Universitat Autònoma de Barcelona

# Estudio de las subunidades reguladas por SUR1 (Kir6.2 y TRPM4) en las contusiones cerebrales traumáticas y la isquemia cerebral focal. Desarrollo de un modelo animal de infarto maligno en cerdo

**Lidia Castro González**

UNIVERSIDAD AUTÓNOMA DE BARCELONA

**Institut de Recerca Vall d'Hebron (VHIR)**

Departamento de Cirugía

TESIS DOCTORAL

# Estudio de las subunidades reguladas por SUR1 (Kir6.2 y TRPM4) en las contusiones cerebrales traumáticas y la isquemia cerebral focal. Desarrollo de un modelo animal de infarto maligno en cerdo.

Director de tesis: Juan Sahuquillo Barris

Doctoranda: Lidia Castro González

Doctorado en Cirugía y Ciencias Morfológicas

Barcelona, 2019

Universitat Autònoma de Barcelona

Programa de doctorado en Cirugía y Ciencias Morfológicas Barcelona

# Estudio de las subunidades reguladas por SUR1 (Kir6.2 y TRPM4) en las contusiones cerebrales traumáticas y la isquemia cerebral focal. Desarrollo de un modelo animal de infarto maligno en cerdo.

Memoria de Tesis presentada por **Lidia Castro González** para obtener el grado de Doctora por la Universidad Autónoma de Barcelona.


**Director de tesis** **Doctoranda**

**Juan Sahuquillo Barris** **Lidia Castro González**


Tesis realizada en la Unidad de Investigación de Neurotraumatología y Neurocirugía (UNINN), Institut de Recerca Vall d'Hebron (VHIR)

Barcelona, 2019

# AYUDAS RECIBIDAS Y CONFLICTOS DE INTERÉS

Esta tesis doctoral ha sido realizada en la Unidad de Neurotraumatología y Neurocirugía (UNINN), acreditada como "Grupo de Investigación Consolidado" por la Generalitat de Catalunya (SGR2009-00495). Los artículos que forman el cuerpo de esta tesis, han sido financiados por el Fondo de Investigación Sanitaria (Instituto Carlos III) con la beca PI15/01228, cofinanciada a su vez por el *European Regional Development Fund* y otorgada al Dr. Sahuquillo.

El Dr. J. Marc Simard tiene la patente de Estados Unidos número 7285574 "*A novel non-selective cation cannel in neural cells and methods for treating brain swelling*". Además, es miembro del consejo asesor científico y posee acciones de *Remedy Pharmaceuticals*. Sin embargo, no se recibió soporte (ni directo ni indirecto) para el desarrollo de los trabajos presentados, por parte de esa compañía. El resto de autores de los trabajos presentados no tienen ningún conflicto de interés en relación con los materiales y métodos utilizados en estos estudios ni con los resultados mostrados.

***Convendría sentir menos curiosidad por las personas y más por las ideas.***

*Marie Curie*

# ÍNDICE

**ÍNDICE** ..... **1**

**TABLA DE ABREVIATURAS** ..... **5**

**INTRODUCCIÓN** ..... **7**

**Resumen** ..... **9**

**Abstract** ..... **11**

1. **Traumatismo craneoencefálico** ..... **15**

1.1.Contusión cerebral ..... 17

2. **Infarto cerebral maligno** ..... **18**

3. **Barrera hematoencefálica** ..... **19**

4. **Edema cerebral** ..... **21**

4.1.Clasificación actual del edema cerebral ..... 22

4.1.1. Edema citotóxico ..... 22

4.1.2. Edema iónico ..... 23

4.1.3. Edema vasogénico ..... 24

4.1.4. Transformación hemorrágica ..... 25

5. **Receptor de la sulfonilurea 1** ..... **27**

5.1.Canal SUR1-TRPM4 ..... 28

5.2.Canal SUR1-Kir6.2 ..... 29

6. **Monitorización multimodal** ..... **30**

6.1.Monitorización sistémica ..... 30

6.2.Monitorización cerebral ..... 31

6.2.1. Presión intracraneal ..... 31

6.2.2. Oxigenación cerebral ..... 32

6.2.2.1. Saturación de oxígeno del bulbo de la yugular ..... 32

6.2.2.2. Presión tisular de oxígeno ..... 33

6.2.3. Metabolismo cerebral ..... 35

6.2.3.1. Concepto de recuperación relativa ..... 37

6.2.3.2. Intervalos de referencia de los metabolitos ..... 38

6.2.3.3. Aplicación clínica de la microdiálisis cerebral ..... 40

7. **Modelos animales ..... 41**

**HIPÓTESIS Y OBJETIVOS ..... 43**

1. **Hipótesis ..... 45**

2. **Objetivos ..... 46**

**CAPÍTULO 1 ..... 47**

**CAPÍTULO 2 ..... 83**

**RESULTADOS Y DISCUSIÓN ..... 119**

1. **Modelo animal porcino de infarto maligno de la arterial cerebral media ..... 121**

1.1.Grupo de estudio ..... 122

1.2.Período de isquemia y tamaño del infarto ..... 122

1.3.Monitorización de la $PtiO_2$ ..... 123

1.4.Monitorización de la microdiálisis cerebral ..... 124

1.5.Análisis del perfil iónico en el espacio extracelular .127

1.6.Expresión de SUR1 y TRPM4 ..... 127

1.7.DISCUSIÓN ..... 129

2. **Expresión de Kir6.2 en las contusiones cerebrales post-traumáticas ..... 136**

2.1.Grupo de estudio ..... 136

2.2.Grupo control ..... 137

2.3.Expresión global de Kir6.2 ..... 138

2.4.Expresión de Kir6.2 en diferentes tipos celulares .... 139

2.5.DISCUSIÓN ..... 141

**CONCLUSIONES ..... 147**

**ANEXOS ..... 151**

**Anexos I ..... 153**

I. **Estudio de la función de Kir6.2 en cultivos primarios de astrocitos humanos ..... 185**

I.I.Efectos de la hipoxia en los astrocitos ..... 185

I.II.Captación de glutamato bajo condiciones de normoxia e hipoxia ..... 186

I.III.Captación de glutamato tras el bloqueo selectivo de Kir6.2 a nivel de membrana ..... 187

I.IV.Captación de glutamato tras el bloqueo selectivo de los canales $K_{ATP}$ en mitocondria ..... 187

I.V.DISCUSIÓN ..... 188

I.VI.CONCLUSIONES (ANEXOS) ..... 194

# LISTA DE ABREVIATURAS

**5-HD:** 5-Hidroxidecanoato

**ABC:** *ATP-binding cassette*

**ACM:** Arteria cerebral media

**ATP:** Adenosín trifosfato

**BHE:** barrera hematoencefálica

**BTF:** *Brain Trauma Fundation*

**DMSO:** dimetilsulfóxido

**GCS:** Escala de coma de Glasgow

**HIF1α:** factor inducible por hipoxia 1α

**HSA:** hemorragia subaracnoidea

**IMACM:** Infarto maligno de la arteria cerebral media

**$K_{ATP}$:** Canal de potasio dependiente de ATP

**Kir6.2:** canal iónico rectificador de entrada de potasio 6.2

**MD:** Microdiálisis cerebral

**MM:** monitorización multimodal

**MMP9:** metaloproteasa de matriz 9

**NKCC1:** co-transportador $Na^+/K^+/Cl^-$

**RM:** Resonancia magnética

**RR:** Recuperación relativa

**$SjO_2$:** Saturación de oxígeno del bulbo de la yugular

**SNC:** Sistema nervioso central

**Sp1:** proteína de especificidad 1

**SUR1:** Receptor de sulfonilurea 1

**PIC:** Presión intracraneal

**PPC:** Presión de perfusión cerebral

**$PtiO_2$:** Presión tisular de oxígeno

**TC:** Tomografía computarizada

**TCE:** Traumatismo craneoencefálico

**TRPM4:** Receptor de potencial transitorio de la melastatina 4

**VEGF:** factor endotelial de crecimiento vascular

**WB:** western blot

# INTRODUCCIÓN

# RESUMEN

El traumatismo craneoencefálico (TCE) tiene un gran impacto socio-económico y sanitario en todo el mundo[1], y es una de las principales causas de mortalidad y discapacidad entre la población adulta menor de 40 años[2]. El infarto cerebral maligno, es un tipo de infarto cerebral isquémico, que tiene una mortalidad de alrededor del 80%[3], y su incidencia aumenta con la edad del paciente. Ambas patologías se caracterizan porque su evolución puede provocar graves desequilibrios iónicos a nivel de las neuronas y de las células gliales, con el consecuente arrastre osmótico de agua y la formación de edema citotóxico[4]. El edema puede evolucionar provocando un efecto de masa que causa la compresión, deformación y herniación de las estructuras cerebrales, pudiendo provocar la muerte del paciente, debido entre otras cosas al aumento de la presión intracraneal (PIC)[5]. Los TCEs y los infartos malignos se abordan siguiendo las mismas estrategias de tratamiento, que pasan por el seguimiento de la evolución de la lesión, la monitorización multimodal del paciente, y en último caso su intervención quirúrgica.

Entender los procesos implicados en la patofisiología del TCE y del infarto, es esencial para su correcto tratamiento. Muchos de los estudios actuales, dirigen su atención a los mecanismos implicados en la formación del edema citotóxico inicial, y en concreto al estudio de un nuevo canal iónico involucrado en su progresión. Este canal está formado por una subunidad reguladora que recibe el nombre de receptor de sulfonilurea 1 (SUR1) y una subunidad formadora de poro, el receptor de potencial transitorio de la melastatina 4 (TRPM4). Juntos constituyen el canal SUR1-TRPM4, que ha demostrado estar sobre-expresado en pacientes y modelos animales de TCE e infarto cerebral, entre otras patologías[6–9]. El bloqueo de

este canal con fármacos como la glibenclamida (un inhibidor de sulfonilureas), ha demostrado mejorar el pronóstico neurológico en modelos animales de roedores y estudios clínicos con pacientes[8,10,11]. La subunidad reguladora SUR1, además de asociarse con TRPM4, también regula la apertura de canales de potasio dependientes de adenosín trifosfato (ATP) ($K_{ATPs}$), entre los que se encuentra el canal iónico rectificador de entrada de potasio 6.2 (Kir6.2). El canal SUR1-Kir6.2 ha sido estudiado ampliamente en células del páncreas y cardiomiocitos, entre otros[12,13]. Sin embargo, la expresión de este canal no ha sido estudiada en profundidad a nivel cerebral en humanos. Este canal acopla el metabolismo de la célula a la actividad eléctrica, mediante la regulación del flujo de $K^+$ a través de la membrana celular. Se considera que tiene una función neuroprotectora, induciendo la hiperpolarización celular durante episodios de hipoxia y/o isquemia[14].

Lo que esta tesis pretende es, en primer lugar, el desarrollo de un nuevo modelo animal de isquemia regional en cerdo común, que sea estable y reproducible. Este modelo permitirá una mejor comprensión de los procesos isquémicos que tienen lugar en pacientes que han sufrido un infarto cerebral maligno, para poder extrapolarlos en un segundo paso a las lesiones cerebrales traumáticas. El uso de modelos animales es esencial para conseguir una mejor comprensión de los mecanismos implicados en cualquier patología, así como para poder desarrollar nuevas estrategias protectoras contra esta. En segundo lugar, se pretende profundizar en el estudio de los canales regulados por SUR1, en concreto Kir6.2, el menos estudiado a nivel del SNC en humanos hasta la fecha. Para ello, se estudió su expresión en tejido pericontusional cerebral de humanos con la pretensión de conocer mejor su función en este tipo de patologías.

# ABSTRACT

Traumatic brain injury has a great socio-economic and sanitary impact in the whole world[1] and is one of the leading causes of mortality and disability in adult population with less than 40 years[2]. Malignant cerebral infarction is a type of ischemic cerebral infarct that has an elevated mortality of around 80%[3], and its incidence increases with the age of the patient. The evolution of both pathologies can lead to severe ionic disarrangements in neurons and glial cells, osmotic water displacement and cytotoxic edema formation[4]. Edema can evolve causing a mass effect that causes compression, deformation and herniation of the cerebral structures that can result in patient's death, due to the increase of the intracranial pressure, among other causes[5]. TBIs and malignant infarcts are treated following the same strategies, which are the monitoring of lesion evolution, multimodal monitoring of the patient and as a last resort, surgical intervention.

Understanding the processes involved in the pathophysiology of the TBI and cerebral infarct, is essential for their correct treatment. Many of the current studies, focus their attention on the mechanisms involved in the formation of the initial cytotoxic edema and specially, in the study of a new ionic channel that is related to the progression of the edema. This channel is constituted by a regulator subunit named sulfonylurea receptor 1 (SUR1) and a pore forming subunit called transient receptor potential melastatin 4 (TRPM4). Both subunits together form the channel SUR1-TRPM4 that is overexpressed in patients and in animal models of TBI and cerebral infarct, among other pathologies[6–9]. The blockage of this channel with drugs like glibenclamide (an inhibitor of sulfonylureas), has demonstrated to improve neurological outcome in rodent animal

models and also in clinical assays with patients[8,10,15]. Regulator subunit SUR1 is not only associated to TRPM4, but also regulates the opening of adenosine phosphate (ATP)-sensitive potassium channels ($K_{ATPs}$), which include the inwardly rectifier potassium ion channel 6.2 (Kir6.2). The channel SUR1-Kir6.2 has been well studied in pancreatic and cardiac cells, among others[12,13]. However, the expression of this channel has not been deeply studied in the human brain. This channel couples cell metabolism to electric activity, regulating the K+ flux through the cell membrane. It is considered that it has a neuroprotective function, inducing the cell hyperpolarization during hypoxic and/or ischemic episodes[14].

The aim of this doctoral thesis is, first of all, the development of a new animal model of regional ischemia in common pig, stable and reproducible. This model will allow a better understanding of the ischemic processes that occur in patients with a malignant cerebral infarction, to extrapolate it in second place to traumatic brain lesions. The use of animal models is essential to achieve a better understanding of the mechanisms involved in any pathology, and to develop new treatment strategies. The aim of the second part of this thesis was to study in detail the channels regulated by SUR1, and especially Kir6.2 channel, the less studied in human brain to the date. For this purpose, Kir6.2 expression was studied in human pericontusional brain tissue, with the aim to achieve a better understanding of its function in this kind of pathologies.

## 1. Traumatismo craneoencefálico

El TCE es considerado una epidemia silenciosa. Aunque la sociedad no es consciente de ello, tiene un gran impacto a nivel económico, social y de salud en todo el mundo[1]. Es una de las principales causas de muerte en la población adulta menor de 40 años[2]. Estimar la incidencia de los TCEs no es algo sencillo, ya que hay mucha variación entre diferentes regiones del mundo. Sin embargo, un estudio transversal realizado en 24 países europeos durante 2012 muestra una incidencia de 2872 casos por millón de habitantes[16]. En España, los datos publicados más recientes engloban el período de 2000 a 2009, donde la incidencia es de 472,6 casos por millón de habitantes[17]. Una de las causas más comunes de los TCEs son los accidentes de tráfico. Sin embargo, en los últimos años se ha visto un cambio en su epidemiología, convirtiéndose las caídas accidentales en la primera causa de TCE debido, entre otras cosas, al envejecimiento de la población en los países más desarrollados[2].

El TCE se define como una alteración de la función cerebral u otra evidencia de patología cerebral, causada por una fuerza externa[18]. Debido a su complejidad, no existe una única clasificación de los TCEs, sino que hay varias basadas en diferentes aspectos de esta patología[19]:

- En función del **mecanismo físico** que los genera, se dividen en lesiones penetrantes o no penetrantes.
- En función de su **pato-anatomía**, existen diferentes escalas de clasificación entre las que destaca la escala de Marshall[20], que

divide las lesiones en focales o difusas con diferentes grados de complejidad.

- En función del **pronóstico** del paciente. Esta es la clasificación más reciente, que usa modelos matemáticos para predecir la evolución del paciente en función de su pronóstico inicial[21].
- En función de su **gravedad**. Esta última clasificación es la más usada en la actualidad, y se basa en la denominada escala de coma de Glasgow[22] (GCS) para establecer diferentes niveles de gravedad, en función de las respuestas motora, verbal y ocular de los pacientes (**Tabla 1**). La GCS tiene una puntuación máxima de 15 y mínima de 3, y permite diferenciar los TCEs entre leves (GCS entre 13 y 15), moderados (GCS entre 9 y 12) y graves (GCS entre 3 y 8).

**Tabla 1.** Escala de coma de Glasgow.

| | Variables | Puntuación |
|---|---|---|
| **Respuesta verbal** | Orientada, conversa | 5 |
| | Desorientada, confusa | 4 |
| | Palabras inapropiadas | 3 |
| | Sonidos incomprensibles | 2 |
| | Sin respuesta | 1 |
| **Respuesta ocular** | Espontánea | 4 |
| | Al estímulo verbal | 3 |
| | Al dolor | 2 |
| | Sin respuesta | 1 |
| **Respuesta motora** | Obedece órdenes | 6 |
| | Localiza el dolor | 5 |
| | Flexión normal | 4 |
| | Flexión anormal | 3 |
| | Extensión | 2 |
| | Sin respuesta | 1 |

Los TCEs pueden ocasionar lesiones primarias y secundarias. Las lesiones primarias (fracturas, contusiones, lesión axonal difusa, etc) son inevitables al ser consecuencia directa de las fuerzas mecánicas externas que tienen lugar tras el traumatismo (fuerzas lineales como la aceleración-desaceleración y rotacionales, entre otras). Estas lesiones primarias, producen deformación del tejido cerebral y daño celular, y pueden complicarse hasta derivar en lesiones secundarias. Las lesiones secundarias desencadenan una serie de procesos bioquímicos y metabólicos patológicos (inflamación, excitotoxicidad, apoptosis, desajustes metabólicos...), que en último término dan lugar a la formación de edema cerebral, hipoxia isquémica o no isquémica y un aumento de la PIC, entre otros. Al contrario que las lesiones primarias, estas se consideran por definición potencialmente tratables y evitables[23].

## 1.1 Contusión cerebral

Las contusiones cerebrales son lesiones primarias focales muy frecuentes en los pacientes que han sufrido un TCE moderado o grave. Se producen como consecuencia de las fuerzas mecánicas originadas por el traumatismo, que inducen el contacto entre el parénquima cerebral y la bóveda craneal o la base del cráneo[23]. Son lesiones evolutivas y dinámicas, que pueden aumentar su tamaño en las primeras horas o incluso días después del TCE. Provocan la muerte celular necrótica y la ruptura o compresión de los capilares sanguíneos cerebrales. Ambos procesos están involucrados en la extravasación de sustancias potencialmente tóxicas para el sistema nervioso central (SNC). La pérdida de capilares, además, puede dar lugar a la isquemia cerebral. Estos fenómenos, provocan la evolución de las lesiones primarias a lesiones

secundarias, que pueden derivar en la formación de edema perilesional y/o la transformación hemorrágica de la contusión[24].

El tratamiento actual de las contusiones cerebrales pasa por el seguimiento de la evolución de la contusión, la monitorización multimodal, y en el caso de que ninguna de estas estrategias funcionen, la resección quirúrgica de la zona afectada y/o la craniectomía descompresiva[5]. Alrededor de las áreas isquémicas y necrosadas de las contusiones cerebrales, hay una región perilesional que podría identificarse con el concepto de "penumbra traumática"[25], por su similitud con la penumbra isquémica definida en los casos de infarto cerebral. Las zonas de penumbra identifican regiones en las que el tejido está en riesgo, pero potencialmente recuperables y susceptibles de ser tratadas. El desarrollo de nuevas estrategias enfocadas al tratamiento de estas zonas sería de gran utilidad en esta patología, para la que las actuales estrategias son muy limitadas.

## 2. Infarto cerebral maligno

El infarto cerebral se define como un déficit neurológico focal, secundario a una disrupción del flujo sanguíneo en el área correspondiente del cerebro[26]. Es la segunda causa más común de mortalidad en todo el mundo. En 2013, se estimaron un total de 110,1 muertes por cada 100.000 personas, a nivel mundial[27]. La incidencia del infarto cerebral, aumenta con la edad, duplicándose cada década después de superar los 55 años[28].

Existen dos tipos de infarto cerebral en función del mecanismo que los genera: el **infarto hemorrágico**, que es debido a la ruptura de los vasos sanguíneos cerebrales; y el **infarto isquémico**, que es el más común y que se debe a la oclusión o al bloqueo de los vasos sanguíneos cerebrales.

El denominado infarto cerebral maligno es un tipo de infarto o ictus isquémico, que fue descrito por primera vez en el año 1996 por Hacke y colaboradores[29]. El término "maligno" hace referencia a un tipo específico de infarto que afecta al territorio completo de la arteria cerebral media (ACM), pudiendo extenderse a otros territorios. Este tipo de patología tiene una mortalidad muy alta de alrededor del 80%[30]. El infarto maligno de la ACM (IMACM) se caracteriza por la formación de edema cerebral citotóxico, que da lugar a un efecto de masa que causa la compresión, deformación e incluso herniación de las estructuras cerebrales[3]. Todos estos fenómenos pueden ocasionar el aumento de la PIC[5]. El tratamiento de los IMACMs, igual que en el caso del TCE, pasa por el seguimiento de la evolución del infarto, su monitorización y en último caso la craniectomía descompresiva.

## 3. Barrera hematoencefálica

La barrera hematoencefálica (BHE) es una barrera de difusión que separa el SNC de la circulación sistémica, regulando el intercambio de iones y moléculas orgánicas entre ambos. El primer estudio que evidenció la existencia de la BHE fue el llevado a cabo por Paul

Ehrlich en 1885, quien tras inyectar un colorante soluble en el sistema circulatorio, vio que todos los órganos se teñían, a excepción del SNC[31]. Sin embargo, no fue hasta 1967 cuando se evidenció su existencia a nivel ultraestructural, gracias al trabajo de Reese y Karnovsky con microscopía electrónica[32].

A nivel anatómico, la BHE está constituida por varios elementos interconectados: células endoteliales, astrocitos, pericitos y membrana basal, como se muestra en la **Fig. 1.** Algunos trabajos también incluyen dentro de su estructura, las proyecciones neuronales en contacto con los elementos anteriormente nombrados y la microglía, que juntos forman la unidad neurovascular[33].

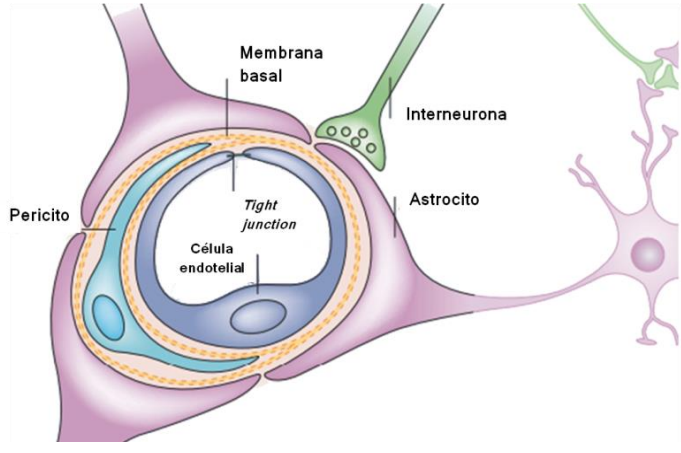


**Fig.1. Estructura de la unidad neurovascular.** Imagen modificada del trabajo de Abbot *et al* [34].

**Células endoteliales:** las células endoteliales de la BHE, constituyen la primera línea de defensa entre la circulación sistémica y el SNC. Se diferencian de las células endoteliales del resto del organismo por

su falta de fenestraciones, su reducida actividad pinocítica y la formación de las llamadas uniones estrechas o *tight junctions*[31,35].

**Astrocitos:** son células gliales que interaccionan a través de sus pies con las células endoteliales, contribuyendo a la formación de la BHE y a su mantenimiento[36]. También están implicados en la formación y el mantenimiento de las uniones estrechas entre las células endoteliales[37].

**Pericitos:** son células derivadas de músculo liso, que tienen como principal función el mantenimiento de la homeostasis y hemostasia en la BHE[36]. Estas células regulan además la formación de las uniones estrechas y la permeabilidad de la BHE[34].

**Membrana basal:** es una lámina de 30-40nm de grosor cuya principal función es la de soporte estructural. Está compuesta de colágeno tipo IV, proteoglicanos, laminina, fibrinonectina y otras proteínas de matriz. Se encuentra alrededor de las células endoteliales y los pericitos y es contigua a la membrana plasmática de los pies de los astrocitos[37,38].

## 4. Edema cerebral

El edema cerebral se asocia a una gran variedad de condiciones patológicas, como los TCEs, los IMACMs, tumores del SNC, etc. Este término fue establecido por Reichardt en 1905. Sin embargo, la primera clasificación conocida del edema, fue llevada a cabo por Klazto en el año 1967[39]. Klazto definió el edema cerebral como una

acumulación anómala (localizada o difusa) de fluido más o menos rico en proteínas, asociado con un aumento del volumen cerebral. A su vez, clasificó el edema cerebral en citotóxico y vasogénico, en función de si la BHE permanecía intacta o se veía estructuralmente afectada, de forma respectiva.

La formación del edema cerebral sigue el principio de Starling[40], que se basa en dos fenómenos principales: la presencia de una denominada "fuerza conductora" (formada por la suma de los gradientes osmóticos e hidrostáticos) que permite la entrada o salida de substancias al interior o exterior del tejido, y la "permeabilidad de poro", que permite el paso de substancias desde el espacio intravascular al extracelular.

## 4.1 Clasificación actual del edema cerebral

A lo largo de la historia, se han establecido muchos posibles modelos de clasificación del edema cerebral, todos basados en el original de Klatzo[39]. Sin embargo, no ha sido hasta el año 2007 en el que el trabajo de Simard *et al* [4] dio lugar a una nueva clasificación, que sigue siendo la más usada en la actualidad. Esta nueva clasificación incorporaba tanto los edemas citotóxico y vasogénico, como los términos edema iónico y transformación hemorrágica como nuevas fases en la evolución del edema, y además introducía una modificación de la ecuación de Starling.

### 4.1.1 Edema citotóxico

El edema citotóxico se considera un proceso pre-mórbido en el que se produce un influjo de osmolitos (especialmente $Cl^-$ y $Na^+$) desde el espacio extracelular al intracelular. En condiciones fisiológicas normales (**Fig. 2A**), la permeabilidad selectiva de la

membrana celular y la actividad de la bomba $Na^+/K^+$-ATPasa, mantienen la concentración de $Na^+$ más elevada en el espacio extracelular que en el intracelular. Sin embargo, bajo condiciones patológicas, como la isquemia y la hipoxia, existe una entrada anómala de iones al interior celular, que genera un gradiente osmótico (**Fig. 2B**). Este gradiente va a favorecer la entrada de agua al interior celular, provocando un aumento del volumen de la célula, que no se produce a nivel tisular. Esto es debido a que lo único que ocurre durante esta etapa del edema, es una redistribución del agua localizada a nivel del parénquima cerebral[4,41].

La entrada de iones al interior de la célula tiene lugar gracias a dos tipos de transporte: 1) el **transporte activo primario** (bomba $Na^+/K^+$-ATPasa, etc), que es dependiente de ATP y 2) el **transporte activo secundario**, que usa la energía almacenada en la membrana celular, proveniente de los gradientes iónicos ya existentes. En condiciones patológicas, la disminución en la disponibilidad de ATP da lugar a que los mecanismos ATP-independientes adquieran mayor importancia. Estos provocarán la entrada masiva de $Na^+$ al espacio intracelular, mediante transportadores constitutivos como el co-transportador $Na^+/K^+/Cl^-$ (NKCC1), así como mediante transportadores de nueva síntesis. Entre estos últimos, cabe destacar el canal SUR1-TRPM4, que se ha demostrado que se sintetiza *de novo* a nivel cerebral bajo condiciones patológicas[7,42].

### 4.1.2 Edema iónico

Como se ha explicado anteriormente, durante el edema citotóxico se produce una entrada anómala de $Na^+$ al interior celular. Esto provoca que sus niveles en el espacio extracelular sean muy

reducidos, formándose un gradiente de concentración que induce la entrada de $Na^+$ desde el espacio vascular al extracelular (**Fig. 2C**). El transporte de $Na^+$ tiene lugar principalmente gracias a canales constitutivos como el NKCC1 (presente en la pared luminal de los vasos) y la $Na^+/K^+$-ATPasa (situado en la membrana abluminal de los mismos). Se ha comprobado que este transporte ocurre también gracias a canales de nueva síntesis como el canal SUR1-TRPM4[42]. El paso de $Na^+$ a través de la BHE origina un gradiente eléctrico y osmótico que da lugar a la entrada de $Cl^-$ y de agua al espacio extracelular[4,41].

En esta fase del edema, se produce entonces una alteración funcional de la permeabilidad de la BHE. Sin embargo, la integridad de esta permanece intacta, así como las uniones estrechas entre las células endoteliales que la componen. Por esta razón, no se produce la entrada de macromoléculas y proteínas plasmáticas al parénquima cerebral.

### 4.1.3 Edema vasogénico

El edema vasogénico se caracteriza por la ruptura de la BHE. Los principales mecanismos que provocan la formación de poros o canales interendoteliales en la BHE son la desestabilización de las uniones estrechas endoteliales, la pinocitosis inversa[43], la interrupción de la vía de señalización del calcio[44], y la retracción celular. La presencia del factor endotelial de crecimiento vascular (VEGF) y de la metaloproteasa de matriz 9 (MMP9), que ven aumentada su expresión durante la isquemia cerebral[45], favorece también a la desestabilización de las uniones interendoteliales y a la degradación de la membrana basal del endotelio. Este conjunto de fenómenos, provoca la disrupción de la BHE permitiendo el paso de

macromoléculas y diversas proteínas del plasma (albúmina, dextranos, etc) al espacio extracelular (**Fig. 2D**).

En esta fase del edema, aunque se haya producido la ruptura de la BHE, la integridad estructural de los capilares sanguíneos no se ve afectada, lo que impide el paso de eritrocitos hacia el espacio extracelular[41].

### 4.1.4 Transformación hemorrágica

La transformación hemorrágica representa la fase final de la disfunción endotelial que se inicia con el edema iónico. Durante esta fase, la integridad estructural de los capilares sanguíneos mantenida durante el edema vasogénico, se pierde. La ruptura de los capilares provoca la extravasación de eritrocitos y otras moléculas de la sangre al parénquima cerebral. Los mecanismos implicados en la transformación hemorrágica son diversos: degradación de la laminina, activación de las células endoteliales, migración de los leucocitos a través de la pared vascular, etc.

Durante esta fase también se ven implicados algunos de los mecanismos que inducían la formación del edema vasogénico, entre los que cabe destacar el VEGF, la MMP9 y el canal SUR1-TRPM4, responsable de la muerte oncótica (**Fig. 2D**) de las células endoteliales[4,41].

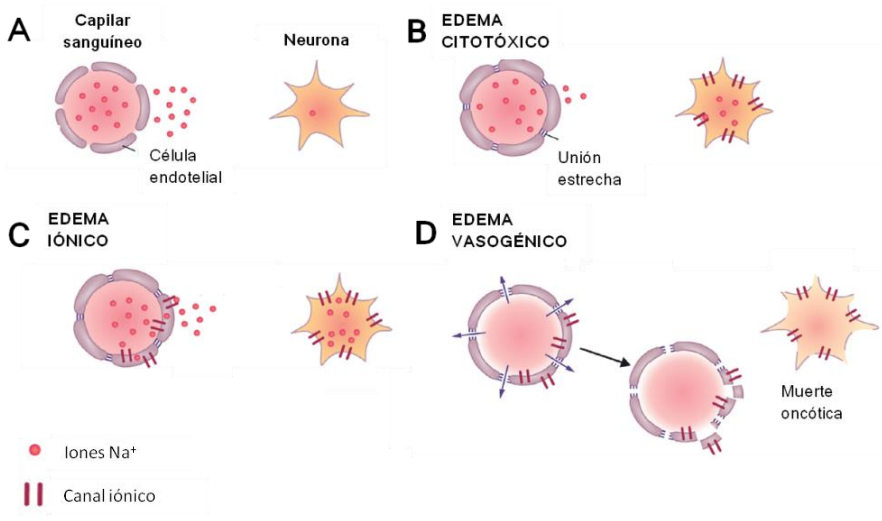


**Fig. 2. Esquema representativo de las diferentes fases de la formación y progresión del edema cerebral. A) Condiciones fisiológicas.** La concentración de $Na^+$ se mantiene en equilibrio, siendo mayor en el exterior celular y en el plasma, que en el interior de la neurona. **B) Edema citotóxico.** La sobreexpresión de canales iónicos, genera un aumento de $Na^+$ en el interior celular y una disminución de este ion en el espacio extracelular. **C) Edema iónico.** El gradiente generado entre el contenido intravascular y el espacio extracelular, provoca la sobreexpresión de canales iónicos en las células endoteliales. Se produce la entrada masiva de $Na^+$ intravascular al espacio extracelular. **D) Edema vasogénico.** La ruptura de las uniones estrechas entre las células endoteliales induce la extravasación de macromoléculas y proteínas plasmáticas. Se produce la muerte oncótica de las células endoteliales. La muerte oncótica y la pérdida de la integridad vascular, entre otras cosas, son las responsables del proceso denominado conversión hemorrágica. Esquema modificado del trabajo de Leinonen *et al* [46].

## 5. Receptor de la sulfonilurea 1

SUR1 es una proteína codificada por el gen *ABCC8*, que pertenece a la familia de transportadores *ATP-binding cassette* (ABC). Los transportadores ABC son proteínas de membrana que acoplan el transporte de moléculas, con la hidrólisis del ATP[47]. Aunque SUR1 pertenezca a esta familia, no actúa como un transportador de membrana, si no que su principal función es la de regulador de canales iónicos[48]. La estructura de SUR1 está constituida por dos dominios transmembrana y dos dominios de unión a nucleótidos. Su asociación más conocida es con el canal iónico Kir6.2, aunque también se ha estudiado en profundidad su asociación con la unidad formadora de poro TRPM4. Se ha demostrado que SUR1 se expresa de forma constitutiva en algunas neuronas, pero siempre asociado al canal Kir6.2[49]. Sin embargo, hay trabajos que indican que en diversas patologías del SNC como el TCE[7], la hemorragia subaracnoidea (HSA)[50], el infarto cerebral[51], etc, existe una sobre-expresión de SUR1 en diversos tipos celulares (vasos sanguíneos, células gliales, neuronas...). En estos casos se considera que SUR1 se encuentra asociado a la subunidad formadora de poro TRPM4.

Los canales SUR1-TRPM4 y SUR1-Kir6.2 son funcionalmente contrarios. La activación del primero provoca la despolarización celular (dando lugar a la muerte celular oncótica), y la activación del segundo, provoca la hiperpolarización celular (que se considera neuroprotectora). Los dos canales comparten la misma estructura: ambos están constituidos por un octámero formado por 4 subunidades de SUR1 y 4 subunidades de TRPM4 o Kir6.2, respectivamente. Sus estructuras aparecen representadas en la **Fig. 3.**

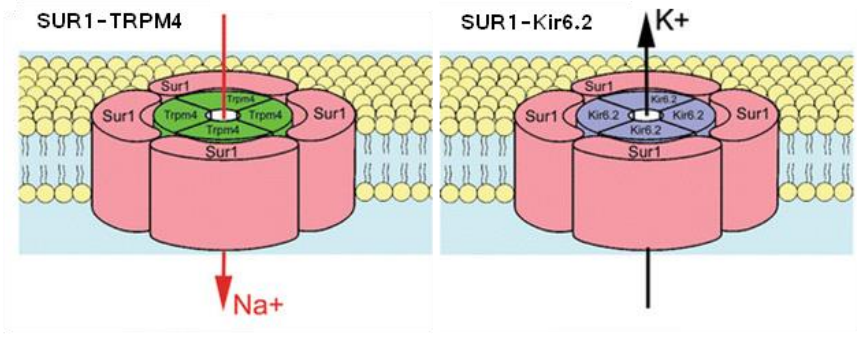


**Fig 3. Estructura de los canales SUR1-TRPM4 y SUR1-Kir6.2.** Estos canales se encuentran formando un octámero constituido por 4 subunidades reguladoras (SUR1, en rosa) y 4 subunidades formadoras de poro (TRPM4, en verde o Kir6.2, en violeta). Modificado de Simard *et al* [8].

## 5.1 Canal SUR1-TRPM4

TRPM4 forma parte de la familia de canales de cationes no selectivos, activados por $Ca^{2+}$. A su vez, esta familia forma parte de la subfamilia de 8 miembros que constituyen los receptores de potencial transitorio[52]. TRPM4 tiene la capacidad de transportar cationes monovalentes inorgánicos ($Na^+$, $K^+$, $Cs^+$, $Li^+$), y aunque se activa gracias al $Ca^{2+}$, es impermeable a este ion, así como a otros iones divalentes como el magnesio[53].

TRPM4 se expresa a nivel de membrana en gran variedad de tejidos, y en diferentes tipos celulares como los linfocitos, las células β del páncreas, las neuronas, las células del músculo liso, etc[54–56].

La asociación de TRPM4 con la subunidad reguladora SUR1, fue descrita por primera vez en el año 2003 por Cheng *et al* [57]. Tras la publicación de este trabajo, fueron muchos los que demostraron que durante diversas patologías del SNC (TCE, HSA, infarto cerebral, etc)[7,9,50], la expresión del canal SUR1-TRPM4 se veía

aumentada. Estos hallazgos, demuestran la gran importancia que tiene este canal en el desarrollo de procesos como el edema cerebral y la neuroinflamación.

Se ha comprobado en diversos estudios llevados a cabo en modelos animales, así como en ensayos clínicos en humanos[8,10], que la inhibición del canal SUR1-TRPM4 con el fármaco glibenclamida (inhibidor selectivo de SUR1), da lugar a mejores resultados neurológicos. El bloqueo de este canal con glibenclamida produce una reducción del volumen del edema cerebral y de las hemorragias secundarias, inhibe la muerte neuronal, tiene efectos neuroinflamatorios y además, promueve la neurogénesis[58].

## 5.2 Canal SUR1-Kir6.2

El canal SUR1-Kir6.2 pertenece a la familia de los canales $K_{ATP}$. Estos canales acoplan el metabolismo de la célula a la actividad eléctrica, mediante la regulación del flujo de $K^+$ a través de la membrana celular[59]. Los $K_{ATPs}$, fueron descubiertos por Noma en el año 1983, en miocitos cardíacos[13], y posteriormente descritos en otros tejidos y tipos celulares como las células β del páncreas, los músculos liso y esquelético, el riñón, la pituitaria, la placenta y el cerebro[60–66].

La asociación de Kir6.2 con SUR1 ha sido muy estudiada, especialmente en órganos como el páncreas, donde el canal SUR1-Kir6.2 regula la liberación de insulina[67]. Hasta la fecha, este canal no ha sido estudiado en profundidad a nivel del SNC en humanos, al no ser considerado relevante en el desarrollo de las patologías que afectan a este sistema. Sin embargo, se han llevado a cabo estudios en modelos animales de roedor, donde se han demostrado los efectos neuroprotectores de SUR1-Kir6.2[68,69], que se plantea

como una posible futura diana terapéutica en pacientes que han sufrido un infarto cerebral o un TCE, entre otras patologías del SNC.

## 6. Monitorización multimodal

Como ya se ha comentado en apartados anteriores, tras un TCE o un infarto, los pacientes afectados sufren una serie de daños tisulares cerebrales inmediatos. Pasados los minutos, las horas o incluso los días, estos daños evolucionan dando lugar a lesiones secundarias, que como hemos dicho anteriormente, se consideran potencialmente tratables y evitables. En estos casos, la monitorización multimodal (MM) es esencial para la optimización del diagnóstico y del tratamiento del paciente, ya que permite la medida de múltiples parámetros sistémicos y cerebrales a tiempo real y de forma continua[70].

### 6.1 Monitorización sistémica

La monitorización sistémica mide diferentes parámetros en los pacientes neurocríticos, entre los que destacan la electrocardiografía, la medida de la saturación de oxígeno arterial, la capnografía, la medida de la presión arterial sanguínea, la medida de la presión venosa central, los gases sanguíneos arteriales, y la osmolaridad y los electrolitos séricos. Dentro de esta categoría también podemos incluir parámetros como el gasto cardíaco, sobre todo en pacientes hemodinámicamente inestables[71].

## 6.2 Monitorización cerebral

La monitorización cerebral se puede realizar mediante métodos invasivos y no invasivos. Los métodos no invasivos son cada vez más populares, ya que permiten reducir los riesgos derivados de los métodos invasivos (infección de la zona de inserción, dolor, molestias...). Sin embargo, muchos no han mostrado ser tan eficaces a la hora de monitorizar de forma fiable determinados parámetros. Todavía quedan por realizar grandes mejoras para que estos métodos se usen de manera rutinaria.

Entre los métodos **no invasivos** destacan 1) el *Doppler* transcraneal, que permite medir el flujo sanguíneo cerebral, 2) el electroencefalograma, que permite detectar anomalías en la actividad eléctrica del cerebro, 3) la espectroscopía del infrarrojo cercano, que nos aporta información sobre la oxigenación vascular del tejido cerebral y 4) las técnicas de neuroimagen, como la tomografía computarizada (TC) y la resonancia magnética (RM)[71]. En cuanto a los métodos **invasivos** usados de forma rutinaria en el tratamiento de pacientes neurocríticos, podemos diferenciar entre métodos para medir la PIC, la oxigenación y el metabolismo cerebral, en los cuales nos vamos a centrar.

### 6.2.1 Presión intracraneal

La monitorización de la PIC es el método invasivo más usado en la monitorización cerebral[72]. La PIC estima la presión que ejercen el parénquima cerebral, el líquido cefalorraquídeo y el flujo sanguíneo, sobre el cráneo. Se mide en milímetros de mercurio (mm Hg). En adultos, en situaciones fisiológicas, la PIC se encuentra entre 7 y 15 mm Hg. En pacientes neurocríticos, cuando

la PIC es mayor de 20 mm Hg de forma persistente, se considera que hay hipertensión intracraneal[72].

Según la cuarta edición de la *Brain Trauma Fundation* (BTF), la PIC debe ser monitorizada en los pacientes con una GCS de entre 3 y 8 y con anormalidades en la TC. En el caso de que la TC sea normal, la monitorización de la PIC también está indicada si el paciente es mayor de 40 años, tiene para o hemiparesia o tiene una presión sistólica menor de 90 mm Hg[73]. Los sensores de PIC más utilizados actualmente en pacientes neurocríticos son los intraparenquimales, ya que son fáciles de colocar y además permiten una monitorización continua[74].

La monitorización de la PIC permite entre otras cosas, la detección temprana de efecto masa intracraneal, la optimización del tratamiento de los pacientes, el cálculo y mejor manejo de la presión de perfusión cerebral (PPC), y una mejor estimación del pronóstico de los pacientes[71].

### 6.2.2 Oxigenación cerebral

Mantener unos niveles de oxigenación adecuados, es esencial en los pacientes neurocríticos. Existen varios sistemas de monitorización del oxígeno cerebral. La medida se puede hacer a nivel global, midiendo la saturación de oxígeno del bulbo de la yugular ($SjO_2$) o a nivel focal, midiendo la presión tisular de oxígeno ($PtiO_2$)[75].

#### *6.2.2.1 Saturación de oxígeno del bulbo de la yugular*

Es un método invasivo que permite estimar el ratio entre el flujo sanguíneo y el consumo metabólico de oxígeno, a nivel cerebral[71]. Para su medida, se introduce un catéter de fibra óptica a nivel del

bulbo de la vena yugular interna dominante. Los niveles normales de la $SjO_2$ se encuentran entre un 60 y un 75%. Cuando los niveles bajan de 50%, se considera que el paciente está en riesgo de isquemia, mientras que si estos suben de 75%, indican hiperemia o tejido infartado[74].

La medida de la $SjO_2$ puede ser continua o discontinua, y está indicada en pacientes con hiperventilación[73]. Al ser global, no es una medida tan específica como la de la $PtiO_2$, que nos permite obtener valores de oxigenación de zonas concretas del cerebro del paciente. Ambas medidas suelen ser complementarias.

#### *6.2.2.2 Presión tisular de oxígeno*

Es un método invasivo que permite medir la $PtiO_2$ en una región concreta del cerebro, de forma continua. La medida se hace mediante la inserción de un catéter a nivel de la sustancia blanca del parénquima cerebral. Este valor se mide en mm Hg, y sus rangos de normalidad se sitúan entre 20 y 35. Los niveles de $PtiO_2$ inferiores a 10-15 mm Hg, suelen asociarse a una mayor morbi-mortalidad de los pacientes, así como a una mayor evidencia de crisis metabólicas a nivel celular[72]. Actualmente, existen dos métodos validados para medir la $PtiO_2$, el polarográfico y el colorimétrico.

El **método colorimétrico** es un método óptico que se basa en el principio de desactivación por fluorescencia, también conocido como "*quenching*" (explicado con detalle en la **Fig. 4**). Es el método que usan los sensores Neurovent-TO® (Raumedic AG; Münchberg, Alemania) y OxyLab pO2™ (Oxford Optronix Ltd; Oxford, United Kingdom)[76,77].

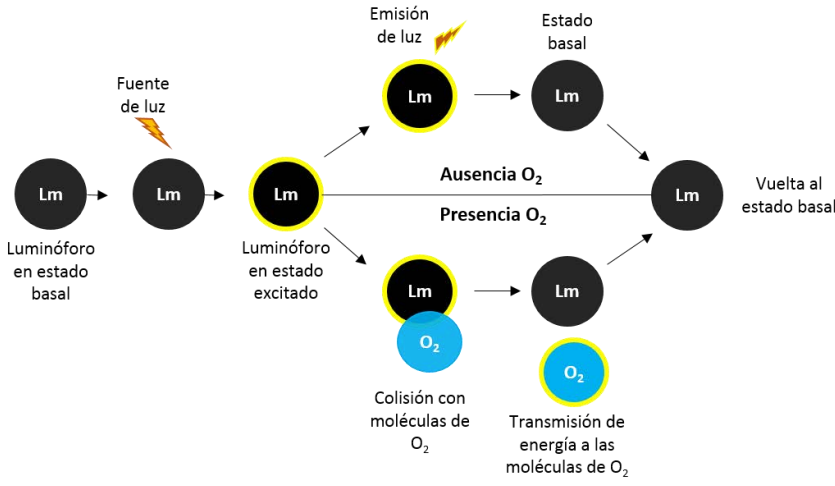


**Fig. 4. Método colorimétrico para la medida de la $PtiO_2$.** Las sondas usadas por los sensores que usan este método, contienen un luminóforo que cuando absorbe luz, cambia su frecuencia y pasa a un estado excitado. En ausencia de oxígeno, cuando el luminóforo vuelve a su estado normal, emite luz de una longitud de onda determinada. En presencia de oxígeno, lo que ocurre es que el luminóforo colisiona con las moléculas de oxígeno, perdiendo energía y volviendo a su estado basal sin producirse la emisión de luz esperada. Figura modificada de Orakcioglu *et al* [76].

El **método polarográfico** usa un electrodo tipo Clark, que está compuesto por un electrodo de plata (el ánodo) y un electrodo de platino (el cátodo), cubiertos por una membrana. El oxígeno pasa por difusión a través de la membrana que recubre los electrodos, y es reducido en el cátodo mediante una serie de reacciones. La corriente galvánica generada por estas reacciones, se convierte en presión parcial de oxígeno, que puede ser registrada por un monitor[77]. Este método (representado en la **Fig. 5**), es el que usan

los sensores Licox® (Integra Neuroscience; Plainsboro, New Jersey). Es el más utilizado en la actualidad.

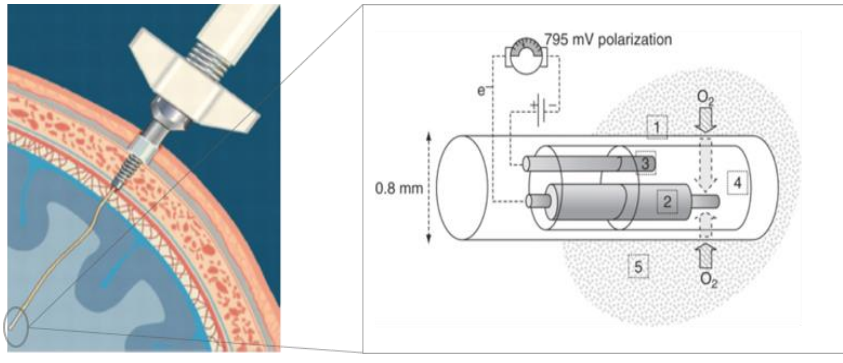


**Fig. 5. Método polarográfico para la medida de la $PtiO_2$.** A la izquierda, representación de un sensor de Licox® localizado en la sustancia blanca del parénquima cerebral. A la derecha, representación de la punta del sensor. 1: membrana; 2: cátodo; 3: ánodo; 4: celda electrolítica; 5: parénquima cerebral. Modificado de Martini *et al* [78] y Nortje *et al* [79].

La medida de la $PtiO_2$ puede hacerse en diferentes zonas del parénquima cerebral. Si se sitúa en el hemisferio dañado, en la zona de penumbra de la lesión, proporciona información sobre el área que se encuentra en riesgo de verse afectada por la lesión secundaria. En el lado contralateral a la lesión, permite una visión más global de la oxigenación cerebral[75].

### 6.2.3 Metabolismo cerebral

La microdiálisis cerebral (MD) permite la monitorización horaria del metabolismo energético de las células. De forma habitual se usa para medir la concentración de metabolitos como la glucosa, lactato y piruvato (marcadores de hipoxia y/o isquemia), así como

el glutamato (marcador de excitotoxicidad) y el glicerol (marcador de daño tisular)[70], en el fluido extracelular cerebral.

La MD es un método invasivo que utiliza la inserción de un catéter intraparenquimal a nivel de la sustancia blanca subcortical. Se trata de un catéter compuesto por una sonda de doble luz, que termina en una membrana semipermeable con punta de oro. Como se muestra en la **Fig. 6**, a través de una de las luces de la sonda, se perfunde hacia la membrana una solución isotónica de composición conocida, a una velocidad de entre 0,1-5µl/min. En la membrana se produce un intercambio entre el líquido perfundido y el fluido cerebral extracelular, en función de un gradiente de concentración. Finalmente, se recoge el microdializado procedente del intercambio en un recipiente denominado microvial, que estará situado en la salida de la otra luz de la sonda. La composición del microdializado se estudiará en un analizador de microdiálisis IscusFlex (M Dialyisis AB, Solna, Suecia).

El catéter de MD puede colocarse en diferentes zonas del tejido cerebral, en función de lo que se quiera monitorizar. Si se coloca en la zona de penumbra de la lesión (como se recomienda en caso de HSA), se podrán observar los cambios bioquímicos que suceden en la zona más vulnerable a las lesiones secundarias. En otros casos (como sucede en la lesión axonal difusa), se recomienda la inserción de un catéter en la zona frontal derecha. Incluso existe la posibilidad de colocar dos catéteres en zona de penumbra y en tejido normal (como se recomienda en las lesiones focales)[80]. La localización de la MD se puede comprobar fácilmente tras la realización de una TC, gracias a la punta de oro de su membrana.

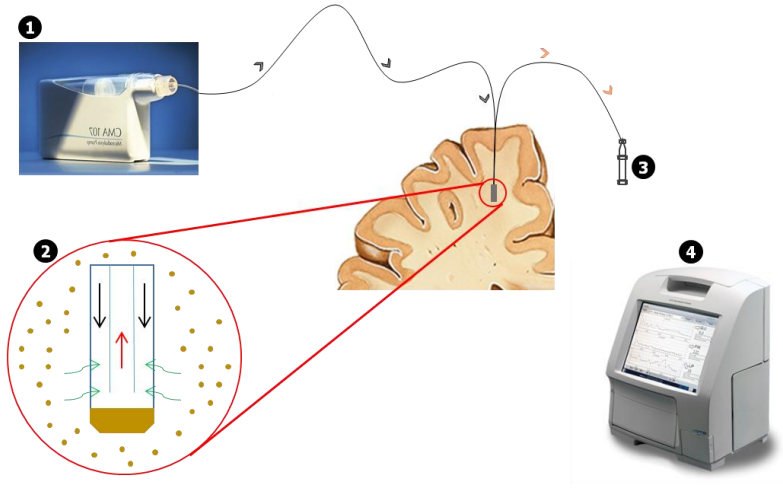


**Fig. 6. Técnica de microdiálisis cerebral. 1)** Microbomba de perfusión. **2)** Membrana semipermeable con punta de oro. **3)** Microvial de recogida de microdializado. **4)** Analizador de microdiálisis IscusFlex.

### *3.2.3.1 Concepto de recuperación relativa*

La concentración de metabolitos en el microdializado nunca es exacta a la concentración en el fluido extracelular cerebral, siempre será menor. Esto se debe a que la eficiencia de paso de la membrana no alcanza el 100%. Es por esto, que la composición del microdializado dependerá de un parámetro denominado "recuperación relativa" (RR), que será específico para cada metabolito. La RR se define como la proporción entre la concentración obtenida en nuestra muestra de microdializado y la concentración real del fluido extracelular (cuando hablamos de estudios *in vivo*) o de la muestra a estudiar (cuando hablamos de estudios *in vitro*)[81]. El cálculo de este parámetro *in vivo* no es posible, debido a que no podemos saber la concentración real del fluido extracelular cerebral. Por ello, siempre que se hace referencia a la RR, hablamos de estudios *in*

*vitro* en los que la muestra de la que partimos tiene una concentración conocida del metabolito a estudiar. La ecuación empleada habitualmente para el cálculo de la RR es la siguiente:

$$\mathbf{RR} = \left(\frac{\mathbf{Cmd}}{\mathbf{Cmatriz}}\right) \times \mathbf{100};$$

donde **Cmd** corresponde a la concentración del metabolito de estudio en el microdializado y **Cmatriz** hace referencia a la concentración del metabolito en la muestra de la que partimos. La RR se expresa en porcentaje (%).

Se considera que la RR es dependiente, entre otras cosas, del tamaño de la molécula de estudio, de la velocidad de flujo de perfusión de la microbomba y del tamaño del poro de la membrana del catéter de MD. Los catéteres de MD más usados en clínica son los que tienen un *cut-off* de 20KDa (CMA70, CMA/Microdialysis) y de 100KDa (CMA71, CMA/Microdialysis)[82]. En este estudio siempre haremos referencia a los catéteres CMA71.

#### *3.2.3.2 Intervalos de referencia de los metabolitos*

Una de las principales limitaciones de la técnica de MD es que no hay definidos intervalos de referencia para los diferentes metabolitos. Algunos trabajos han intentado definirlos, monitorizando con catéteres de MD las zonas sanas del cerebro de pacientes con diferentes patologías del SNC: tumores benignos[83], epilepsia[84], HSA[85], etc. Recientemente, nuestro grupo ha publicado un trabajo en el que se han definido estos intervalos de referencia en pacientes con lesiones de la fosa posterior y supratentoriales, en pacientes despiertos y anestesiados[86]. En la **Tabla 2** se indican estos intervalos.

**Tabla 2.** Intervalos de referencia de los metabolitos

| Condición | **Glucosa** (mmol/L) | **Lactato** (mmol/L) | **Piruvato** (µmol/L) | **Glicerol** (µmol/L) | **Ratio L/P** |
|---|---|---|---|---|---|
| Anestesiados (0,3µL/min) | 1.25 (0.64-3.53) | 1,40 (1,10-3,84) | 73,8 (36,6-149,7) | 53,8 (24,2-205,1) | 23,3 (12,8-34,5) |
| Despiertos (0,3µL/min) | 1.55 (0.29-3.01) | 3,41 (1,56-5,62) | 137,1 (85,0-192,0) | 79,8 (29,3-346,4) | 24,9 (16,9-35,1) |

Los intervalos se expresan como la mediana (valor mínimo-valor máximo)

### *3.2.3.2 Aplicación clínica de la MD*

El empleo de la MD junto con otras técnicas de monitorización cerebral en pacientes neurocríticos, permite orientar el tratamiento de estos pacientes para predecir y evitar el avance de las lesiones secundarias, y por lo tanto mejorar sus resultados neurológicos. El uso de la MD ha demostrado ser de gran utilidad en pacientes con HSA[87], TCE[88] e infarto cerebral[89], entre otras patologías del SNC. A nivel clínico, los metabolitos más empleados en la monitorización de la MD son la glucosa, el lactato, el piruvato, el glutamato y el glicerol, debido a su amplia disponibilidad comercial. En la **Tabla 3** se resumen las variaciones registradas en estos metabolitos, consecuencia de distintos procesos patológicos.

**Tabla 3.** Marcadores de lesión secundaria. Adaptado de Borg *et al* [82].

| Cambios en los metabolitos | Procesos patológicos asociados |
|---|---|
| **Reducción de los niveles de glucosa** | ▪ Hipoxia/isquemia<br>▪ Disminución del aporte de glucosa<br>▪ Hiperglicólisis |
| **Incremento del ratio L/P** | ▪ Hipoxia/isquemia<br>▪ Disminución del aporte de glucosa<br>▪ Disfunción mitocondrial<br>▪ Reducción del estado redox celular |
| **Incremento del glicerol** | ▪ Hipoxia/isquemia<br>▪ Degradación de la membrana celular |
| **Incremento del glutamato** | ▪ Hipoxia/isquemia<br>▪ Excitotoxicidad |

## 7. Modelos animales

El uso de modelos animales es esencial para conseguir una mejor comprensión de los mecanismos implicados en cualquier patología, así como para poder desarrollar nuevas estrategias protectoras contra esta. Los modelos animales en roedores son los más utilizados en la actualidad, debido a la facilidad en su manejo, su reducido tamaño y su bajo coste[90]. Existen diferentes modelos de TCE en roedor, tanto de lesión focal (modelo de percusión lateral por fluido, impacto cortical controlado, etc) como de lesión difusa (modelos de aceleración-desaceleración)[91]. También es frecuente el uso de modelos de infarto cerebral en roedor (modelos de oclusión de la arteria cerebral media, modelos de infarto embólico, etc)[92]. Sin embargo, las diferencias neuroanatómicas entre humanos y roedores son algunas de las causas por las que en este tipo de patologías, tratamientos que han demostrado ser eficaces en animales, han fracasado al ser trasladados a humanos[93].

La introducción de modelos animales girencefálicos y con un porcentaje de sustancia gris-sustancia blanca similar al humano, y por lo tanto más parecidos anatómica y funcionalmente a este, es un paso necesario para diseñar mejores estrategias de tratamiento de estas patologías. En la actualidad, ya existen modelos animales de TCE e infarto cerebral en animales con estas características, como los cerdos, las ovejas e incluso primates no humanos[94]. Sus características fenotípicas y su disponibilidad, hacen del cerdo común uno de los modelos más adecuados para el estudio de este tipo de patologías. Las dificultades y consideraciones éticas a la hora de diseñar un modelo de TCE en estos animales, hacen que el diseño de un modelo de isquemia regional sea menos complejo. El estudio

de las alteraciones moleculares de la isquemia y la posterior extrapolación de estas a las contusiones cerebrales postraumáticas, parece una aproximación más factible. Las similitudes entre estas dos patologías del SNC[95], y el papel que ha demostrado la subunidad reguladora SUR1, de la que hemos hablado previamente, en estudios previos de ambas patologías[67], hacen posible que estrategias protectoras contra la isquemia, también puedan ser aplicadas a pacientes con lesiones focales traumáticas.

# HIPÓTESIS Y OBJETIVOS

# HIPÓTESIS Y OBJETIVOS

En esta sección se resumen las principales hipótesis de este proyecto de tesis, así como los objetivos llevados a cabo para validar o refutar dichas hipótesis.

## 1. Hipótesis

### *CAPÍTULO 1*

- El desarrollo de un modelo porcino de isquemia focal puede proporcionar una mejor comprensión de los mecanismos implicados tanto en la isquemia como en las lesiones cerebrales traumáticas. La aplicación de este modelo, permite la medida de parámetros –como la oxigenación y el metabolismo cerebral- en diferentes zonas de la lesión, que no sería posible en modelos animales de menor tamaño, como los roedores.
- La obtención de muestras cerebrales, procedentes de las diferentes zonas de la lesión isquémica, nos permite estudiar la expresión de canales que han demostrado su implicación en el desarrollo de la lesión, como SUR1-TRPM4. Su expresión mimetiza los resultados obtenidos en el humano.

### *CAPÍTULO 2*

- El tejido cerebral pericontusional de pacientes que han sufrido un TCE, presenta una sobreexpresión de Kir6.2, subunidad formadora de poro de los canales $K_{ATP}$.

- La subunidad Kir6.2 se encuentra sobre-expresada en células endoteliales y gliales de tejido cerebral pericontusional humano, actuando como un biomarcador de lesión cerebral traumática.

## 2. Objetivos

### *CAPÍTULO 1*

- Desarrollar un modelo animal porcino de isquemia cerebral focal, estable y reproducible.
- Medir la oxigenación y el metabolismo cerebral del animal mediante la monitorización de la $PtiO_2$ y de diferentes metabolitos (glucosa, lactato, piruvato y glicerol) por MD.
- Obtener muestras de las diferentes zonas de la lesión isquémica (core, penumbra y tejido sano contralateral a la lesión), para estudiar la expresión del canal SUR1-TRPM4.

### *CAPÍTULO 2*

- Comparar la expresión de Kir6.2 en muestras cerebrales de tejido pericontusional humano con muestras de tejido sano control.
- Estudiar la expresión de Kir6.2 en diferentes tipos celulares (neuronas, células endoteliales y células gliales).
- Determinar si el grado de expresión de Kir6.2 está relacionado con el tiempo transcurrido entre el TCE y el momento de recogida de las muestras de tejido.

# CAPÍTULO 1

**Malignant infarction of the middle cerebral artery in a porcine model. A pilot study.**

PLoS One. 2017 Feb 24; 12(2):e0172637.

DOI: 10.1371/journal.pone.0172637

PLoS One. 2017 Feb 24; 12(2):e0172637.
doi: 10.1371/journal.pone.0172637

# Malignant infarction of the middle cerebral artery in a porcine model. A pilot study.

**Fuat Arikan[1,2☯*], Tamara Martínez-Valverde[2], Ángela Sánchez-Guerrero[2], Mireia Campos[3], Marielle Esteves[3], Dario Gandara[1], Ramon Torne[1,2], Lidia Castro[2], Antoni Dalmau[4], Joan Tibau[4], Juan Sahuquillo[1,2☯]**

**1** Department of Neurosurgery, Vall d'Hebron University Hospital, Universitat Autònoma de Barcelona, Barcelona, Spain, **2** Neurotraumatology and Neurosurgery Research Unit (UNINN), Vall d'Hebron Research Institute (VHIR), Universitat Autònoma de Barcelona, Barcelona, Spain, **3** Experimental Surgery Unit, Vall d'Hebron Research Institute (VHIR), Universitat Autònoma de Barcelona, Barcelona, Spain, **4** IRTA, Animal Breeding and Genetics Program, Monells, Girona, Spain.

☯ These authors contributed equally to this work.
* arikan@neurotrauma.net

## Abstract

### Background and purpose

Interspecies variability and poor clinical translation from rodent studies indicate that large gyrencephalic animal stroke models are urgently needed. We present a proof-of-principle study describing an alternative animal model of malignant infarction of the middle cerebral artery (MCA) in the common pig and illustrate some of its potential applications. We report on metabolic patterns, ionic profile, brain partial pressure of oxygen ($PtiO_2$), expression of sulfonylurea receptor 1 (SUR1), and the transient receptor potential melastatin 4 (TRPM4).

### Methods

A 5-hour ischemic infarct of the MCA territory was performed in 5 2.5-to-3-month old female hybrid pigs (Large White x Landrace) using a frontotemporal approach. The core and penumbra areas were intraoperatively monitored to determine the metabolic and ionic profiles. To determine the

infarct volume, 2,3,5-triphenyltetrazolium chloride staining and immunohistochemistry analysis was performed to determine SUR1 and TRPM4 expression.

**Results**

$PtiO_2$ monitoring showed an abrupt reduction in values close to 0 mmHg after MCA occlusion in the core area. Hourly cerebral microdialysis showed that the infarcted tissue was characterized by reduced concentrations of glucose (0.03 mM) and pyruvate (0.003 mM) and increases in lactate levels (8.87mM), lactate-pyruvate ratio (4202), glycerol levels (588 μM), and potassium concentration (27.9 mmol/L). Immunohistochemical analysis showed increased expression of SUR1-TRPM4 channels.

**Conclusions**

The aim of the present proof-of-principle study was to document the feasibility of a large animal model of malignant MCA infarction by performing transcranial occlusion of the MCA in the common pig, as an alternative to lisencephalic animals. This model may be useful for detailed studies of cerebral ischemia mechanisms and the development of neuroprotective strategies.

## Introduction

Stroke is the second most common cause of death and the third most common cause of disability-adjusted life years worldwide[1]. One-third of strokes occur in children and young and middle-aged adults[1], ischemic stroke (IS) being the most common subtype[2]. The rationale for aggressive therapy in IS is based on the fact that after acute ischemia, a variable amount of hypoperfused brain is at risk of permanent infarction (ischemic penumbra), but it may be potentially salvaged by early restoration of cerebral blood flow (CBF). The aim of translational research in IS is to improve neurological outcomes: it is the focus for basic science and clinical researchers, funding agencies, and the industry as a whole[3]. Despite remarkable advances in the understanding of the pathophysiology of ischemic lesions, however, ongoing efforts to identify novel molecular targets have not yet yielded new pharmacological therapies[4].

The term `malignant' middle-cerebral artery (MCA) infarction was coined by Hacke et al. in 1996 to describe a form of IS that involved at least 50% of the MCA territory, followed an uniform clinical course, and resulted in transtentorial herniation and death in most patients despite optimal medical treatment[5]. To elucidate the pathophysiology of IS and develop neuroprotective therapies, animal models have been widely used. Despite limitations and ethical concerns, animal models are invaluable for investigating the pathogenesis of cerebral ischemia and evaluating the consequences of pharmacological intervention[6]. Since the early 1980s, the traditional animal model of IS has been occlusion of the MCA in the rat[7]. However, therapeutic strategies that appear efficacious in these experimental models have not been proven so when translated to patients. One explanation for this failure may be interspecies variability in cerebrovascular physiology, which may contribute to the divergent outcomes observed in rodent and human studies. The lysencephalic rodent brain is barely one-thousandth of the weight of the human brain and the proportions of grey and white matter also differ when comparing humans and rodents[8]. Humans, like other gyrencephalic species, have a considerably higher percentage of white matter (>60%) compared to lissencephalic species, such as rats or mice, which have only ~10%[8-10]. As a consequence of the recurrent failed translation to humans, the Stroke Therapy Academic Industry Roundtable (STAIR) recommended the use of large animal stroke models-e.g. pigs or nonhuman primates-before testing drugs or endovascular recanalization strategies in clinical trials[11].

Pigs have been described as excellent experimental animals for medical research because of the similarities between human and porcine biology. The pig brain is gyrencephalic and has a white-gray matter ratio similar to that of the human brain[10-12]. In a pivotal paper, Imai et al. presented a new, well-designed model of focal IS in the miniature pig that produced remarkable consistency in terms of infarct size, which was achieved by electrocoagulation of the 2 MCAs[13]. The aim of the present work is to present a proof-of-principle study describing a feasible large animal model of large hemispheric stroke in the common pig (*Sus scrofa domestica*) and to elucidate some of its potential advantages as an alternative to the few

gyrencephalic models already available. Furthermore, this model will allow the use of all the modern neuromonitoring clinical tools that cannot be used easily in rodents.

In the present study we will show and discuss the results obtained using a porcine model. We characterized the volume of the infarction, the metabolic patterns of the ischemic tissue, the partial pressure of brain tissue oxygen ($PtiO_2$), and the ionic profile of the extracellular space. We also explored at a molecular level the expression of sulfonylurea receptor 1 (SUR1) and transient receptor potential melastatin 4 (TRPM4), previously described in the brain of patients with multiple sclerosis [14], in subarachnoid hemorrhage[15], in cerebral infarcts[16], and in posttraumatic brain contusions[17]. TRPM4 is a calcium-activated nonselective cation channel that is expressed *de novo* after brain ischemia and injury. It is involved in the modulation of the brain immune response and the development of ischemic brain edema-and oncotic cell death-through the regulation of Ca2+ homeostasis, cationic fluxes, and membrane depolarization [14-18]. To our knowledge, this is the first study to explore these receptors in large IS-induced gyrenchephalic mammals.

## Material and methods

### Experimental procedures and ethics statement

All procedures described in this study were approved by the animal experimentation ethics committee of the Vall d'Hebron Research Institute (protocol number 69/14) and were conducted in compliance with Spanish legislation and the directives of the European Union for animal research (2010/63/EU). All experiments were performed in 2.5-to-3-month-old female hybrid pigs (Large White x Landrace) weighing 30 to 40 Kg. Animals were sourced from A.M. Animalia Bianya S.L. animal center (Girona, Spain) and recorded in the registry of breeding centers, suppliers, and users of experimental animals with reference number G9900009. The transport company was authorized and certified to perform this service. Animals were previously acclimated to our facilities and housed in

conventional pens for at least 1 week with free access to water and twice-daily feedings using a conventional diet. Animals underwent fasting for 12 hours before surgery but had free access to water with diluted sucrose. Only specimens with a satisfactory examination were included in the study. The pigs were kept under general anesthesia for the entire duration of the experiment and they did not experience any pain or distress.

## Housing conditions and diet

Environmental parameters were recorded and regulated daily. Temperature was maintained within a range of 19 to 21°C and humidity was 45 to 65%. Driven air was 100% external, prefiltered, filtered with 95% efficiency, and processed with a renewal rate of 15 to 20 cycles per hour. The photoperiod was programmed for 12 hours of light and 12 hours of darkness, daylight hours being from 8:00 a.m. to 8:00 p.m. The animals had a minimum floor space of 0.5 $m^2$. They were usually housed as a group of 4 to 6 animals with an area of 8 to 12 $m^2$. Beds of wood shavings were provided, and for environmental and social enrichment we installed chains, balls, cylinders, hot plates of soil, an infrared plate in the ceiling, and alfalfa and sugar lumps as positive reinforcement.

The animals were monitored daily using the following criteria: appearance and body condition, observed behavior and habits, food and drink intake, and clinical follow-up after the procedure. Any anomalies or incidences were recorded. Observation of the animals was carried out by caregivers, technicians, research personnel, animal welfare advisers, and the veterinarians attending the animals. During the 24-hour period, a remote surveillance system involving a webcam was used to allow animals to be recorded and to study and assess their state, with the additional advantage of studying their behavior without the presence of people. In accordance with Spanish regulations (the Department of Agriculture, Food and Rural Affairs), all pigs went through a program of prevention and health surveillance and were vaccinated against Aujeszky disease.

## Anesthesia and analgesia

While still in the pen, animals were sedated with an intramuscular injection of 4 mg/kg of Tiletamine+ Zolazepam (Zoletil 100®, Virbac SA, Esplugues del Llobregat, Barcelona, Spain) and 2 mg/kg of Xylacine (Xilagesic 20%®, Laboratorios Calier SA, Les Franqueses del Valles, Barcelona, Spain). After loss of reflexes, the pigs were transported on a trolley. A venous catheter was placed in the auricular vein and an arterial catheter was placed in the auricular artery. Preoxygenation with 100% oxygen was applied using a facemask while the animals were aseptically washed. In the operating room, intravenous (IV) anesthesia was induced with Propofol (Propofol®, B Braun Medical SA, Melsungen AG, Germany) at 4 mg/kg. Endotracheal intubation was immediately performed and anesthesia maintained with 60% oxygen and 2% isoflurane (Isoflo, Abbott laboratories Ltd, Saint-Laurent, Quebec, Canada) for the duration of the experiment. Ringer lactate (Ringer lactate, B Braun Medical SA) was continuously infused at 10 ml/kg/h and an IV constant-rate infusion of 6 µg/kg/h of Fentanyl (Fentanest®, KernPharma SL, Terrasa, Barcelona, Spain) was also administered for analgesia. In order to prevent an increase in intracranial pressure (ICP), a single bolus of 10% mannitol (Fresenius Kabi Espana SA, Barcelona, Spain) was infused at 0.5 g/kg immediately before craniotomy.

## Physiological monitoring

Venous and arterial blood pressures were continuously monitored using arterial catheters placed in the cava vein and the femoral artery, respectively. Both catheterizations were performed through an ultrasound-guided technique. Anesthesia and ventilation parameters were controlled with an Aespire-79001 device (GE Healthcare, General Electric Company, Fairfield, CT, USA), while heart rate, oxygen saturation, end-tidal $CO_2$, and respiratory rate were monitored with an S/5TM Compact anesthesia monitor Datex-Ohmeda1 (Datex-Ohmeda, Inc, Madison, WI, USA). A urinary catheter was also inserted. Core temperature was monitored with a rectal thermometer and controlled with a heating pad in order to maintain a stable core temperature of 38.5°C.

## Surgical approach and occlusion of the middle cerebral artery

A frontotemporal approach was performed in the lateral position according to the surgical description by Imai et al.[13]. A curved skin incision was performed starting at the zygoma and extending to just above the right orbit. The frontotemporal bone and the orbital rim were exposed. Craniotomy was performed with a single burr hole made on the anterior aspect of the superior temporal line and then expanded using a Kerrison rongeur. The bone in the lateral part of the roof of the orbit was aggressively removed to facilitate access to the basal cisterns. The dura mater was opened with a semicircular flap. Two different brain regions were monitored intraoperatively by placing a polarographic Clark-type electrode (CC1.2 sensor, Integra Neurocare, Plainsboro, NJ, USA) and a CMA microdialysis probe (CMA-71, 8010320, MDialysis AB, Solna, Sweden). The first area was labeled as the core area (CORE), with probes placed in the rostral sylvian gyrus of the frontal lobe corresponding to the vascular territory of the MCA in the common pig[13, 19]. These catheters recorded brain oxygenation and metabolism of the infarction area induced by the occlusion of the MCA. The second area, labeled the penumbra area (PENUMBRA), was monitored with 1 microdialysis probe placed in the ectosagittal rostral gyrus of the frontal lobe corresponding to a border area of the vascular territory between the MCA and the anterior cerebral artery (ACA)[13, 19]. Once the dura was opened, the operating microscope was positioned and a brain retractor was gently used to open the arachnoid and expose the basal cisterns, the optic nerve, the internal carotid artery, and the 2 MCAs. Ischemia was induced by clipping both MCAs (**Fig 1**), after which a control angiography was performed. Using a right femoral approach and a 5-French intravascular sheath, the carotid artery was catheterized with a 5-French intra-arterial catheter (Tempo 5, Cordis Corporation, Miami, FL, USA) to anatomically confirm the correct clipping of the 2 MCA branches. Euthanasia was scheduled at least 5 hours after the cerebral infarction was established: pigs received an IV dose of 2 g of thiobarbital (Thiopental, B Braun Medical SA).

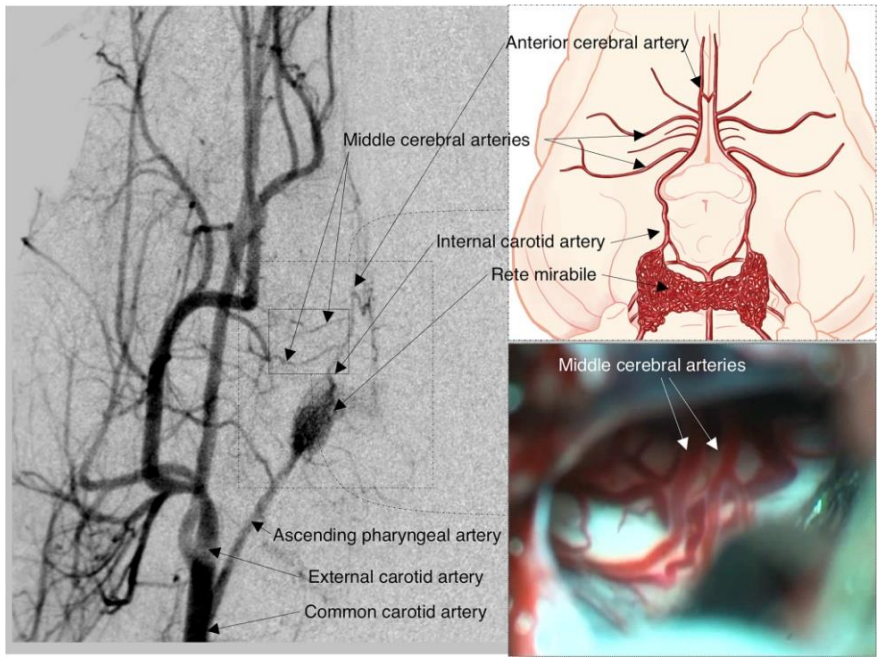


**FIG. 1. Basal vascular supply (1), angiographic study (2), and surgical view of the basal circulatory anastomosis (3) in the common pig.** The most relevant arteries in the pig are shown in the angiographic study. Note that the animal presents a network of small bilaterally interconnected vessels called rete mirabile, the site from which the internal carotid artery originates intracranially. Rete mirabile are perfused on both sides by the ascending pharyngeal artery, which originates from the common carotid artery. In contrast to humans, it should be noted that in each hemisphere 2 middle cerebral arteries (MCAs) emerge from the internal carotid arteries, 1 coursing laterally and the other rostrally (the latter provides vascularization to the olfactory tract).

## Brain tissue oxygen monitoring and microdialysis

Polarographic Clark-type electrodes (CC1.P1 sensor, Integra Neurocare) were connected to a tissue oxygen pressure monitor (Licox1 CMP system, Integra Neurocare), and the data obtained throughout the entire $PtiO_2$ monitoring period were stored in a laptop and exported to a flat file for statistical analysis. The main objective of using these probes was to obtain real-time brain oxygenation levels and confirm that the surgical procedure was successful in establishing a reliable ischemic model with a severe drop in $PtiO_2$. Cerebral MD probes were perfused with a sterile isotonic central

nervous system fluid containing 147 mmol/L of NaCl, 1.2 mmol/L of $CaCl_2$, 2.7 mmol/L of KCl, and 0.85 mmol/L of $MgCl_2$ (P000151, MDialysis AB, Stockholm, Sweden) at a fixed flow rate of 0.3 µL/min using a microinfusion pump (CMA-402, MDialysis AB). During the non-ischemic monitoring period (basal), microvials were changed every 30 minutes, while during ischemia microdialysate samples were collected every 60 minutes until death. Lactate ([Lac]brain), pyruvate ([Pyr]brain), glucose ([Glu]brain), and glycerol ([Gly]brain) were monitored using the point-of-care IscusFlex analyzer (M Dialysis AB). After hourly measurements were completed, microvials were placed on a rack designed to seal them and prevent evaporation (M Dialysis AB). All racks were stored at -20°C until ion analysis was carried out.

## Histological examination and infarct volume assessment

Immediately after death, brains were carefully extracted and placed on ice for 15 minutes. Microdialysis and $PtiO_2$ probes were not removed in order to identify the exact insertion site. Five-mm coronal slices were obtained and stained with 2,3,5-triphenyltetrazolium chloride (TTC; 93140; Sigma-Aldrich, Inc., St. Louis, MO, USA) to determine the infarct volume. Each brain slice was placed in a 60-mm dish, covered with 1% TTC solution (dissolved in 0.9% saline), and incubated at 37°C under dark conditions for 30 minutes. Using TTC staining, viable gray matter was stained red or pink and infarcted tissue remained a pale cream or white color (**Fig 2**). Next, both sides of each section were rinsed twice in 0.9% saline solution and fixed with 4% formol for 7 days. The placement of the catheters was identified post-mortem and classified using 3 possible categories: infarct core, ischemic penumbra, and healthy brain. All brain slices were photographed (Nikon D750, Nikkon 50mm Lens, Nikon and Essilor International Joint Research Center Co., Ltd., Kanagawa, Japan). For infarct volume assessment, TTC images from both sides of the brain slices were digitalized by using a flatbed scanner (HP Scanjet G4010, Hewlett Packard Enterprise, Sant Cugat del Valles, Barcelona, Spain). The final infarct volume of all animals was quantified by 1 of the investigators (TMV) using ImageJ software (Wayne Rasband, National Institutes of

Health, USA). We calculated the volume of the infarct by adding the infarct volumes of each cut, which were obtained by multiplying the mean of the infarct area (the area that remains pale cream or white after TTC staining) of the anterior and posterior surface of each sample by the thickness of each slice. The total volume of the supratentorial brain was also obtained using the same software to sum up the volume of each slice (also obtained by multiplying the thickness of each slice by the mean of the anterior and posterior areas). The infarct volume was expressed in $cm^3$ and as a percentage of the total volume of the brain in each animal.

### Immunohistochemistry

For immunohistochemistry analysis, samples from the different areas (core, penumbra, and healthy contralateral brain) were obtained. All samples were dehydrated with different alcohol solutions (70°, 90°, and 100°). Brain tissue samples were cryoprotected using 30% sucrose and embedded in a Tissue-Tek optimal cutting temperature compound (4583; Sakura Finetek Europe B.V, Alphen aan den Rijn, The Netherlands). From these blocks, 10-µm sections were obtained using a cryostat (Leica CM3050 S; Leica Biosystems, Heidelberg, Germany), mounted on glass slides, and stored at -20°C until analysis was carried out. For immunohistochemistry analysis, sections were incubated in a blocking solution containing 2% donkey serum (D9663; Sigma-Aldrich) and 0.2% Triton-X (T8787; Sigma-Aldrich) in 0.1M phosphate-buffered saline for 1 h. Next, cryosections were incubated for 1 hour at room temperature and then for 48 hours at 4°C with the primary antibodies goat anti-SUR1 1:100 (Santa Cruz Biotechnology, Santa Cruz, CA, USA) and chicken anti-TRPM4 1:500 (custom anti-TRPM4 antibodies described by Woo et al.[2]). Fluorescent-labeled, species-appropriate secondary antibodies (Invitrogen™, Eugene, OR, USA) were used for visualization. Omission of primary antibodies served as a negative control. Sections were cover-slipped with polar mounting medium containing antifade reagent and the nuclear dye 4,6-diamino-2-phenylindole (P36935; Invitrogen). Fluorescent signals were visualized using an epifluorescence microscope (BX61 Olympus; Olympus Corporation, Tokyo, Japan).

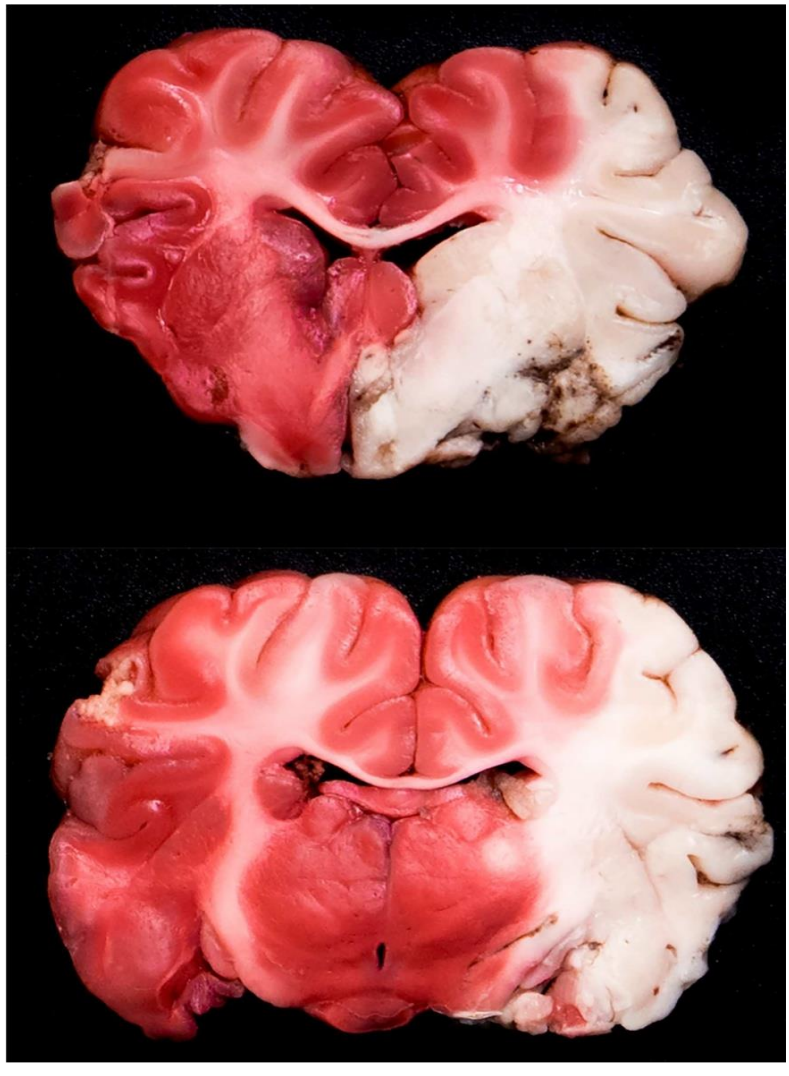

**FIG. 2. Two representative 5-mm brain coronal slices from animal #3 stained with 1% 2,3,5-Triphenyltetrazolium chloride (TTC) solution and showing the ischemic core at 7.5 h after left MCA occlusion.** Note how with TTC staining the entire territory of the left MCA (i.e. the infarcted territory) remains a pale cream or white color, while the non-infarcted viable brain stains red or pink. In this particular case, the entire MCA territory was affected, including the 3 MCA subterritories (deep, superficial anterior, and posterior). The deep territory of the MCA includes the caudate nucleus, the internal and the external capsules, the preoptic area, and the hypothalamus.

### Quantitative immunohistochemical analysis in neurons and vessels

To calculate SUR1/TRPM4-positive neurons and endothelial cells, between 4 and 8 randomly captured 440×330-$\mu m^2$ images from the cortex (NEURONS) and the white and grey matter (VESSELS) were taken with an epifluorescence BX61 Olympus microscope. The primary antibodies used were mouse anti-NeuN 1:100 (MAB377, Millipore Corporation, Billerica, MA, USA) for neurons and CD31: mouse anti-CD31 1:100 (M082329; Dako, Carpinteria, CA, USA) for vessels. Next, all images were quantified using the plugin Cell Counter (Kurt De Vos; http://rsb.info.nih.gov/ij/plugins/cell-counter.html) from the Image J 1.47v program (Wayne Rasband, National Institutes of Health, Bethesda, MD). Using the total number of neurons and vessels (NeuN and CD31-positive cells, respectively), the percentage of SUR1/TRPM4-positive cells was calculated.

### Semi-quantitative immunohistochemical analysis in astrocytes

To evaluate SUR1 and TRPM4 expression in the astrocytes, we used an anti-GFAP 1:3000 mouse antibody (C9205, Sigma-Aldrich). Next, the whole section was quantified by a single observer using a semi-quantitative scale to count the following: 1) GFAP-positive cells (0: absent, 1: scant, 2: moderate, and 3: numerous) and 2) SUR1-positive cells and TRPM4-positive cells of each type (0: none; 1: in a few cells; 2: in many cells, and 3: in almost all or all cells).

### Ionic profile of the extracellular space

After hourly microdialysis measurements were completed, the microvials were placed in a rack designed to seal them and prevent evaporation (MDialysis AB). All racks were stored at -20°C until analysis could be performed. Prior to analysis, the microvials were defrosted on ice and the ionic profile was determined using an ICP-MS analyzer (Agilent 7500ce, Agilent Technologies, Santa Clara, CA, USA) with collision cell technology using He as inert gas at 5 mL/ min. All concentrations obtained were corrected using a previously-defined linear model described previously[20].

### Statistical analysis

Data were analyzed and summarized using the SPSS program for Mac (Version 20, SPSS, Inc., New York, USA). Because most variables followed a non-normal distribution, data were summarized using the median, minimum, and maximum. Immunohistochemical findings of SUR1 and TRPM4 were compared using nonparametric tests and statistical significance was defined as $p$_0.05. Graphics were created using R v3.2.0 (R Foundation for Statistical Computing, Vienna, Austria; http://www.R-project.org) and the integrated development environment R Studio v0.99.903 (RStudio, Inc., Boston, MA, USA; http://www.rstudio.com).

## Results

### Ischemic period and infarct volume

A total of 5 animals were included in the study. Two of the 5 animals (#1 and #4) died early after ischemic induction and did not complete the study protocol. Both animals presented severe hypotension 30 min after MCA occlusion that could not be reverted with fluid therapy and vasoactive drugs, resulting in cardiac arrest before the experiment could be completed. Despite active resuscitation, animal #1 died 4.5 hours after MCA occlusion and in animal #4 death occurred 4 hours after MCA clipping. The median ischemic time achieved in our study was 6.5 hours (min: 4, max: 7.5 h). The median infarct volume was 12.3 $cm^3$ (min: 6.6, max 15.8 cm3), representing on average 18.4% of the total brain volume (min: 9.5%, max: 25.1%). **Table 1** summarizes data on the ischemic period and the infarct volume for all animals. Animals with a larger infarcted area (14.2 $cm^3$ in animal #3 and 15.8 $cm^3$ in animal #5) had a longer clipping time (7.5 h and 7 h respectively). Animal #4, which had a shorter ischemic period (4 h), had the lowest volume of infarcted tissue (6.6 cm3).

### $PtiO_2$ monitoring

$PtiO_2$ values are summarized in **Table 2.** With the exception of animal #5, $PtiO_2$ monitoring was very reliable in confirming the establishment of the

infarction. $PtiO_2$ levels dropped immediately after clipping the arteries, reaching minimum values approximately 60 min after clip placement. In a sole animal (#5), no changes in $PtiO_2$ were observed after MCA occlusion, despite confirmation by cerebral angiography of the correct clipping of the 2 branches. In this animal, post-mortem study revealed that the $PtiO_2$ probe had been placed outside the area of infarction, while an angiographic control confirmed the occlusion of both MC arteries. $PtiO_2$ data for this animal was excluded from statistical analysis, but its metabolic data was used. Ischemia values are expressed as median (minimum-maximum). $PtiO_2$ data of animal #5 was excluded from statistical analysis after confirming in the post-mortem study that the $PtiO_2$ probe had been placed outside the area of infarction. For the sake of clarity, values under detection were considered to be 0, although the lower detection limits were 0.1 mmol/L for glucose and 0.01 mmol/L for pyruvate. When pyruvate was under this limit, an L/P index was not calculated (N/A).

Basal levels in the penumbra area were only available in the animal #5, and therefore minimum and maximum values in the penumbra area were not available in the basal determination.

**Table 1. Ischemic period and infarct volume in pig specimens**

| Animal | Ischemic period (h) | Infarct volume($cm^3$) | Infarct volume (%) |
|---|---|---|---|
| **1** | 4.5 | 12.3 | 18.4 |
| **2** | 6.5 | 9.1 | 13.8 |
| **3** | 7.5 | 14.2 | 23.6 |
| **4** | 4 | 6.6 | 9.5 |
| **5** | 7 | 15.8 | 25.1 |

TTC images from both sides of the brain slices were digitalized and the final infarct volume was quantified by adding the volume of each slice, which was obtained by multiplying the thickness by the mean area of the anterior and posterior areas of each slice.

**Table 2. Metabolite values and $PtiO_2$ measurements in the entire animal group during basal and ischemic periods in CORE and PENUMBRA**

| Condition | TIME | $PtiO_2$ (mmHg) | MD CORE (n= 5) | MD CORE (n= 3) | MD CORE (n= 3) | MD CORE (n= 3) | MD CORE (n= 3) | MD PENUMBRA (n= 3) | MD PENUMBRA (n= 3) | MD PENUMBRA (n= 3) | MD PENUMBRA (n= 3) | MD PENUMBRA (n= 3) |
|---|---|---|---|---|---|---|---|---|---|---|---|---|
| BASAL OR ISCHEMIA | (h) | CORE (n=4) | Glucose (mM) | Lactate (mM) | Pyruvate (mM) | LPR | Glycerol (μM) | Glucose (mM) | Lactate (mM) | Pyruvate (mM) | LPR | Glycerol (μM) |
| BASAL | 0 | 27.5 (24.4-39.2) | 1.59 (0.92-2.25) | 1.80 (1.2-2.5) | 0.101 (0.072-0.131) | 17.40 (16.1-18.8) | 44.20 (23.0-65.5) | 2.72 | 2.40 | 0.243 | 9.88 | 15.1 |
| ISCHEMIA | 1 | 0.45 (0-3.2) | 0.70 (0.14-2.08) | 8.18 (1.56-13.4) | 0.074 (0.016-0.142) | 64.90 (19.5-853) | 77.60 (37.5-217) | 1.22 (0.55-2.19) | 4.54 (4.40-7.32) | 0.25 (0.019-0.321) | 29.9 (13.72-244.5) | 148 (119-244) |
| ISCHEMIA | 2 | 2.8 (1.0-4.6) | 0.09 (0-1.88) | 8.25 (7.25-9.85) | 0.015 (0-0.050) | 3241 (27.2-N/A) | 319 (116-544) | 1.40 (1.13-1.84) | 4.06 (2.62-4.97) | 0.18 (0.096-0.379) | 27.20 (10.7-27.7) | 103 (98.5-507) |
| ISCHEMIA | 3 | 2.2 (1.0-3.1) | 0.18 (0-2.59) | 7.29 (6.85-9.43) | 0.011 (0-0.047) | 3225 (187-N/A) | 462 (187-734) | 1.21 (1.01-1.64) | 2.94 (2.58-3.40) | 0.26 (0.095-0.292) | 11.70 (9.89-31.2) | 111 (90.2-660) |
| ISCHEMIA | 4 | 0.0 (0-4.7) | 0.15 (0-2.46) | 6.68 (5.84-10.7) | 0.008 (0-0.034) | 6282 (315-N/A) | 545 (306-794) | 1.13 (0.29-1.15) | 3.06 (1.91-4.85) | 0.21 (0.062-0.251) | 22.90 (7.6-49.5) | 115 (75.8-882) |
| ISCHEMIA | 5 | 2.0 (0-3.4) | 0.03 (0-2.02) | 8.87 (5.16-11.2) | 0.003 (0-0.032) | 4202 (346-N/A) | 588 (311-790) | 1.13 (0.05-1.24) | 2.62 (1.98-8.13) | 0.25 (0.023-0.298) | 27.30 (7.87-116) | 141 (73.3-751) |

Ischemia values are expressed as median (minimum-maximum). $PtiO_2$ data of animal #5 was excluded from statistical analysis after confirming in the post-mortem study that the $PtiO_2$ probe had been placed outside the area of infarction. For the sake of clarity, values under detection were considered to be 0, although the lower detection limits were 0.1 mmol/L for glucose and 0.01mmol/L for pyruvate. When pyruvate was under this limit, an L/P index was not calculated (N/A). Basal levels in the penumbra area were only available in the animal #5, and therefore minimum and maximum values in the penumbra area were not available in the basal determination.

## Brain microdialysis monitoring

Values for the different metabolites measured at baseline and after ischemia in the core and penumbra are summarized in **Table 2.** A cerebral MD catheter was implanted in the ischemic core in all the animals and in the ischemic penumbra in the final 3 animals.

**Changes in the core.** A significant decrease in [Glu]brain in the core was observed in all animals soon after occlusion, with the exception of animal #4. Post-mortem analysis of the brain of this animal showed that the cerebral MD probe had been placed in an infarcted area, but there had been significant collateral circulation around the necrotic tissue that might explain the observed readings in [Glu]brain. In all animals, the drop in [Glu]brain was followed by a significant drop in [Pyr]brain to undetectable levels and a significant increase in [Lac]brain, with a consequent increase in the lactate/pyruvate ratio (LPR) (**Fig 3** and **Table 2**). A typical example of the metabolic changes observed in both the core and the penumbra in 1 animal (#5) is shown in **Fig 3.** A significant increase in [Gly]brain was observed in the core of all animals and reached a maximum value of 794 µmol/L in 1 animal.

**Changes in the penumbra.** Heterogeneous changes were found in all metabolites for the penumbra, showing a variable degree of metabolic stress (**Table 2**) or even progression to nonviable tissue at the end of the experiment in 2 animals (#3 and #4). The small number of animals in this pilot study precludes a statistical analysis of the metabolic profile of the penumbra, however it may be noted that a significant reduction in [Glu]brain (~50%) with respect to the baseline values was observed in most animals. In 2 animals (#3 and #4) the decrease was more marked at the end of the experiment, indicating recruitment of the penumbra into the core. [Lac]brain increased in the penumbra, but it was less marked than in the core (**Fig 3** and **Table 2**). The same trend was observed with LPR. [Gly]brain also increased in all animals but did not reach the levels observed in the core, with the exception of animal #5.

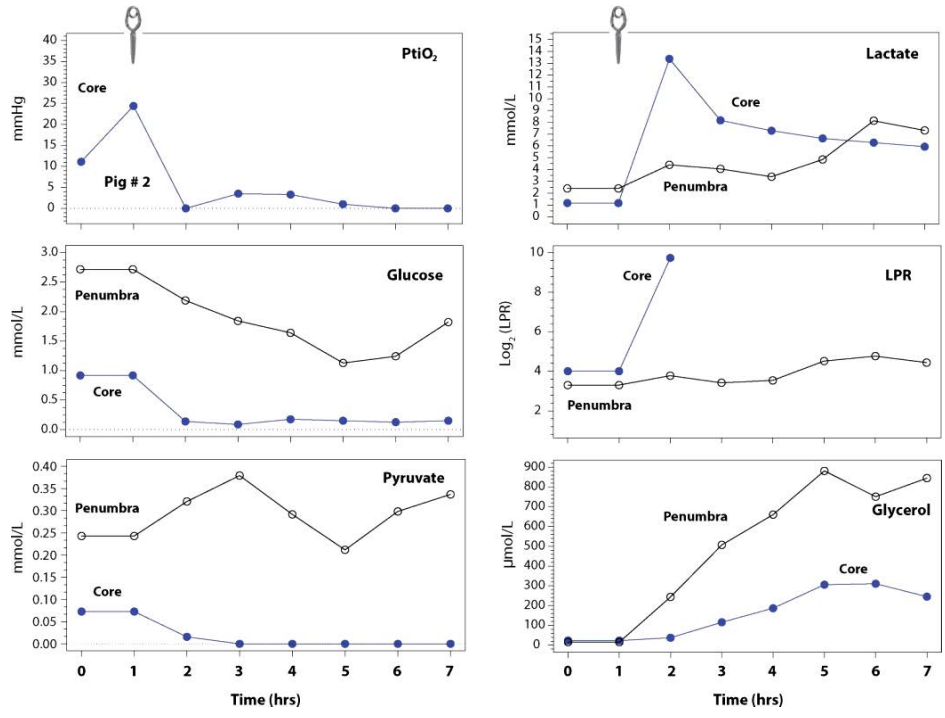


**FIG. 3. The representative pattern of microdialysis values in the ischemic core and in the penumbra of animal #5.** We used $PtiO_2$ data from animal #2 to represent the $PtiO_2$ drop after clipping both MCAs because the probe had been misplaced outside the core in animal #5 (image not shown) and because baseline data was missing in some of the remaining animals. The increase in $PtiO_2$ in the first 2 hours may be explained by the running time of $PtiO_2$ probes. The clip illustrated at the top of the diagram shows the time in which clipping of both MCAs was carried out. $PtiO_2$ data in animal #2 was consistent with the typical $PtiO_2$ profile observed in all but 1 animal (#5). In the ischemic core, a rapid decrease in [Glu]brain was observed after occlusion, followed by a significant drop in [Pyr]brain and a significant increase in [Lac]brain and in the lactate/pyruvate ratio (LPR). LPR values 2 hours after clipping could not be calculated because [Pyr]brain levels were undetectable and therefore LPR rose to infinite values. A significant increase in [Gly]brain was also observed in the core, reaching a plateau at 5 h post-ischemia. In the penumbra area, [Lac]brain and the LPR values also increased, but they were not as pronounced as in the core. [Pyr]brain levels were unstable in the penumbra and at 4 to 7 h after clipping followed the same pattern as [Glu]brain. Glycerol also increased in the penumbra, reaching levels well above those observed in the samples taken from the core.

## Ionic profile of the extracellular space

After MCA clipping, ionic data were obtained hourly for the entire period in both brain regions. Due to the minimum required dialysate for the ionic analysis, it was not possible to obtain the medians, minimums, and maximums of the 3 ions during the baseline period. During the ischemic period the ionic profile in the core was compiled from 24 valid determinations, and in the penumbra area the ionic profile was made from 19 valid determinations. The ionic profile was significantly different for each monitored brain area. The ischemic core was characterized by an increase in median $K^+$ to 27.9 mmol/L (min: 4.0, max: 49.4), while penumbra presented increased Na+ levels (median 164.0 mmol/L; min: 130.7, max: 208.0). **Table 3** summarizes the ionic data of the extracellular space.

**Table 3. Ionic data of the extracellular space in both monitored brain areas.**

| Monitored area | $[Na^+]$ mmol/L | $[K^+]$ mmol/L | $[Cl^-]$ mmol/L |
|---|---|---|---|
| **Ischemic core** | 154.1 (135.3–199.8) | 27.9 (4.0–49.4) | 157.0 (132.3–187.0) |
| **Ischemic penumbra** | 164.0 (130.7–208.0) | 7.5 (3.7–44.0) | 157.7 (147.2–208.0) |

Values are summarized as median (min-max). Due to the minimum required volume for ion analysis, the median, minimum, and maximum values of the 3 ions in the core were made from 24 valid determinations, and in the penumbra area they were made from 19 valid determinations.

## SUR1-TRMP4 expression

All sections were examined by a single observer (LC), who carried out a quantitative or semiquantitative analysis, depending on the cell type, for SUR1 and TRPM4 expression (**Fig 4**). In neurons, immunofluorescence showed that the expression of both the regulatory subunit (SUR1) and the pore forming subunit (TRPM4) were significantly increased in the neurons in the penumbra area and in the ischemic core when compared with the contralateral healthy hemisphere (Kruskal-Wallis, $p$ = 0.01 in both cases). A summary of the semi-quantitative findings for SUR1-positivity and TRMP4-positivity are shown in **Table 4**. A mild overexpression of SUR1 and

TRPM4 was detected in the GFAP-positive cells in the normal brain tissue samples. Both the penumbra and core samples presented strong SUR1 overexpression, with moderate expression of the TRPM4 channel (**Fig 4**). For endothelial cells (CD31+ cells), we did not find any significant difference in SUR1 expression when comparing the core, the penumbra, and the contralateral healthy tissue. However, we did find a significant difference in TRPM4 expression when comparing the 3 different regions in all cells (Kruskal-Wallis, $p$ = 0.02) (**Fig 4** and **Table 4**).

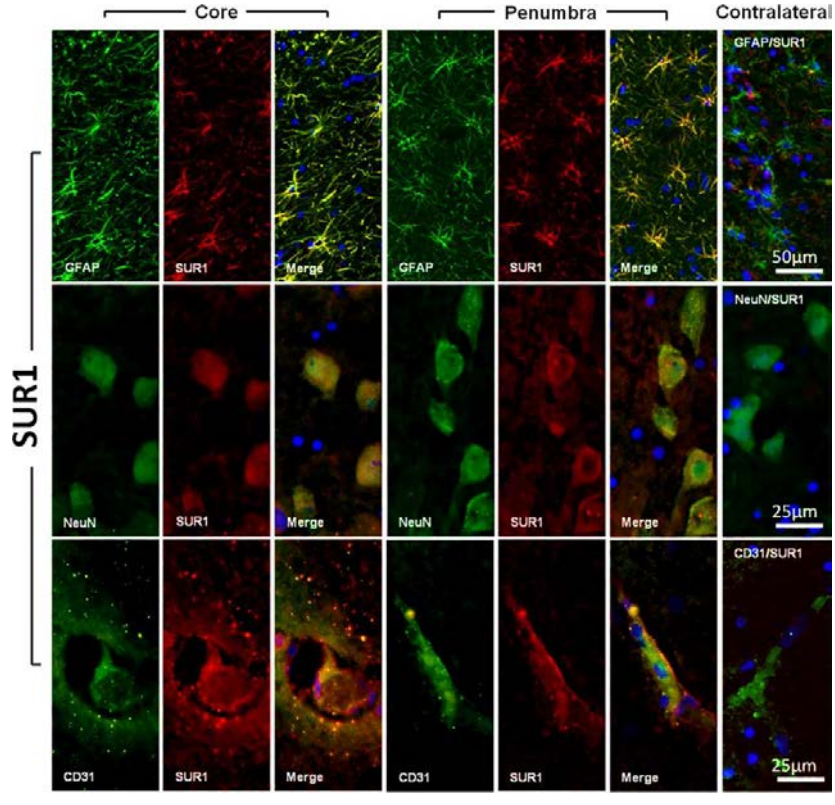


**FIG. 4. SUR1 expression in astrocytes, neurons, and capillary endothelial cells.** The figure shows fluorescent double labeling for GFAP (panel A), NeuN (panel B), CD31 (panel C) and SUR1 in the core and penumbra regions. The most lateral column on the right shows the merged images of the controls (i.e. contralateral healthy tissue). Original magnification = 20x (A) and 40x (B, C). Nuclei were counterstained with DAPI. All tissue sections were obtained from animal #5 7 hours after ischemia onset.

**Table 4. Expression of SUR1 and TRPM4 in neurons and vessels.**

| Cell type | SUR1 expression (%) Contralateral | SUR1 expression (%) Penumbra | SUR1 expression (%) Core | TPRM4 expression (%) Contralateral | TRPM4 expression (%) Penumbra | TRPM4 expression (%) Core |
|---|---|---|---|---|---|---|
| **Neurons** | 3.63 (0-22.3) | 52.0 (18.6-62.6) | 79.3 (66.9-86.8 | 4.7 (0-19.9) | 32.9 (22.4-37.5) | 58.5 (40.1-64.5) |
| **Vessels** | 40 (4.6-55.7) | 65.3 (51.2-83.9) | 72.8 (32.2-88.7) | 61.3 (43.7-79.6 | 77.8 (75.6-79) | 87.2 (83.3-91.1) |

Results are shown as median (min± max) of the percentage of SUR1/TRPM4-positive neurons and vessels versus the total number in these 2 cell types.

## Discussion

Most treatments used to manage patients with IS (e.g. intravenous rtPA, intra-arterial treatments, and mechanical thrombectomy) seek to obtain rapid recanalization of the occluded artery and reperfuse the ischemic brain to reduce the final amount of necrotic brain[3, 21]. However, no effective neuroprotective strategies have been found to reduce either brain edema or the amount of ischemic brain that is recruited to the core once the attempt to reopen the occluded artery has failed. Sudden deprivation of oxygen and glucose to the brain elicits a series of pathological cascades that contribute to the affected brain tissue's progression to necrosis. Excitotoxicity, metabolic derangements, tissue acidosis, accumulation of intracellular calcium cations, neuroinflammation, excessive production of free radicals, disrupted BBB and brain edema, apoptosis, and the overexpression of channels involved in regulating sodium and potassium all play critical roles in ischemic damage and in the deterioration of the penumbra [22]. Many drugs and agents that have been shown to reduce the infarct size in animal models -mostly in rodents- have failed dramatically in the clinical arena[4, 22]. This is

particularly relevant for patients with malignant IS for whom space-occupying brain edema is the most important cause of death and disability[23] and the only treatment option is to conduct decompressive craniotomy to reduce the dismal mortality they nonetheless present with maximal medical treatment[23]. Among the many reasons suggested for the clinical trial failures, a very important factor is the lack of an animal model to reproduce the complex cascades observed in humans after IS[22]. To date, most experimental animal models use animals with lissencephalic brains, such as the mouse or the rat. The proportions of grey and white matter in rodents differ from that of humans. Gyrencephalic species have a higher percentage of white matter than lissencephalic species[8, 9], an anatomical difference that may lead to different mechanisms of cellular injury and recovery[24]. Recent studies have shown that in patients with stroke, the degree of affected motor function is more closely related to white matter integrity than to the BOLD response of cortical motor areas[25]. In addition, aquaporin-4 (AQP-4) -a main player in ischemic brain edema- is exclusively expressed by astrocytes. Stokum et al. have shown in a rodent experimental model of ischemia that subcortical white matter is much more susceptible to post-ischemic tissue swelling than cortical grey matter, and that cortical astrocytes exhibit unchanged expression in AQP-4, while white matter astrocytes exhibit a significant increase in AQP-4 expression after induced ischemia[26]. Those authors confirmed their findings in humans and suggested that white matter may play an underestimated active role in the formation of cerebral edema following ischemia[26]. There is a wide consensus that developing new therapeutic strategies in animal models is crucial despite the ethical concerns that animal experimentation raises. As some authors emphasize, ethical issues and animal welfare constitute an important limitation that should be clearly weighed against their scientific potential, medical benefit, and the availability of appropriate alternative approaches[27, 28]. For animal experiments on cerebral ischemia, Kuroiba and Okeda described the criteria that should be considered when selecting an appropriate species to ensure the findings have clinical relevance[8]. The animal whose brains are closest to human brains are non-human primates. However, modelling brain disorders in primates is very expensive,

availability is limited, and relevant ethical considerations remain unresolved [28].

## The pig: A neglected animal model

In the rat, unilateral common carotid artery occlusion and intraluminal thread occlusion of the internal carotid artery are classic procedures for inducing focal brain ischemia without intracranial manipulation[8]. Transitioning IS modelling from rodents to large mammals with gyrencephalic brains that possess a white-gray matter ratio that is closer to the human brain is crucial for new preclinical models. Pigs are an alternative to primates as a non-rodent species because of their anatomical and physiological similarities to humans. The pig brain is only 7.5 times smaller than the human brain and is composed of >60% white matter[12, 22]. An added value of using pigs as experimental animals is that they are widely available due to commercial production and less constrained by ethical and economic considerations. Pigs have been widely used in toxicology and experimental surgery, but are only occasionally used in neuroscientific research, something that has progressively increased only in the past decade[12]. As Lind et al. report, most agricultural pigs are derived from the Eurasian wild boar (*Sus scrofa*) but there are a large number of breeds with significant anatomical differences[12]. In addition, pig-producing countries do not generally supply pure breeds, but rather crossbreeds of various recognized breeds (e.g. Landrace, Yorkshire, Hampshire, and Duroc)[29].

In modelling brain ischemia, researchers should be familiar with the important anatomic, histopathologic, and clinicopathologic features of the pig brain and neurovascular supply in order to reproduce a valid model of focal ischemia. Pigs, like other experimental large animals, have the disadvantage of having a prominent external carotid circulation from which a rete mirabilis is formed and from which the internal carotid artery originates (**Fig 1**)[13, 30]. This collateral circulation, described angiographically by Burbridge et al., has caused some authors to rule out swine for brain ischemic models. Rete mirabilis restricts the occlusion of the carotid artery and their branches by intravascular methods and the use of microcatheters[30]. However, this anatomical variant is also present in other mammals, such as cats, goats,

dogs, and sheep[31]. The second important difference between pigs and humans is that the posterior communicating artery in pigs is comparable in size to the ICA. As a result, the connection between the anterior and posterior circulation systems is very well developed when compared with humans. An additional important difference is that in each hemisphere 2 MCAs originate from the ICA, 1 coursing laterally and another rostrally over the olfactory tract[13].

## Considerations when modelling focal brain ischemia in the pig

The same limitations raised by our group concerning the use of models in rodents led a team at the Aarhus University of Denmark to propose for the first time animal models of infarction using common pigs with transorbital occlusion of the MCA[32]. That group made important contributions to the understanding of the cerebrometabolic changes that occur after irreversible occlusion in pigs. However, in our opinion, that animal model was not introduced in more centers due to the complexity of surgical access, which is less common in neurosurgery. Another factor could have been that infarct volumes obtained in this animal model showed a greater variability, probably due to the non-complete occlusion of the entire territory of the MCA; the surgical corridor only gives access to 1 of the 2 branches of the MCA present in the pig[32-36].

The main anatomical consideration in the model of permanent arterial occlusion we present is that MCA occlusion involves an open surgical frontotemporal approach and the clipping of both MCAs. After a learning curve, the total surgical procedure took approximately 60 minutes. We believe this model has many advantages over the classic rodent model. We found that our model gives a satisfactory representation of malignant IS with a dense, reproducible infarction that causes early death if untreated. Moreover, the percentage of infarcted volumes we obtained from animal modeling appears to be consistent and is comparable to the volumes obtained in the classical models of malignant infarction in rats[37-40]. In addition, this model allows the use of conventional angiography to confirm optimal arterial occlusion. Like the minipig model presented by Imai et al., our model is a feasible, large gyrencephalic model of focal IS that may be

more useful than alternative models of focal cerebral ischemia in medium gyrencephalic animals, such as dogs, cats, or even subhuman primates. The use of vascular clips instead of coagulation of both MCAs allows for the design of experimental models in which the clips can be removed at different times after ischemia, modelling temporary ischemia and allowing for the study of reperfusion phenomena. In addition, this model allows for the use of $PtiO_2$ and cerebral MD probes to study the metabolic disorders induced by ischemia, as well as the ionic disturbances of the ischemic brain and its potential reversibility through use of various therapeutic strategies. The main disadvantages of using large animals are handling difficulties within experimental facilities and the increased workload for the research group resulting from multi-hour experiments. When considering which swine species to use when establishing an animal model, domestic pigs have several advantages over minipigs, including lower cost and greater availability.

## Metabolic and ionic profile in ischemia

Continuous $PtiO_2$ monitoring is a reliable surrogate measure of rCBF and can detect ischemic and non-ischemic causes of brain hypoxia, such as low-extractivity hypoxia, shunt hypoxia, or dysperfusion hypoxia[41-43]. In all cases in which the probe was correctly inserted, $PtiO_2$ levels dropped immediately and were thus a reliable indicator of the complete occlusion of both MCAs. After a careful anatomical examination of the brain in the only animal in which $PtiO_2$ values did not change, the probe's tip was found to be located outside the ischemic lesion. To our knowledge, this is the first report of the ionic profile monitored hourly together with energy metabolism in a brain IS, with results that are consistent with the patterns found in the human brain[44]. Malignant strokes cause massive ionic fluxes, with consequent osmotic water movement across cells and cerebral edema formation. Changes in ionic concentrations induce water accumulation in the intracellular and extracellular space and cause the injured brain tissue to swell, resulting in neurological worsening[45]. These ionic disorders are directly related to the overexpression of different ion channels that can be constitutive or newly synthesized, such as the SUR1-regulated channel

TRPM4[16, 45]. TRPM4 belongs to a large family of proteins that share certain structural similarities. Most members of the TRP family are permeable to divalent cations. However, TRPM4 is impermeable to Ca2+ because it exclusively and non-selectively transports monovalent cations. In situations of ischemia there is an increase in the transcription of SUR1 that is accompanied by overexpression of TRPM4. TRPM4 channels are activated either by an increase in cytosolic Ca2+ or by a decrease in the ATP/ADP ratio in the cytosolic space. SUR1-TRPM4 is not constitutively present in cells of the central nervous system, but its transcription increases in neurons, the capillary endothelium, and astrocytes several hours after the onset of cerebral ischemia. In the absence of ATP this channel is activated, favoring edema and oncotic cell death due to the massive entry of ions[16, 18, 46]. The use of brain MD in large animal models offers a unique opportunity to observe the dynamic ionic changes in the brain over time and opens up a new path to explore the ionic profile during edema formation and its changes after different therapies. From a metabolic perspective, our model allowed us to reproduce the changes expected in permanent focal ischemia and detect the metabolic deterioration of the penumbra (**Fig 3**). Furthermore, we found that [Gly]brain increased with time and can be used in experimental models as a biomarker for the progression of the damaged brain. Glycerol is considered a biomarker of brain tissue damage and its concentrations rise during cellular energy failure and cell damage[47, 48]. However, it is presently unclear whether increased [Gly]brain is associated with the destruction of the cell membrane and cell death, or whether it is a marker of cell "suffering" with the possibility of reversal. To clarify this distinction, further studies using the same experimental model are needed.

## Limitations of the study

The main limitation of our study was the small sample size inherent to most animal-based experimental studies. Both cost and ethical issues (ensuring animal welfare) constitute a limitation and the number of animals must be reduced to the minimum required to obtain answers to predefined scientific questions. The aim of this article is to present a proof-of-principle

study, using a small sample of subjects as per Directive 2010/63/EU of the European Commission for the protection of animals used for scientific purposes. Due to its small sample size, our study did not try to look for statistically significant results, but rather described the feasibility of a large hemispheric stroke in the common pig and elucidated some of its potential advantages as an alternative to rodents. Therefore, we cannot rule out that increasing the sample size could introduce more variability in the final infarction size. A second limitation is that our study was not designed to reproduce a reperfused focal infarction, and therefore we cannot present data on the lesions found after reperfusion or report on the time needed to obtain a complete infarction versus a reversible focal lesion. Our main goal was to determine the feasibility of obtaining a reproducible malignant infarction, and transient ischemia was not an endpoint in our model. Another drawback is that our model was designed to study only the early phenomena occurring at the very first stages of complete arterial occlusion, and therefore we cannot present data on the survival of animals, the degree of brain swelling -which in humans with malignant stroke develops many hours after the ischemic insult- or the long-term neurological sequelae that have been extensively studied in rodents that survive an IS. Finally, we must also highlight as a possible limitation of our study the need for anesthetic agents with possible neuroprotective effects, including propofol, zolazepam, and mannitol. However, we emphasize the difficulty in limiting their use in big-animal models since they are needed to facilitate microsurgical access of the cisterns for the clipping of both MCA branches, thus minimizing injuries secondary to the cerebral retraction.

## Conclusions

We report on the development of a porcine model of malignant IS involving craniotomy and the clipping of both MCAs as a feasible model that allows for the study of both ischemia-induced metabolic disorders and disturbances in the ionic profile. We believe that this model provides an excellent opportunity to better understand the mechanisms of cerebral ischemia in a human-like gyrencephalic brain and the neglected importance of white matter

in post- ischemic brain edema, aiding in the development of novel therapeutics that can potentially be translated to patients. In addition, this model may help in elucidating the mechanisms that lead to the recruitment of the penumbra to the infarction core and the pathophysiology of ischemic brain edema. Furthermore, it will allow researchers to test new therapeutic strategies that, alone or in combination, may target some of the many molecular cascades (specifically, the SUR1-regulated TRPM4 channel) that may be useful in reducing edema-induced brain swelling and therefore improving the functional outcome of patients with malignant IS. Our animal model allows for the study of the temporal profile of TRPM4 overexpression in the ischemic brain, as well as the other ionic and water channels involved in focal brain ischemia. More importantly, it may open up a clear line of research on the effects of SUR1-antagonists as neuroprotective drugs in gyrencephalic animals, the brains of which are very similar to those of humans.

## Acknowledgments

We are grateful for the assistance of Jessica Shull in preparing the drawings in this study, as well as the collaboration of Albert Cored and Angel Lorente of the Animal Facility Unit, who carefully assisted with animal management. We also thank Dr. J.M. Simard (Department of Neurosurgery) for providing us with the TRPM4 antibody used in this study.

## Author Contributions

**Conceptualization:** FA JS.

**Data curation:** FA.

**Formal analysis:** FA ASG LC JS.

**Funding acquisition:** FA JS.

**Investigation:** FA TMV ASG MC ME DG RT LC.

**Methodology:** FA TMV ASG MC ME DG RT LC.

**Project administration:** FA JS.

**Resources:** TMV ASG MC ME.

**Supervision:** FA JS.

**Validation:** FA TMV ASG AD JT JS.

**Visualization:** FA TMV ASG LC JS.

**Writing original draft:** FA JS.

**Writing review & editing:** FA TMV ASG MC ME DG RT LC AD JT JS.

## References

**1.** Feigin VL, Forouzanfar MH, Krishnamurthi R, Mensah GA, Connor M, Bennett DA, et al. Global and regional burden of stroke during 1990-2010: findings from the Global Burden of Disease Study 2010. Lancet. 2014; 383(9913):245-54. PMID: 24449944.

**2.** Bennett DA, Krishnamurthi RV, Barker-Collo S, Forouzanfar MH, Naghavi M, Connor M, et al. The global burden of ischemic stroke: findings of the GBD 2010 study. Global heart. 2014; 9(1):107-12. doi: 10.1016/j.gheart.2014.01.001 PMID: 25432120

**3.** Prabhakaran S, Ruff I, Bernstein RA. Acute stroke intervention: a systematic review. Jama. 2015; 313 (14):1451-62. doi: 10.1001/jama.2015.3058 PMID: 25871671

**4.** Xu SY, Pan SY. The failure of animal models of neuroprotection in acute ischemic stroke to translate to clinical efficacy. Medical science monitor basic research. 2013; 19:37-45. doi: 10.12659/MSMBR. 883750 PMID: 23353570

**5.** Hacke W, Schwab S, Horn M, Spranger M, De Georgia M, von Kummer R. 'Malignant' middle cerebral artery territory infarction: clinical course and prognostic signs. Archives of neurology. 1996; 53(4):309-15. PMID: 8929152

**6.** Mhairi Macrae I. New models of focal cerebral ischaemia. British journal of clinical pharmacology. 1992; 34(4):302-8. PMID: 1457262

**7.** Tamura A, Graham DI, McCulloch J, Teasdale GM. Focal cerebral ischaemia in the rat: Description of technique and early neuropathological consequences following middle cerebral artery occlusion. Journal of cerebral blood flow and metabolism: official journal of the International Society of Cerebral Blood Flow and Metabolism. 1981; 1(1):53-60.

**8.** Kuroiwa T, Okeda R. Checkpoints and pitfalls in the experimental neuropathology of circulatory disturbance. Neuropathology: official journal of the Japanese Society of Neuropathology. 2003; 23(1):79-89.

**9.** Frahm HD, Stephan H, Stephan M. Comparison of brain structure volumes in Insectivora and Primates. I. Neocortex. Journal fur Hirnforschung. 1982; 23(4):375-89. PMID: 7161477

**10.** Ventura-Antunes L, Mota B, Herculano-Houzel S. Different scaling of white matter volume, cortical connectivity, and gyrification across rodent and primate brains. Frontiers in neuroanatomy. 2013; 7:3. doi: 10.3389/fnana.2013.00003 PMID: 23576961

**11.** Fisher M, Feuerstein G, Howells DW, Hurn PD, Kent TA, Savitz SI, et al. Update of the stroke therapy academic industry roundtable preclinical recommendations. Stroke. 2009; 40(6):2244-50. doi: 10.1161/STROKEAHA.108.541128 PMID: 19246690

**12.** Lind NM, Moustgaard A, Jelsing J, Vajta G, Cumming P, Hansen AK. The use of pigs in neuroscience: modeling brain disorders. Neuroscience and biobehavioral reviews. 2007; 31(5):728-51. doi: 10.1016/j.neubiorev.2007.02.003 PMID: 17445892

**13.** Imai H, Konno K, Nakamura M, Shimizu T, Kubota C, Seki K, et al. A new model of focal cerebral ischemia in the miniature pig. Journal of neurosurgery. 2006; 104(2 Suppl):123-32. doi: 10.3171/ped.2006.104.2.123 PMID: 16506500

**14.** Schattling B, Steinbach K, Thies E, Kruse M, Menigoz A, Ufer F, et al. TRPM4 cation channel mediates axonal and neuronal degeneration in experimental autoimmune encephalomyelitis and multiple sclerosis. Nature medicine. 2012; 18(12):1805-11. doi: 10.1038/nm.3015 PMID: 23160238

**15.** Tosun C, Kurland DB, Mehta R, Castellani RJ, deJong JL, Kwon MS, et al. Inhibition of the Sur1-Trpm4 channel reduces neuroinflammation and cognitive impairment in subarachnoid hemorrhage. Stroke. 2013; 44(12):3522-8. doi: 10.1161/STROKEAHA.113.002904 PMID: 24114458

**16.** Mehta RI, Tosun C, Ivanova S, Tsymbalyuk N, Famakin BM, Kwon MS, et al. Sur1-Trpm4 Cation Channel Expression in Human Cerebral Infarcts. Journal of neuropathology and experimental neurology. 2015; 74(8):835-49. doi: 10.1097/NEN.0000000000000223 PMID: 26172285

**17.** Martinez-Valverde T, Vidal-Jorge M, Martinez-Saez E, Castro L, Arikan F, Cordero E, et al. Sulfonylurea Receptor 1 in Humans with Post-Traumatic Brain Contusions. Journal of neurotrauma. 2015; 32 (19):1478-87. doi: 10.1089/neu.2014.3706 PMID: 26398596

**18.** Simard JM, Kent TA, Chen M, Tarasov KV, Gerzanich V. Brain oedema in focal ischaemia: molecular pathophysiology and theoretical implications. The Lancet Neurology. 2007; 6(3):258-68. doi: 10.1016/S1474-4422(07)70055-8 PMID: 17303532

**19.** Barone R, Bortolami R. Anatomie comparee des mammifères domestiques. Tome 6, Neurologie I, système nerveux central: Vigot; 2004. 652 p.

**20.** Martinez-Valverde T, Vidal-Jorge M, Montoya N, Sanchez-Guerrero A, Manrique S, Munar F, et al. Brain microdialysis as a tool to explore the ionic profile of the brain extracellular space in neurocritical patients: a methodological approach and feasibility study. Journal of neurotrauma. 2015; 32(1):7-16. doi: 10.1089/neu.2014.3473 PMID: 25019674

**21.** Goyal M, Menon BK, van Zwam WH, Dippel DW, Mitchell PJ, Demchuk AM, et al. Endovascular thrombectomy after large-vessel ischaemic stroke: a meta-analysis of individual patient data from five randomized trials. Lancet. 2016; 387(10029):1723-31. doi: 10.1016/S0140-6736(16)00163-X PMID: 26898852

**22.** Cheng YD, Al-Khoury L, Zivin JA. Neuroprotection for ischemic stroke: two decades of success and failure. NeuroRx: the journal of the American Society for Experimental NeuroTherapeutics. 2004; 1(1):36-45.

**23.** Simard JM, Sahuquillo J, Sheth KN, Kahle KT, Walcott BP. Managing malignant cerebral infarction. Current treatment options in neurology. 2011; 13(2):217-29. doi: 10.1007/s11940-010-0110-9 PMID: 21190097

**24.** Zhang K, Sejnowski TJ. A universal scaling law between gray matter and white matter of cerebral cortex. Proceedings of the National Academy of Sciences of the United States of America. 2000; 97 (10):5621±6. doi: 10.1073/pnas.090504197 PMID: 10792049

**25.** Qiu M, Darling WG, Morecraft RJ, Ni CC, Rajendra J, Butler AJ. White matter integrity is a stronger predictor 9of motor function than BOLD response in patients with stroke. Neurorehabilitation and neural repair. 2011; 25(3):275-84. doi: 10.1177/1545968310389183 PMID: 21357529

**26.** Stokum JA, Mehta RI, Ivanova S, Yu E, Gerzanich V, Simard JM. Heterogeneity of aquaporin-4 localization and expression after focal cerebral ischemia underlies differences in white versus grey matter swelling. Acta neuropathologica communications. 2015; 3:61. doi: 10.1186/s40478-015 0239-6 PMID: 26419740

**27.** Singer P. In defense of animals: the second wave. In: Malden M, editor.2006. p. 248.

**28.** Russell WMS BR, Hume CW. The principles of humane experimental technique: Univ Federation for Animal Welfare; 1992 238p.

**29.** B Bollen JA, Hansen AK, Alstrup AKO. The Laboratory Swine. 2 ed. Suckow MA, editor. Boca Raton, FL, USA: CRC Press; 2010.

**30.** Burbridge B, Matte G, Remedios A. Complex intracranial arterial anatomy in swine is unsuitable for cerebral infarction projects. Canadian Association of Radiologists journal = Journal l'Association canadienne des radiologistes. 2004; 55(5):326-9. PMID: 15646463

**31.** Gillilan LA. Extra- and intra-cranial blood supply to brains of dog and cat. The American journal of anatomy.
1976; 146(3):237-53. doi: 10.1002/aja.1001460303 PMID: 941852

**32.** Sakoh M, Ostergaard L, Rohl L, Smith DF, Simonsen CZ, Sorensen JC, et al. Relationship between residual cerebral blood flow and oxygen metabolism as predictive of ischemic tissue viability: sequential multitracer positron emission tomography scanning of middle cerebral artery occlusion during the critical first 6 hours after stroke in pigs. Journal of neurosurgery. 2000; 93(4):647-57. doi: 10.3171/jns.2000. 93.4.0647 PMID: 11014544

**33.** Sakoh M, Gjedde A. Neuroprotection in hypothermia linked to redistribution of oxygen in brain. American journal of physiology Heart and circulatory

physiology. 2003; 285(1):H17-25. doi: 10.1152/ ajpheart.01112.2002 PMID: 12793975

**34.** Sakoh M, Ostergaard L, Gjedde A, Rohl L, Vestergaard-Poulsen P, Smith DF, et al. Prediction of tissue survival after middle cerebral artery occlusion based on changes in the apparent diffusion of water. Journal of neurosurgery. 2001; 95(3):450-8. doi: 10.3171/jns.2001.95.3.0450 PMID: 11565867

**35.** Sakoh M, Rohl L, Gyldensted C, Gjedde A, Ostergaard L. Cerebral blood flow and blood volume measured by magnetic resonance imaging bolus tracking after acute stroke in pigs: comparison with [(15)O] H(2)O positron emission tomography. Stroke. 2000; 31(8):1958-64. PMID: 10926964

**36.** Watanabe H, Sakoh M, Andersen F, Rodell A, Sorensen JC, Ostergaard L, et al. Statistical mapping of effects of middle cerebral artery occlusion (MCAO) on blood flow and oxygen consumption in porcine brain. Journal of neuroscience methods. 2007; 160(1):109-15. doi: 10.1016/j.jneumeth.2006.08.016 PMID: 17129609

**37.** Doerfler A, Forsting M, Reith W, Staff C, Heiland S, Schabitz WR, et al. Decompressive craniectomy in a rat model of "malignant" cerebral hemispheric stroke: experimental support for an aggressive therapeutic approach. Journal of neurosurgery. 1996; 85(5):853-9. doi: 10.3171/jns.1996.85.5.0853 PMID: 8893724

**38.** Engelhorn T, Doerfler A, Kastrup A, Beaulieu C, de Crespigny A, Forsting M, et al. Decompressive craniectomy, reperfusion, or a combination for early treatment of acute "malignant" cerebral hemispheric stroke in rats? Potential mechanisms studied by MRI. Stroke. 1999; 30(7):1456-63. PMID: 10390323

**39.** Morancho A, Garcia-Bonilla L, Barcelo V, Giralt D, Campos-Martorell M, Garcia S, et al. A new method for focal transient cerebral ischaemia by distal compression of the middle cerebral artery. Neuropathology and applied neurobiology. 2012; 38(6):617-27. doi: 10.1111/j.1365-2990.2012.01252.x PMID: 22289071

**40.** Simard JM, Yurovsky V, Tsymbalyuk N, Melnichenko L, Ivanova S, Gerzanich V. Protective effect of delayed treatment with low-dose glibenclamide in three models of ischemic stroke. Stroke. 2009; 40 (2):604-9. doi: 10.1161/STROKEAHA.108.522409 PMID: 19023097

**41.** Arikan F, Vilalta J, Minoves T, Moncho D, Vilalta A, Moguer M, et al. [Detection of episodes of ischemic tissue hypoxia by means of the combined intraoperative neurophysiologic monitoring with the tissue oxygenation monitoring in aneurysm surgery]. Neurocirugia. 2008; 19(2):113-20. PMID: 18500409

**42.** Arikan F, Vilalta J, Noguer M, Olive M, Vidal-Jorge M, Sahuquillo J. Intraoperative monitoring of brain tissue oxygenation during arteriovenous malformation resection. Journal of neurosurgical anesthesiology.2014; 26(4):328-41. doi: 10.1097/ANA.0000000000000033 PMID: 24492516

**43.** Sahuquillo J, Amoros S, Poca MA, Mena MP, Ibanez J, Baguena M, et al. Coexistence of regional cerebral hypoxia with normal or hyperemic brain detected by global monitoring methods. Analysis of apparently contradictory findings based on the Siggaard-Andersen model of tissue hypoxia. Acta neurochirurgica Supplement. 2002; 81:303-5. PMID: 12168332

**44.** Martinez-Valverde T, Sanchez-Guerrero A, Vidal-Jorge M, Torne R, Castro L, Gandara D, et al. Characterization of the Ionic Profile of the Extracellular Space of the Injured and Ischemic Brain: A Microdialysis Study. Journal of neurotrauma. 2016.

**45.** Stokum JA, Gerzanich V, Simard JM. Molecular pathophysiology of cerebral edema. Journal of cerebral blood flow and metabolism: official journal of the International Society of Cerebral Blood Flow and Metabolism. 2016; 36(3):513-38.

**46.** Woo SK, Kwon MS, Ivanov A, Gerzanich V, Simard JM. The sulfonylurea receptor 1 (Sur1)-transient receptor potential melastatin 4 (Trpm4) channel. The Journal of biological chemistry. 2013; 288 (5):3655-67. doi: 10.1074/jbc.M112.428219 PMID: 23255597

**47.** Hillered L, Valtysson J, Enblad P, Persson L. Interstitial glycerol as a marker for membrane phospholipid degradation in the acutely injured human brain. Journal of neurology, neurosurgery, and psychiatry. 1998; 64(4):486-91. PMID: 9576540

**48.** Peerdeman SM, Girbes AR, Polderman KH, Vandertop WP. Changes in cerebral interstitial glycerol concentration in head-injured patients; correlation with secondary events. Intensive care medicine. 2003; 29(10):1825-8. doi: 10.1007/s00134-003-1850-8 PMID: 12827237

# CAPÍTULO 2

## Kir6.2, the Pore-Forming Subunit of ATP-Sensitive K+ Channels, Is Overexpressed in Human Posttraumatic Brain Contusions

JOURNAL OF NEUROTRAUMA 35:1–11 (XXXX 00, 2018)

DOI: 10.1089/neu.2017.5619

JOURNAL OF NEUROTRAUMA 35:1–11 (XXXX 00, 2018)
DOI: 10.1089/neu.2017.5619

# Kir6.2, the Pore-Forming Subunit of ATP Sensitive K+ Channels, Is Overexpressed in Human Posttraumatic Brain Contusions

**Lidia Castro[1], Noelia Montoya[1], Marian Vidal-Jorge[1], David Sánchez-Ortiz[1], Darío Gándara[1,3], Elena Martínez-Saez[2], Marta Cicuéndez[3], Maria-Antonia Poca[1,3], J. Marc Simard[4] and Juan Sahuquillo[1,3].**

**1** Neurotraumatology and Neurosurgery Research Unit (UNINN), Vall d'Hebron Research Institute (VHIR), Universitat Autònoma de Barcelona, Barcelona, Spain, **2** Department of Pathology, Vall d'Hebron University Hospital, Barcelona, Spain, **3** Department of Neurosurgery, Vall d'Hebron University Hospital, Universitat Autònoma de Barcelona, Barcelona, Spain, **4** Departments of Neurosurgery, Physiology and Pathology, University of Maryland School of Medicine, Baltimore, MD, USA.

## Abstract

Brain contusions (BCs) are one of the most frequent lesions in patients with moderate and severe traumatic brain injury (TBI). BCs increase their volume due to peri-lesional edema formation and/or hemorrhagic transformation. This may have deleterious consequences and its mechanisms are still poorly understood. We previously identified de novo upregulation sulfonylurea receptor (SUR) 1, the regulatory subunit of adenosine triphosphate (ATP)-sensitive potassium (KATP) channels and other channels, in human BCs. Our aim here was to study the expression of the pore-forming subunit of KATP, Kir6.2, in human BCs, and identify its localization in different cell types. Protein levels of Kir6.2 were detected by western blot (WB) from 33 contusion specimens obtained from 32 TBI patients aged 14–74 years. The evaluation of Kir6.2 expression in different cell types was performed by immunofluorescence in 29 contusion samples obtained from 28 patients with a median age of 42 years. Control samples were obtained from limited brain resections performed to access extra-axial skull base tumors or intraventricular lesions. Contusion specimens showed an

increase of Kir6.2 expression in comparison with controls. Regarding cellular location of Kir6.2, there was no expression of this channel subunit in blood vessels, either in control samples or in contusions. The expression of Kir6.2 in neurons and microglia was also analyzed, but the observed differences were not statistically significant. However, a significant increase of Kir6.2 was found in glial fibrillary acidic protein (GFAP)-positive cells in contusion specimens. Our data suggest that further research on SUR1- regulated ionic channels may lead to a better understanding of key mechanisms involved in the pathogenesis of BCs, and may identify novel targeted therapeutic strategies.

**Keywords:** brain contusion; brain edema; human; Kir6.2; SUR1

## Introduction

Brain contusions (BCs) are one of the most frequent focal primary lesions in patients with moderate and severe traumatic brain injury (TBI).[1] In more than 50% of TBI patients with BCs, contusions increase their volume as a result of an increase in water content in the core of the lesion, edema formation in the perilesional area, and/or hemorrhagic progression.[2,3] The volume increase of BCs is the cause of neurological worsening and in some patients requires craniotomy for mass evacuation to avoid brain herniation and death. One major goal of current TBI research is a better understanding of the molecular pathophysiology of the BC induced edema and its hemorrhagic progression to avoid the neurological deterioration related to these still poorly understood lesions.

Adenosine triphosphate (ATP)-sensitive potassium ($K_{ATP}$) channels -first discovered by Noma in 1983 in the cardiomyocytes of guinea pigs and rabbits[4]- are a collection of structurally distinct channels that couple cell energetic status with electrophysiological membrane potential.[5] In mammals, $K_{ATP}$ channels are expressed in a variety of excitable and endocrine tissues, including cardiomyocytes, pancreatic b-cells, skeletal and smooth muscle, kidney, pituitary, placenta, and brain.[5–7] $K_{ATP}$ channels are hetero-octameric

complexes with four pore-forming, inwardly rectifying potassium channel subunits (Kir6.1 or Kir6.2) and four regulatory sulfonylurea receptor (SUR) subunits (SUR1, SUR2A, or SUR2B).[8] $K_{ATP}$ channels expressed in the mammalian brain have the same structure as the pancreatic β-cell channels -a SUR1 regulatory subunit and a Kir6.2 pore-forming subunit[9]- but their functions are still poorly understood. The activation of $K_{ATP}$ channels in the setting of energy failure, both in the myocardium and the brain, results in cell hyperpolarization and vasodilation, and has cardio- and neuroprotective effects.[10–12]

Paradoxically, experimental evidence has accumulated that in acute lesions of the central nervous system (CNS) such as spontaneous subarachnoid hemorrhage, stroke, TBI, and spinal cord injury, the SURs and specifically SUR1 -the regulatory subunit of pancreatic and neuronal KATP channels- are involved in the generation and propagation of ischemic and contusion-induced brain edema and in the hemorrhagic conversion of ischemic stroke and BCs.[2,13] SURs are not directly involved in ionic transport but must associate with pore-forming subunits to form transmembrane cation channels.[13,14] Therefore, the deleterious effects of SUR1- overexpression or the beneficial effects of its pharmacological modulation are associated with the pore-forming subunit it regulates, not with the SUR subunit by itself.

Simard's group has shown that SUR1 is also the regulatory subunit of a non-constitutive channel formed with transient receptor potential melastatin 4 (TRPM4).[15–17] The SUR1-TRMP4 channel, described by Chen and Simard in 2001,[17] is a nonselective ATP- and calcium-sensitive monovalent cation channel that facilitates Na+ entry into cells and triggers cell depolarization, cerebral vasoconstriction, and brain edema. Upregulation of SUR1- TRPM4 in brain tissue including endothelial cells, astrocytes, and neurons, results in necrotic cell death and promotes brain edema by initiating cytotoxic edema, the driver of all other forms of brain edema, such as ionic or vasogenic edema.[13,17–22] Recently, our group showed SUR1 overexpression in human BCs and that SUR1 was significantly overexpressed in all types of brain cells, but particularly in neurons, glia, and endothelial cells.[23] Kurland and colleagues suggested that in TBI, the endothelial cells of microvessels that

are not disrupted at the time of injury receive kinetic energy that initiates a series of molecular events that results in their structural failure and fragmentation, which contributes to the secondary hemorrhagic progression of BCs.[2] Brain edema and the extravasated blood are extremely toxic to the brain and initiate a strong neuroinflammatory response that is the starting point of a deleterious circle that adds further secondary damage to the already-established primary brain injury.

The clinical relevance of the SUR association with pore-forming subunits is that SUR1 can be modulated by drugs that interact with it and thus influence the opened-closed status of its regulated channels. $K_{ATP}$ channels in any tissue are inhibited by sulfonylureas and are activated by channel-opening drugs, such as diazoxide, pinacidil, or nicorandil.[9,24] Pre-clinical evidence and a recently finished Phase II clinical trial have shown that glibenclamide, a second-generation sulfonylurea used in diabetic patients,[25] significantly reduces brain edema and mass effect in large middle cerebral artery ischemic stroke.[26,27] By inhibiting SUR1-TRPM4 channels, glibenclamide reduced brain swelling and death and was associated with better neurological outcomes than treatment with decompressive craniectomy in a rat model of severe ischemia/reperfusion.[26]

In studying the SUR1-TRPM4 channel in human BCs, by serendipity, we found that the pore-forming subunit Kir6.2 was also expressed in BC specimens. Because SUR1 is the regulatory subunit for both TRMP4 and Kir6.2, and because glibenclamide protects the brain from ischemic swelling, it seemed that their function was contradictory to the role that SUR1-TRPM4 plays in the generation of brain edema and in the ''microvascular failure'' phenomenon in BCs.[2] Our aim in this article was to study Kir6.2 in human BC specimens, including its expression and localization in different cell types, to obtain a better understanding of the role of this subunit in TBI and the potential role of the SUR1-Kir6.2 channel in the pathophysiology of TBI. Here we show that the Kir6.2 pore-forming subunit is significantly overexpressed in the astrocytes of human BC specimens, and we speculate about Kir6.2's potential role in the pathophysiology of BCs and its exploitation as a potential pharmacological target in TBI.

# Methods

## Clinical material and methods

This prospective study included all TBI patients who had an initial computed tomography (CT) scan and underwent surgical evacuation of their BCs at our institution between January 2006 and July 2015. The brain specimens were obtained from surgically resected areas of the BCs that were stored in a biobank collection of TBI specimens at our institution (registration number C0002524 at the Carlos III Institute). The mean contusion volume at the time of evacuation was determined using the ABC/2 method.[28] As suggested by Iaccarino and co-workers, in patients with more than one lesion, the volume of each contusion was calculated and then added to get a total contusion volume.[1] The clinical outcome for each patient was assessed 6 months after the injury, using the Extended Glasgow Outcome Scale (GOSE), by an independent neuropsychologist blinded to the immunolabeling and western blot (WB) data. The control group included tissue specimens obtained from limited brain resections of macroscopically normal brain, which were performed to access extra-axial skull base tumors or intraventricular lesions. These samples were included if the magnetic resonance imaging (MRI) scans did not show any abnormalities in T1-weighted, T2-weighted, or fluid-attenuated inversion recovery (FLAIR) images. Our research was carried out in accordance with the ethical principles for medical research of the Declaration of Helsinki.[29] This study and the tissue collection protocol were approved by the Institutional Ethics Committee of Vall d'Hebron University Hospital (protocols PR-ATR-68/2007 and PR-ATR- 286/2013) and written informed consent was obtained from all of the patients (including the controls) or the patient's legally authorized representative.

## Criteria for surgical evacuation of brain contusions

At our institution, patients must fulfill at least one of the following criteria to be considered for surgical evacuation: (1) for patients with intracranial pressure (ICP) monitoring, the ICP exceeds 20mm Hg and the total volume of a single contusion or multiple contusions exceeds the 25-mL

threshold; (2) for patients without ICP monitoring (mostly moderate TBI), the total contusion volume (hemorrhagic and edematous components) is above the 25- mL threshold; (3) any temporal contusion that produces a significant mass effect and/or compresses the basal cisterns; and (4) contusions that induce a significant midline shift (> 5 mm) despite having an ICP <20mm Hg. The surgical approach in non-eloquent brain areas is usually excision of the necrotic tissue with variable margins but without external bone decompression.

## Brain tissue collection

After surgical resection, all of the specimens were immediately transported to the laboratory on ice. Using dissection material and phosphate buffer (0.2 M), the cauterized and necrotic zones of the resected tissues were removed; excess blood and hematomas were also eliminated. Samples (the minimum size was $5mm^3$) were obtained from the processed tissue. The specimens with preserved anatomical structures were selected from areas of the resected tissue, corresponding to penumbral zones or the interface of the penumbra/core using the terminology described by Kurland and associates.[2] The surgical samples were processed following different protocols. For WB analysis, specimens were rapidly frozen on dry ice and stored at -80°C until analysis. For immunohistochemistry, samples were fixed with 4% formaldehyde for 48 h and cryoprotected using 30% sucrose solution. After cryoprotection, the specimens were embedded in Tissue-Tek optimal cutting temperature (OCT) compound (OCT 4583; Sakura Finetek Europe B.V., Alphen aan den Rin, The Netherlands) and frozen on dry ice. From these blocks, 10-µm-thick sections were obtained using a cryostat (Leica CM3050 S; Leica Biosystems, Heidelberg, Germany), mounted on glass slides, and stored at -20°C until further analysis.

The MRI images of all controls were independently assessed by two of the authors (JS and JMS), who were blinded to the immunolabeling data. The tissue quality was evaluated in the hematoxylin and eosin (H&E)-stained sections by a neuropathologist (EMS), who was blinded to the immunolabeling data, using one scale for edema and another for signs of tissue hypoxia/ischemia (0: absent, 1: mild, 2: moderate, or 3: severe).

The patients with edema and/or ischemia scores >2 were excluded as controls.

## Western blot

Protein extracts were homogenized by tissue lysis via sonication in ice-cold RIPA buffer (R0278; Sigma-Aldrich, St. Louis, MO). To avoid protein degradation, proteases were inhibited by a protease inhibitor cocktail (11697498001; Roche Diagnostics, Mannheim, Germany). After homogenization, samples were put on ice for 20 min and centrifuged at 12,000 rpm for 15 min at 4°C. The pellet was discarded and the supernatant was used to quantify the protein concentration by the Bradford's method[30] using bovine serum albumin as the standard (A2153; Sigma-Aldrich). Once the concentration was determined, 15 µg of denatured protein (5 min at 100°C) from each sample were loaded on a 10% SDSpolyacrylamide gel, separated electrophoretically, and transferred in a tank filled in with 1x running buffer (Tris/Glycine/SDS; 161073; Bio-Rad, Hercules, CA) to a polyvinylidene difluoride (PVDF) membrane. A standard molecular weight marker (Precision Plus Protein Standards-Dual Color; Bio-Rad) was included in a separate lane. The transferred membrane was incubated at 4°C overnight in blocking solution with a primary antibody (rabbit anti-Kir6.2 at 1:10,000; APC-020; Alomone Labs, Jerusalem, Israel). Blocking solution was composed of 5% skimmed milk powder and Tris-buffered saline (TBS) containing 0.1% Tween-20 (TBSTween-20; P9416; Sigma-Aldrich). Alomone's APC-020 is an affinity purified, polyclonal rabbit antibody raised against amino acid sequence 372-385 of rat Kir6.2, which is homologous to human Kir6.2. After washing in TBS Tween-20 the horseradish peroxidaselabeled species-appropriate secondary antibody (A0545; Sigma- Aldrich) was applied at a dilution of 1:2000 for 1 h. The blot was washed again in TBS-Tween-20 and then positive signals were developed using enhanced chemiluminescence (RPN2232; Amersham Biosciences, Bucks, UK) and detected by a 30-sec exposure to radiographic films. The relative optical density of the resulting bands was determined by Quantity One 1-D Analysis Software v4.6.6 (Bio-Rad) and, for quantification, was normalized to the β-actin loading control. We tested

whether there were some significant differences between b-actin concentration in contusion (optical density units; median: $1.2x10^{11}$; min-max: 0.6 to $30.4x10^{11}$) and controls (optical density units; median: $1.3x10^{11}$; min-max: 1.2 to $1.8x10^{11}$). The differences in actin concentration observed between contusions and controls were not statistically significant (Mann-Whitney Wilcoxon test, p = 0.11).

## Immunohistochemistry

Before immunolabeling, to reduce autofluorescence, the samples were pre-treated by immersing the 10-µm-thick sample sections for 7 min in 0.1% sodium borohydride ($NaBH_4$) diluted in 0.1M phosphate-buffered saline (PBS).[31] After this treatment, sections were incubated in a blocking solution containing 4% donkey serum (D9663; Sigma-Aldrich) and 0.2% Triton-X (T8787; Sigma- Aldrich) diluted in PBS for 1 h and then overnight at 4°C with the primary antibodies indicated in **Table 1**. Fluorescent-labeled, species-appropriate secondary antibodies (also indicated in **Table 1**) were used for signal visualization. The omission of primary antibodies was used as a negative control. Sections were cover-slipped with polar mounting medium containing anti-fade reagent and the nuclear dye 4,6-diamino-2-phenylindole (DAPI; P36935; Invitrogen). Fluorescent signals were visualized using an epifluorescence microscope (BX61Olympus; Olympus Corporation, Tokyo, Japan).

## Antibody validation

To avoid reproducibility problems, we validated our Kir6.2 antibody with some of the independent antibody strategies proposed by Uhlen and associates.[32] As a first step, we conducted a comparative analysis between our antibody (APC-020; Alomone Labs) and a second one recognizing a different Kir6.2 epitope (GTX80493; GeneTex, CA). We performed a WB with both antibodies in the same specimens and compared the expression of Kir6.2 by the Pearson correlation coefficient (R = 0.88, p = 0.049) as shown in **Figure 1A**. As a second validation method, we tested our antibody (APC-020; Alomone Labs) by immunofluorescence using a

second antibody against Kir6.2 (G-16; Santa Cruz Biotechnology). We looked for an overlapping distribution of both antibodies, as shown in **Figure 1B**, to ensure accuracy. As the third validation method, we performed a WB using a fragment (amino acids 301 to 390) of the recombinant human Kir6.2 protein (ab114436; Abcam, Cambridge, UK) tagged with green fluorescent protein (GFP) to demonstrate that Alomone's antibody recognized recombinant human Kir6.2 protein.

**Table 1. Antibodies used for immunohistochemistry**

| Primary antibody | Dilution | Supplier | Secondary antibody | Dilution | Supplier |
|---|---|---|---|---|---|
| **Rabbit anti-Kir6.2; APC-020** | 1:300 | Alomone Labs | AlexaFluor® 568; A10042 | 1:400 | Invitrogen |
| **Goat anti-Kir6.2; sc-11228** | 1:50 | Santa Cruz Biotechnology | AlexaFluor® 488; A11055 | 1:400 | Invitrogen |
| **Mouse anti-NeuN; MAB377** | 1:100 | Millipore Corporation | AlexaFluor® 488; A21202 | 1:400 | Invitrogen |
| **Mouse anti-GFAP; C-9205, CY3 conjugated** | 1:3000 | Sigma-Aldrich | – | - | - |
| **Mouse anti-Iba; 174429658** | 1:100 | Thermo Fisher | AlexaFluor® 488; A21202 | 1:400 | Invitrogen |
| **Mouse anti-CD31; M0823** | 1:100 | Dako | AlexaFluor® 488; A21202 | 1:400 | Invitrogen |

A second recombinant protein of GFP (ab134853; Abcam) was used as a negative control. For this test, 1µg of protein was loaded per lane onto a 10% SDSpolyacrylamide gel and transferred to a PVDF membrane that was incubated with the primary antibody from Alomone Labs at a 1:1000 dilution; the secondary antibody was applied at 1:2000. Positive signals were detected by a 1-min exposure to radiographic film.

The results show that our antibody recognized the recombinant protein but not the tags, as shown in **Figure 1C**. Finally, to have a positive control,

we decided to show the expression of Kir6.2 in a cell line of human cardiomyocytes (ScienCell Research Laboratories, San Diego, CA), because these cells express Kir6.2 constitutively.[9,33] As shown in **Figure 1D**, the cardiomyocytes were strongly positive for Kir6.2.

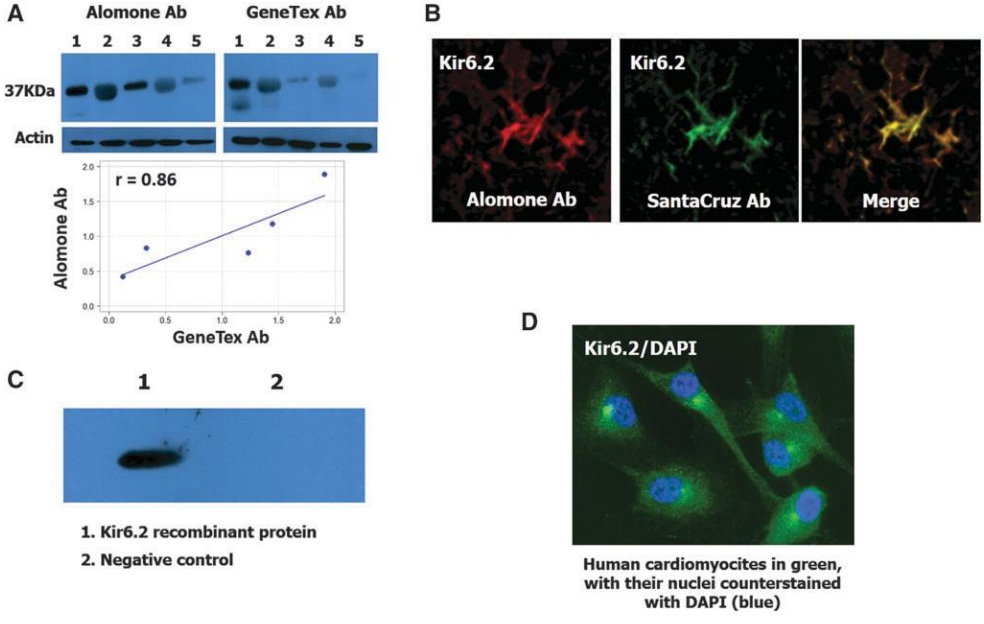


**FIG. 1. Antibody validation. (A)** Upper images show the result of a western blot analysis of human Kir6.2 in five specimens of human brain tissue (lanes 1 to 5: 2, 4 corresponding to contusion specimens and 1, 3, 5 corresponding to healthy tissue) using two independent antibodies (Alomone Ab and GeneTex Ab). The bar graphs are shown as a visual aid for the inmunoblot results. Optical density with both antibodies was compared and resulted in a Pearson correlation coefficient of 0.88 ($p = 0.049$). The scatterplot is shown as a visual aid to the immunoblot results. **(B)** Fluorescence labeling of Kir6.2 using Alomone Ab (red) and SantaCruz Ab (green); merged images in yellow. **(C)** Western blot analysis of a human recombinant Kir6.2 protein (ab114436; Abcam, Cambridge, UK) (1) tagged with Green fluorescent protein (GFP) and GFP recombinant protein (2) used as a negative control. **(D)** Kir6.2 expression (green) in a cell line of human cardiomyocytes (P10451; Innoprot, Derio, Spain) used as a positive control. Nuclei were counterstained with 4,6-diamino-2-phenylindole (DAPI).

## Cross-reactivity between Kir6.2 and Kir6.1

To demonstrate that our Kir6.2 antibody (APC-020; Alomone Labs) was not binding to Kir6.1, we conducted immunofluorescence labeling using our Kir6.2 antibody and a Kir6.1 antibody (APC-105; Alomone Labs) in adjacent sections of a mouse brain sample. The rationale for using mouse brain tissue is that Kir6.2 and Kir6.1 are compartmentalized in mouse brain (Kir6.2 expression is mostly located in neurons and Kir6.1 in astrocytes).[34] We took immunofluorescence images from the same region of our samples using an epifluorescence microscope (BX61, Olympus), and we observed that Kir6.1 and Kir6.2 were labeling different zones and cells. Kir6.2 was restricted to neuronal structures, and Kir6.1 was restricted to blood vessels. Thus, the Kir6.2 antibody does not cross-react with the Kir6.1 epitope.

We also performed an experiment with a lysate of HEK293T cells that overexpress only Kir6.1 (NBL1-12174; Novus Biological, Littleton, CO) but not Kir6.2, to confirm that our antibody was not cross-reacting also with Kir6.1. We simultaneously ran two WBs where 15 µg of the lysate was loaded onto a 10% SDS polyacrylamide gel and transferred to a PVDF membrane. As negative controls, we used HEK293T cells transfected with an empty vector. One of the membranes was incubated with our Kir6.2 antibody at a 1:10,000 dilution and the other one with the Kir6.1 antibody at a 1:200 dilution as recommended by the manufacturer. Both secondary antibodies were applied at a 1:2000 dilution. Signals were detected by exposing the membranes to radiographic films for 1 min. The results obtained showed that only the Kir6.1 antibody was detecting the HEK293T-cells lysate, as is shown in **Figure 2B**.

## Analysis of immunohistochemical findings

**Quantitative immunohistochemical analysis in neurons and endothelial cells.** To calculate the number of Kir6.2-positive neurons and vessels, 4–8 captured 440x330 $\mu m^2$ images from the cortex were taken by the investigator with an epifluorescence microscope (BX61, Olympus) using DAPI as a guide. All images were quantified using the plug-in Cell Counter (Kurt De Vos; http://rsb.info.nih.gov/ij/plugins/cell-counter.html) of the Image J program,

v1.47 (Wayne Rasband, National Institutes of Health, Bethesda, MD). This plug-in allows counting cells manually. The investigator clicks in the cell image and this method marks the cell with a colored square and adds the cell to a tally sheet. The percentage of Kir6.2-positive cells was calculated from the total number of neurons and blood vessels (NeuN/CD31-positive).

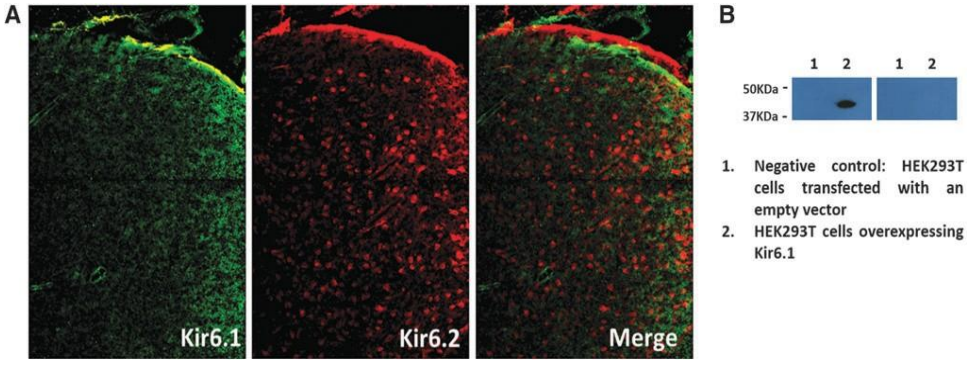


**FIG. 2. Cross-reactivity Kir6.2-Kir6.1. (A)** Staining of Kir6.1 (green; APC-105; Alomone Labs) and Kir6.2 (red; APC-020; Alomone Labs) in the same section of mouse brain tissue. Kir6.1 shows labeling in blood vessel-like structures and Kir6.2 in neuronal-like structures. This shows that the Kir6.2 antibody does not cross-react with the Kir6.1 epitope. **(B)** Western blot analysis of a lysate of HEK293T-cells transfected with an empty vector (lane 1) and HEK293T cells that overexpress Kir6.1 (NBL1-12174; Novus Biological, Littleton, CO) (lane 2). The membrane shown on the left was incubated with an anti-Kir6.1 antibody and the one on the right with an anti-Kir6.2 antibody. Only the Kir6.1 antibody was detecting the HEK293T-cells lysate showing that cross-reactivity does not occur between the Kir6.2 antibody and the Kir6.1 epitope.

**Semi-quantitative immunohistochemical analysis in astrocytes and microglia.** To evaluate whether Kir6.2 was expressed in these cells, specific antibodies were used (anti-GFAP and anti- Iba1, respectively). The whole section was quantified by two independent observers using a semi-quantitative scale to count: (1) the different cell types (0: absent; 1: scanty; 2: moderate; or 3: numerous) and (2) the Kir6.2-positive cells of each type (0: none; 1: in a few cells; 2: in many cells; or 3: in all or almost all cells). The inter-observer agreement (weighted kappa) was 0.83 (min: 0.78, max: 0.94). The statistical analysis was conducted using the average of the assigned scores from the two independent observers. To facilitate data

interpretation, an example of the quantification in different cell types is shown in **Supplementary Figure 1** (see online supplementary material at http://www.liebertpub.com).

## Controls

The tissue quality was evaluated in the H&E-stained sections by a neuropathologist (EMS), who was blinded to the immunolabeling data, using one scale for edema and another for signs of tissue hypoxia/ischemia (0: absent, 1: mild, 2: moderate, or 3: severe). The patients with edema and/or ischemia scores >2 were excluded as controls.

## Statistical analysis

Descriptive statistics were obtained for each variable. For continuous variables, the mean, median, range, and standard deviation were used for normally distributed data and the median, minimum, and maximum values were used for non-Gaussian distributions. The Shapiro-Wilk test and the inverse probability plot were used to test whether the data followed a normal distribution. The percentages and sample sizes were used to summarize the categorical variables. To correlate two continuous variables, the Pearson correlation test was used for data that followed a normal distribution and the more conservative Spearman's rho was used if the data did not follow a normal distribution. For each marker, scatter plots were constructed with time as the abscissa and the percentage/score of positive immunolabeling as the ordinate. A simple linear regression and the ordinary least squares (OLS) method were used. Adjusted $R^2$ values were calculated for all of the models to test whether the linear or non-linear models adequately explained the relationships between both variables. The statistical analyses were performed using Microsoft R Open (version 3.4.2) and the integrated development environment R Studio (version 1.1.383).[35] The car package was used for regression analysis.[36] To calculate the inter-observer agreement between the two independent observers using the immunolabeling ordinal scales, we used weighted kappa with the routine implemented in MedCalc version 12.2 (MedCalc Software, Mariakerke,

Belgium). Statistical significance was considered when $p<0.05$. Data are presented graphically using boxand- whisker plots.

## Results

Small differences regarding the number of control and contusion samples in the different techniques used for the quantification of Kir6.2 are due to the different number of samples obtained from individual patients. When the samples were large enough, they could be processed for immunoblots and for immunochemistry. However, when the samples were small they could only be processed for one of these techniques.

### Descriptive data of patients with contusions

Forty-three contusion specimens were obtained from 42 TBI patients (30 males and 13 females) with a median age of 48 years (min: 14, max: 74 years). The lack of coincidence between number of specimens and samples is due to the fact that we have collected two samples from one single patient—one from the frontal and a second one from the temporal lobe—however, the other specimens each correspond one to one patient. Samples were obtained at a median time post-injury of 23 h (min: 5, max: 246 h). The median contusion volume evaluated by CT was 44mL (min: 13, max: 170 mL). On admission, 21 patients (49%) scored above 9 on the Glasgow Coma Score scale and were thus included in the moderate TBI category. Mortality was 7% in this cohort. The median GOSE of the survivors assessed at 6 months after injury was heterogeneous (median, 3; range, 1–8). The small sample size was not powered for conducting a robust statistical analysis to study the possible relationship between contusion volume, neurological outcome, and Kir6.2 expression.

### Control group

Six control specimens were used. The reduced number of control specimens was due to the exclusion of some of them because of pathological evidence of edema and/or ischemia that could have been caused by the manipulation of tissues during surgery, suboptimal conditions during transport of the samples to the laboratory, or the pre-existence of pathology not

detectable by MRI. Also the variability in the number of controls used for different techniques is due to the different sizes of resected tissues, as explained previously. Demographic data for the 6 control subjects are summarized in **Table 2.**

**Table 2. Descriptive data for control patients**

| | | | | Tissue quality | |
|---|---|---|---|---|---|
| **Case** | **Age** | **Sex** | **Primary pathology** | **Edema** | **Ischemia** |
| **1** | **57** | **F** | **Meningothelial meningioma** | **0** | **2** |
| **2** | **59** | **F** | **Psammomatous meningioma** | **0** | **1** |
| **3** | **31** | **F** | **Facial shwannoma** | **0** | **1** |
| **4** | **2** | **M** | **Rhabdoid tumor** | **1** | **2** |
| **5** | **66** | **M** | **Epidermoid cyst** | **1** | **2** |
| **6** | **25** | **F** | **Left temporal lobe lesion** | **1** | **0** |

Tissue quality scores (edema and ischemia): 0: absent; 1: mild; 2: moderate; and 3: severe. F: female; M: male

## Kir6.2 pore-forming subunit is increased in brain contusions

Kir6.2 levels were evaluated by WB in 33 contusion specimens obtained from 32 TBI patients (21 males and 11 females) ages between 14 and 74 years (median: 49 years). The results were compared with 5 control specimens (cases, 1, 2, 3, 4 and 6 in **Table 2**). On average, Kir6.2 expression, expressed as optical density units, was significantly increased in contusions (median: 1.03; min: 0.32, max: 1.84) compared with controls (median: 0.64; min: 0.38, max: 0.93) (Wilcoxon rank sum test; $p = 0.014$) (**Fig. 3**).

## Kir6.2 expression in different cell types

The expression of the channel subunit was studied by immunofluorescence in 29 contusion specimens from 28 patients (23 males and 5 females) with a median age of 42 years (min: 14, max: 74 years) and in four

controls (cases, 2 to 5 of **Table 2**). In **Figure 4**, a montage of the immunofluorescence for the different cell types is shown.

**Neurons.** The median percentage of Kir6.2-positive neurons in controls was 16.5% (min: 6.1%, max: 59.0%) and 1.8% in contusions (min: 0%, max: 69.3%) (**Fig. 5A**). However, the observed differences were not statistically significant (Mann- Whitney Wilcoxon test, p = 0.293). In contusions, 13 specimens (50%) exhibited Kir6.2-positive neurons but in 13 specimens, Kir6.2 was not observed.

**Endothelial cells.** We did not find expression of Kir6.2 in blood vessels, either in control samples or in contusion specimens. For this reason, we did not quantify Kir6.2 expression for this cell type.

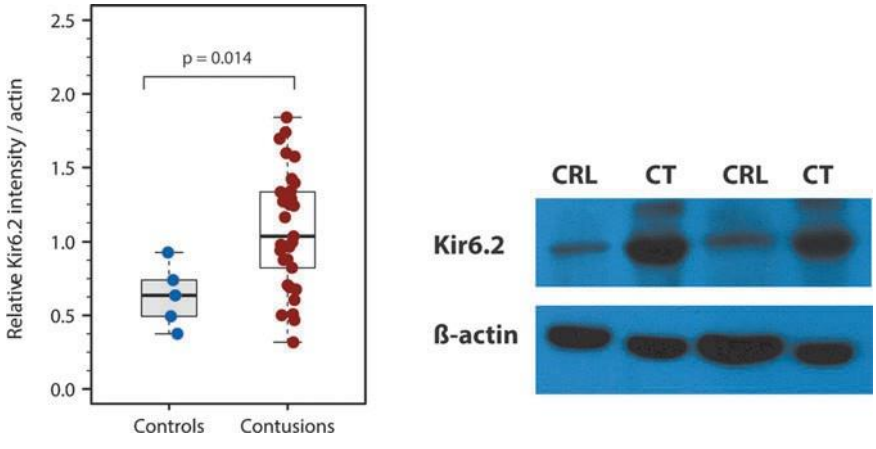


**FIG. 3. Kir6.2 protein levels in control and contusion samples. (A)** Box plots of Kir6.2 relative intensity in control and contusion samples, showing a significant increase of Kir6.2 expression (p = 0.014) in contusion specimens; data normalized to b-actin loading controls. **(B)** Representative image of a western blot showing a clear difference between control and contusion samples.

**Glial cells.** In 1 control and 4 of the 29 contusion specimens, we did not observe GFAP-positive cells, and therefore these specimens were excluded from the semi-quantitative analysis. In the GFAP-positive cells, control specimens showed very low Kir6.2 expression (median: 0.5; min: 0, max: 1) (**Fig. 5B**). A significant increase in Kir6.2 density was found in GFAP-

positive cells in contusion specimens (median: 2; min: 0, max: 3). These differences were statistically significant (Mann-Whitney Wilcoxon test, p = 0.03). However, as shown in **Figure 5B**, a wide variability in Kir6.2 expression was found among GFAP-positive cells. The plot of time versus the number of Kir6.2-positive glial cells (data not shown) did not show any correlation between Kir6.2-positive cells and the time when contusion was surgically evacuated (Spearman rho = 0.1, p = 0.60).

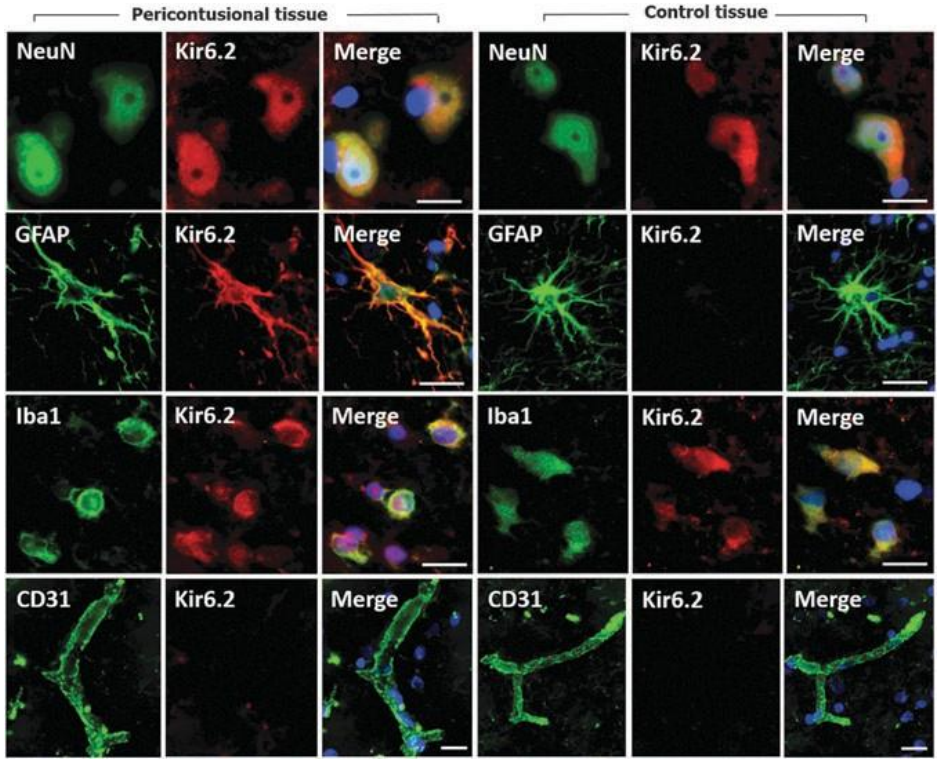


**FIG. 4. Expression of Kir6.2 in different cell types.** The first three columns of the montage show Kir6.2 expression in different cell types of the peri-contusional tissue and the last three show Kir6.2 expression in control tissue. Peri-contusional tissue: fluorescent double labeling for NeuN/ glial fibrillary acidic protein (GFAP)/Iba1/CD31 (green) and Kir6.2 (red). Merged images are presented in the third column. Control tissue: fluorescent double labeling for NeuN/GFAP/Iba1/CD31 (green) and Kir6.2 (red). Merged images are presented in the last column. In controls, the Kir6.2 expression was evident in neurons and microglia but was minimal in astrocytes (GFAPpositive cells). Original magnification = 100x. Scale: 20 µm.

Nuclei were counterstained with 4,6-diamino-2-phenylindole (DAPI).

**Microglia.** In 2 of the 4 controls and 7 of the 29 contusion specimens, we did not observe Iba1-positive cells, and therefore these specimens were excluded from the analysis. In the two controls with Iba1-positive cells, the median density for Kir6.2 was 2 compared with a non-significant increase to 2.25 (min: 1, max: 3) in contusion specimens (Mann-Whitney Wilcoxon test, p = 0.29) (**Fig. 5C**). The scatterplot of time versus percentage of Kir6.2- positive microglia (data not shown) did not show any linear (Spearman rho = 0.01, p = 0.95) or non-linear correlation between Kir6.2-positive cells and time from injury to the surgically evacuation.

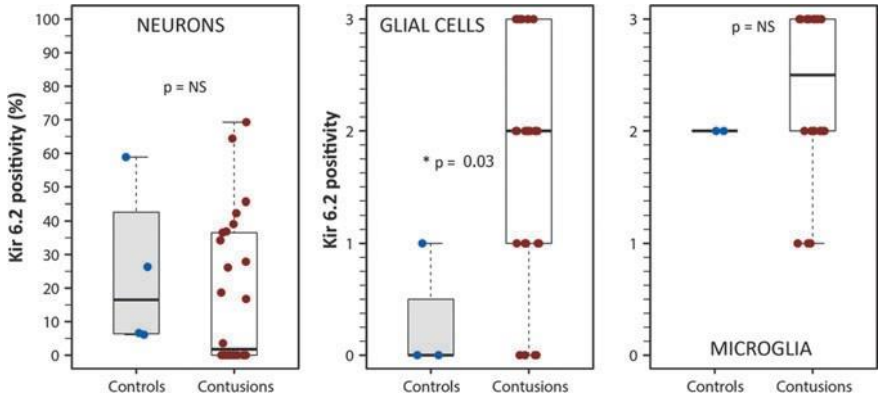


**FIG. 5. Kir6.2 expression in neurons, glial cells, and microglia.** From left to right, representative box plots of Kir6.2 expression in neurons (percentage), in glial cells, and microglia (semi-quantitative scale from 0 to 3). The results show a significantly increased expression of Kir6.2 in glial cells from contusion samples (Wilcoxon rank sum test; p = 0.03), but non-significant differences in neurons and microglia. Asterisks indicate statistically significant differences (*p < 0.05).

## Discussion

Because of its frequency and associated morbidity, BCs remains a serious clinical problem. BCs evolve with time and most of the neurological damage they inflict is a consequence of their increase in volume in the first hours after TBI. The basic mechanisms underlying the growth of posttraumatic

BCs—by either cerebral edema and/or hemorrhagic progression—is complex and involves many interrelated phenomena and biochemical cascades such as alterations in regional cerebral blood flow (rCBF) and in all the components of the multi-cellular neurovascular unit: endothelial cells, neurons, astrocytes, pericytes, and microglia. BCs induce a variable degree of alteration in the blood–brain barrier (BBB) with the consequent increase in permeability to ions at an early stage and protein extravasation and hemorrhagic transformation in later stages.[2] In addition, the contusion ''core''—mainly necrotic brain with blood—induces in the peri-contusional tissue a strong neuroinflammatory response that elicits the release of pro-inflammatory molecules and early upregulation of both systemic and brain gelatinases, proteases that degrade the extracellular matrix and the basement membrane and that are directly implicated in the disruption of the BBB, and in the production of brain swelling after human TBI.[37] Emerging evidence has shown that there are important molecular players involved in the progression of BCs and, among them, dysregulation of cation channels and their regulatory subunits play a crucial role.[2,23] In a series of pivotal studies, Kurland and co-workers have shown that SUR1-TRPM4 channels contribute to brain edema and to the phenomenon of ''microvascular failure'' that explains the hemorrhagic increase observed in BCs.[2] In experimental and clinical studies of ischemic stroke, blockade of the SUR1 regulatory subunit by sulfonylureas consistently reduces ischemia-induced brain edema and swelling,[26,38,39] whereas Kir6.2 and SUR1 null mice are extremely vulnerable to brain hypoxia and exhibit a reduced threshold for hypoxia-induced generalized seizures.[10]

## Kir6.2-pore forming subunit is selectively overexpressed in astrocytes

Our data show that the pore-forming subunit Kir6.2 is overexpressed in BCs and that its expression is weak in neurons, strong in astrocytes (GFAP-positive cells), moderately increased in microglia, and non-detectable in endothelial cells. Because, in most of our specimens, necrotic tissue was excluded from analysis, and analysis was conducted in structurally preserved brain, the overexpression of Kir6.2 is prominent in

what has been called by Kurland and colleagues peri-contusional ''penumbra.''[2] In astrocytes, Kir6.2 was apparently localized not only in the membrane but was observed in the cytoplasm of GFAP-positive cells (**Fig. 3**), suggesting that Kir6.2 could be increased in the plasmalemma but also probably in the mitochondria (mito$K_{ATP}$), as described in the rat liver.40 Mito$K_{ATP}$ regulates mitochondrial volume and membrane potential and could be the key player in the cardio- and neuroprotective molecular processes of ischemic pre-conditioning.[41] Astrocytes are the most important scavengers of glutamate from the brain's extracellular space and regulate glutamate concentrations below toxic levels. In primary cultured astrocytes, Sun and associates showed that mito$K_{ATP}$ activation by KATP channel openers increased glutamate transport into astrocytes,[42] a mechanism that may explain the overexpression of Kir6.2 in BCs and also give a plausible explanation for its observed neuroprotective effects. In experimental models and clinical studies, it has been shown that TBI and specifically BCs increase the extracellular levels of glutamate.[43,44] Using the controlled cortical impact model in rats, Rose and co-workers showed a significant increase in the extracellular concentration of glutamate that was attributed to neuronal depolarization, release from damaged cells, and contusion-induced ischemia.[43] However, we need to consider this as a working hypothesis that needs further data in additional human specimens to be confirmed or refuted.

The non-significant increase of Kir6.2 found in activated microglia was unexpected. In a previous study in BCs, we observed a significant overexpression of the SUR1 regulatory subunit not only in astrocytes but in all the cell types studied (neurons, endothelial cells, astrocytes, and microglia).[23] In most specimens (84%), we observed a moderate increase in the number of cells with the phenotype of activated microglial cells or macrophages. Some of the activated microglial cells -a low to moderate number- were also SUR1-positive, and their numbers increased with time postinjury.[23] Here, we did not find any temporal trend in Kir6.2 labeling in Iba1-positive cells. One difference between our former study and the present one is that in the previous study, we used CD68 as a marker for activated microglia, whereas here we used Iba1 that is a marker for activated and

resting microglial cells, which may explain the difference between our present results and the previous ones.[45]

Ortega and colleagues have shown experimentally that reactive microglia increased the expression of both SUR1 and the $K_{ATP}$ channel after pro-inflammatory stimuli,[46,47] and that under inflammatory conditions, microglial $K_{ATP}$ regulates the release of inflammatory mediators and trophic factors.[47] In our study, only 2 of the 4 controls and 76% of contusions (22 specimens) showed Iba1-positive cells. Iba1-positive cells in contusion specimens exhibited significant variability in the intensity of Kir6.2 labeling and this, together with microglial activation observed in the surgically explanted specimens, prevented us from reaching a conclusion regarding whether Kir6.2 was overexpressed in microglia. To determine the relevance of this finding will require that the sample size of both human contusions and controls be increased. In addition, microglial expression needs to be better explored in animal models in which experimental conditions can be more fully controlled. In this way, the expression of Kir6.2 in microglia might be compared in both the normal brain -not surgically manipulated- and in the injured brain. Because of the importance of microglial response in TBI, further studies are needed to reach any solid conclusion on the role of microglial SUR1-Kir6.2 channels in BCs.

## Kir6.2 and TRPM4 expression in brain contusions: A paradox?

SUR1 co-assembles with both the pore-forming subunits Kir6.1 or Kir6.2 to form the $K_{ATP}$-channel and with the ATP-and-calcium sensitive TRPM4 to form the SUR1-TRPM4 channel. The latter is not constitutively expressed, but is expressed de novo after many types of CNS injury.[15] Hyperactivity, aberrant regulation, or blockade of the different pore-forming subunits have opposite effects in ischemic, traumatic, and inflammatory CNS injuries. The opening of $K_{ATP}$ channels hyperpolarizes the cell and is neuroprotective during ischemia/hypoxia, metabolic stress, and seizures.[10] In contrast, SUR1-TRPM4 channels, which promote $Na^+$ influx accompanied by influx of $Cl^-$ and water to maintain electrical and osmotic neutrality, depolarize the cell and, if overactivated, act as drivers of cytotoxic edema and oncotic cell death.[17,20,48] In the case of endothelium, we previously found that SUR1 is

overexpressed in endothelial cells of human BCs;[23] here we report no expression of Kir6.2 in endothelium, and previously it was found that TRPM4 is overexpressed in endothelium after CNS injury.[15] Thus, SUR1-TRPM4, not $K_{ATP}$, appears to be the dominant SUR1-regulated channel in endothelium of human BCs.

The mechanism of activation of SP1 and NF-kB during mechanical injury remains speculative. However, the diverse pathophysiological mechanisms involved in BCs—absorption of kinetic energy, dysregulated perfusion, hypoxia, extravasated blood, brain edema, etc.—induce the release of many inflammatory mediators, cytokines, and so forth. For a comprehensive review of the molecular mechanisms involved in BCs, the reader is referred to the comprehensive review by Kurland and associated.[2]

## SUR1: Target for pharmacological modulation in BCs

To our knowledge, this is the first study showing that the Kir6.2 pore-forming subunit is overexpressed in human BCs. This evidence complements our previous work, that the expression of the regulatory subunit (SUR1) is also increased in most cells of the neurovascular unit.[23] This information, together with the robust evidence that SUR1-TRPM4 is overexpressed in many forms of CNS injury and that it is an important driver of brain edema, makes the SUR1 subunit an attractive target for pharmacological modulation in BCs. Sulfonylureas, and especially glibenclamide, are powerful inhibitors of SUR1-regulated channel activity with nanomolar affinity and reduce brain edema in many experimental models of CNS injury.[15]

SUR1 blockade has beneficial effects in experimental and clinical studies of ischemia and spinal cord injury.[15,49] Because some experimental findings have shown neuroprotection with the opening of $K_{ATP}$ channels in ischemic stroke, attempts to block SUR1 may seem counterintuitive. However, as noted by Benarroch, the role of KATP channels can be neuroprotective under normal conditions but ''in pathologic conditions their excessive activation may also be deleterious.''[13] Several lines of evidence support the claim that overactivation of KATP channels may be deleterious in different neurological conditions, specifically in ischemic stroke.[50] One potential

explanation for these seemingly contradictory claims is that there are two categories of $K_{ATP}$ channels: plasmalemmal and mito$K_{ATP}$. In a model of brain ischemia in rat brain slices, Nistico and colleagues showed that excessive activation of $K_{ATP}$ channels contributes to the ischemic damage, and that tolbutamide and glibenclamide rescue neurons that are destined to deteriorate in the absence of KATP blockers.[50] The hypothesis put forth by these authors is that excessive activation of KATP channels during ischemia increases the efflux of potassium, thus reducing [K+]i.[50] To compensate for the ischemia-induced ionic disequilibrium, there is an increase in activation of the Na+/K+ pump that depletes the residual ATP under ischemia.[50] Therefore, blocking KATP during ischemia reduces ATP consumption and may preserve cell function.[50] A relevant fact found by the same authors was that the neuroprotective effect of KATP blockers were dependent on the plasmalemmal channels but was not observed when selectively blocking mito$K_{ATP}$ channels by 5-hydroxydecanoate.[50]

Additional findings support the deleterious effects of an increase in function of $K_{ATP}$ channels. The most relevant are observations in the Cantu´ syndrome, and the finding that activation of microglial $K_{ATP}$ channels contributes to the inflammatory response elicited by ischemic stroke.[13,47,51] Cantu syndrome is a rare condition resulting from mutations in the genes that encode SUR2, a regulatory subunit that binds to the Kir6.1 pore-forming subunit.[51] This mutation alters the functionality of the KATP channel and causes the channel to remain open when it should be closed.[51] In this syndrome, it has been suggested that cerebral blood flow autoregulation may be impaired because overactive $K_{ATP}$ channels limit pressure-induced vasoconstriction.51 In a different experimental model, Ortega and associates have shown that reactive microglia overexpresses both SUR1 and the $K_{ATP}$ channel after cerebral ischemia.[47,52] In experimental models, the $K_{ATP}$ channel regulates the microglial reactive state and controls the release of diverse pro-inflammatory mediators such as nitric oxide, interleukin-6 (IL-6), and tumor necrosis factor-alpha (TNFα).[47,52]

In summary, there is increasing evidence that blockade of both SUR-regulated channels, TRPM4 and Kir6.2, could be potentially beneficial in

acute brain injuries, and that in BCs, both are overexpressed. This suggests that modulating these channels is a potential therapeutic target and that the beneficial effects of glibenclamide might be mediated by an additive block of both channels.

## Study limitations

A critical point to note is that we only had a few controls and that they were obtained from patients surgically treated for extra-axial skull base tumors or intraventricular lesions, and therefore they should not be considered comparable to the controls used in animal models or those extracted from fresh human cadavers. In a previous work, we showed a moderate increase in SUR1 in these controls and specifically in endothelial cells.[23] Here we found a moderate increase in Kir6.2 expression in the microglia of controls. In a model of mild/moderate TBI conducted by Patel and co-workers in rats, sham animals (receiving craniotomy without cortical-impact injury) presented some expression of SUR1 in the endothelial cells.[53] This experiment confirms that any intervention, including surgery and brain tissue resection, may induce some upregulation of SUR1 in the mammalian brain. Despite these limitations, we believe our control specimens were adequate ''sham-controls'' and may be more desirable than specimens from cadavers. The apparently better-quality specimens obtained from controls who died of non-neurological disease, probably reflect the inability of the dead brain tissue to initiate any response to tissue manipulation. Therefore, we believe our control specimens are more representative than brain tissue explanted after death.

Our study was not designed to manipulate the Kir6.2 channel but only to describe its expression in the cells that form the neurovascular subunit. Therefore, we can only hypothesize about the potential benefits of manipulating overactive Kir6.2 channels. However, in pilot studies conducted in vitro and in animal models, we have found a very similar pattern of Kir6.2 overexpression. An additional limitation is that we did not try to study the localization of Kir6.2 in specific cell organelles, so we cannot conclude whether the significant increase in the amount of Kir6.2 is

dependent of either the mito-KATP channels, the plasmalemmal channels, or both.

## Conclusions, clinical implications, and future directions

SUR1-regulated ionic channels -specifically SUR1-TRPM4 and SUR1 KIR6.2- likely play a significant role during the pathophysiology of TBI. Previous work and active research by several groups have shown that BCs -primary focal injuries- increase in volume and cause neurological deterioration and death because of BC-induced secondary lesions such as brain edema, hemorrhagic progression, peri-lesional ischemia, brain herniation, and increased ICP. We provide evidence that the Kir6.2 pore-forming subunit, regulated by SUR1, is overexpressed in BCs and this increased expression is predominantly found is astrocytes. This, together with previous studies that have shown the key role of SUR1-TRPM4 in the generation of brain edema suggest the pivotal role of SUR1-regulated channels as attractive potential targets for the prevention of secondary injury in TBI, specifically in BCs. Although significant challenges remain before the molecular pathophysiology of BCs is clarified, the fact that we do not have any effective drug for treating BCs yet makes these new molecular candidates very provocative. There appears to be a great benefit in continuing research in SUR1-regulated ionic channels that should be continued actively to have a better understanding of the key mechanisms involved in the pathogenesis of BCs before they can translate into novel targeted therapeutic strategies. Future research should concentrate on the expression and the role of different $K_{ATP}$ channels (plasmalemmal and mito-$K_{ATP}$), their role in activated microglia, and their manipulation by channel openers and antagonists. A better understanding of the role of ion channels in the mechanisms contributing to TBI may ultimately make it possible to develop novel ion channel based therapies with increased efficacy over the current ineffective treatments.

## Acknowledgments

This work was supported in part by the Fondo de Investigacio´n Sanitaria (Instituto de Salud Carlos III) with grants PI10/00302, PI11/00700, and PI15/01228, which were co-financed by the European Regional Development and awarded to Dr. M.A. Poca and Dr. J. Sahuquillo, respectively. We also thank Dr. T. Martínez-Valverde, former PhD of the Neurotraumatology and Neurosurgery Research Unit (UNINN), for her advice and help during the setting up of the initial experiments. Also, we would like to thank Dr. F. Elortza (Proteomics Platform Manager of CIC bioGUNE) and Dr. J.M. Estanyol (Proteomics Unit Supervisor of the University of Barcelona) for their support and advice in immunoprecipitation and recombinant protein experiments. Finally, we thank Dr. H. Peluffo (PI of the Neuroinflammation and Gene Therapy Laboratory of the Institut Pasteur of Montevideo) for his advice on the treatment and processing of tissue samples. Author contributions to the study and manuscript preparation include the following. Conception and design: Sahuquillo, Castro. Acquisition of data: Castro, Martínez-Saez, Montoya. Analysis and interpretation of data: Sahuquillo and Castro. Statistical analysis: Sahuquillo and Castro. Drafting of the article: Sahuquillo, Simard, Castro. Critical revision of the article: all authors. Reviewing of submitted version of manuscript: all authors. Approval of the definitive version of the manuscript on behalf of all authors: Sahuquillo. Study supervision: Sahuquillo, Simard.

## Author Disclosure Statement

JMS holds a U.S. patent (#7,285,574), ''A novel non-selective cation channel in neural cells and methods for treating brain swelling.'' JMS is a member of the scientific advisory board of and holds shares in Remedy Pharmaceuticals. No support, direct or indirect, was provided to JMS, or for this project, by Remedy Pharmaceuticals. All other authors report no conflict of interest concerning the materials or methods used in this study or the findings specified in this article.

## References

1. Iaccarino, C., Schiavi, P., Picetti, E., Goldoni, M., Cerasti, D., Caspani, M., and Servadei, F. (2014). Patients with brain contusions: predictors of outcome and relationship between radiological and clinical evolution. J. Neurosurg. 120, 908–918.

2. Kurland, D., Hong, C., Aarabi, B., Gerzanich, V., and Simard, J.M. (2012). Hemorrhagic progression of a contusion after traumatic brain injury: a review. J. Neurotrauma 29, 19–31.

3. Katayama, Y., Yoshino, A., Kano, T., Kushi, H., and Tsubokawa, T. (1994). Role of necrosis area in development of the mass effect of cerebral contusion and elevated intracranial pressure, in: Intracranial Pressure IX. H. Nagai, K. Kamiya, and S. Ishii (eds). Springer-Verlag: Tokyo, pps. 324–327.

4. Noma, A. (1983). ATP-regulated K+ channels in cardiac muscle. Nature 305, 147–148.

5. Ashcroft, F.M. (1988). Adenosine 5'-triphosphate-sensitive potassium channels. Annu. Rev. Neurosci. 11, 97–118.

6. Lybaert, P., Hoofd, C., Guldner, D., Vegh, G., Delporte, C., Meuris, S., and Lebrun, P. (2013). Detection of K(ATP) channels subunits in human term placental explants and evaluation of their implication in human placental lactogen (hPL) and human chorionic gonadotropin (hCG) release. Placenta 34, 467–473.

7. Insuk, S.O., Chae, M.R., Choi, J.W., Yang, D.K., Sim, J.H., and Lee, S.W. (2003). Molecular basis and characteristics of KATP channel in human corporal smooth muscle cells. Int. J. Impotence Res. 15, 258–266.

8. Flagg, T.P., and Nichols, C.G. (2011). ''Cardiac KATP'': a family of ion channels. Circ. Arrhythm Electrophysiol. 4, 796–798.

9. Seino, S. (2003). Physiology and pathophysiology of KATP channels in the pancreas and cardiovascular system. J. Diabetes Complications 17, 2–5.

10. Yamada, K., and Inagaki, N. (2005). Neuroprotection by KATP channels. J. Mol. Cell. Cardiol. 38, 945–949.

11. Stoller, D.A., Fahrenbach, J.P., Chalupsky, K., Tan, B.H., Aggarwal, N., Metcalfe, J., Hadhazy, M., Shi, N.Q., Makielski, J.C., and McNally, E.M. (2010). Cardiomyocyte sulfonylurea receptor 2-KATP channel mediates cardioprotection and ST segment elevation. Am. J. Physiol. Heart Circ. Physiol. 299, H1100–H1108.

12. Murry, C.E., Jennings, R.B., and Reimer, K.A. (1986). Preconditioning with ischemia: a delay of lethal cell injury in ischemic myocardium. Circulation 74, 1124–1136.
13. Benarroch, E.E. (2017). Sulfonylurea receptor-associated channels: involvement in disease and therapeutic implications. Neurology 88, 314–321.
14. Nichols, C.G. (2006). KATP channels as molecular sensors of cellular metabolism. Nature 440, 470–476.
15. Simard, J.M., Woo, S.K., Schwartzbauer, G.T., and Gerzanich, V. (2012). Sulfonylurea receptor 1 in central nervous system injury: a focused review. J. Cereb. Blood Flow Metab. 32, 1699–1717.
16. Woo, S.K., Kwon, M.S., Ivanov, A., Gerzanich, V., and Simard, J.M. (2013). The sulfonylurea receptor 1 (Sur1)-transient receptor potential melastatin 4 (Trpm4) channel. J. Biol. Chem. 288, 3655–3667.
17. Chen, M., and Simard, J.M. (2001). Cell swelling and a nonselective cation channel regulated by internal Ca2+ and ATP in native reactive astrocytes from adult rat brain. J. Neurosci. 21, 6512–6521.
18. Gerzanich, V., Woo, S.K., Vennekens, R., Tsymbalyuk, O., Ivanova, S., Ivanov, A., Geng, Z., Chen, Z., Nilius, B., Flockerzi, V., Freichel, M., and Simard, J.M. (2009). De novo expression of Trpm4 initiates secondary hemorrhage in spinal cord injury. Nat. Med. 15, 185– 191.
19. Makar, T.K., Gerzanich, V., Nimmagadda, V.K., Jain, R., Lam, K., Mubariz, F., Trisler, D., Ivanova, S., Woo, S.K., Kwon, M.S., Bryan, J., Bever, C.T., and Simard, J.M. (2015). Silencing of Abcc8 or inhibition of newly upregulated Sur1-Trpm4 reduce inflammation and disease progression in experimental autoimmune encephalomyelitis. J. Neuroinflammation 12, 210.
20. Mehta, R.I., Tosun, C., Ivanova, S., Tsymbalyuk, N., Famakin, B.M., Kwon, M.S., Castellani, R.J., Gerzanich, V., and Simard, J.M. (2015). Sur1-Trpm4 cation channel expression in human cerebral infarcts. J. Neuropathol. Exp. Neurol. 74, 835–849.
21. Kunte, H., Busch, M.A., Trostdorf, K., Vollnberg, B., Harms, L., Mehta, R.I., Castellani, R.J., Mandava, P., Kent, T.A., and Simard, J.M. (2012). Hemorrhagic transformation of ischemic stroke in diabetics on sulfonylureas. Ann. Neurol. 72, 799–806.
22. Simard, J.M., and Chen, M. (2004). Regulation by sulfanylurea receptor type 1 of a non-selective cation channel involved in cytotoxic edema of reactive astrocytes. J. Neurosurg. Anesthesiol. 16, 98–99.
23. Martinez-Valverde, T., Vidal-Jorge, M., Martinez-Saez, E., Castro, L., Arikan, F., Cordero, E., Radoi, A., Poca, M.A., Simard, J.M., and

Sahuquillo, J. (2015). Sulfonylurea Receptor 1 in Humans with posttraumatic brain contusions. J. Neurotrauma 32, 1478–1487.

24. Principalli, M.A., Dupuis, J.P., Moreau, C.J., Vivaudou, M., and Revilloud, J. (2015). Kir6.2 activation by sulfonylurea receptors: a different mechanism of action for SUR1 and SUR2A subunits via the same residues. Physiol. Rep. 3, e12533.

25. Sola, D., Rossi, L., Schianca, G.P., Maffioli, P., Bigliocca, M., Mella, R., Corliano, F., Fra, G.P., Bartoli, E., and Derosa, G. (2015). Sulfonylureas and their use in clinical practice. Arch. Med. Sci. 11, 840–848.

26. Simard, J.M., Tsymbalyuk, N., Tsymbalyuk, O., Ivanova, S., Yurovsky, V., and Gerzanich, V. (2010). Glibenclamide is superior to decompressive craniectomy in a rat model of malignant stroke. Stroke 41, 531–537.

27. Sheth, K.N., Elm, J.J., Molyneaux, B.J., Hinson, H., Beslow, L.A., Sze, G.K., Ostwaldt, A.C., Del Zoppo, G.J., Simard, J.M., Jacobson, S., and Kimberly, W.T. (2016). Safety and efficacy of intravenous glyburide on brain swelling after large hemispheric infarction (GAMES-RP): a randomised, double-blind, placebo-controlled phase 2 trial. Lancet. Neurol. 15, 1160–1169.

28. Kothari, R.U., Brott, T., Broderick, J.P., Barsan, W.G., Sauerbeck, L.R., Zuccarello, M., and Khoury, J. (1996). The ABCs of measuring intracerebral hemorrhage volumes. Stroke 27, 1304–1305.

29. World Medical Association. (2013). World Medical Association Declaration of Helsinki: ethical principles for medical research involving human subjects. JAMA 310, 2191–2194.

30. Bradford, M.M. (1976). A rapid and sensitive method for the quantitation of microgram quantities of protein utilizing the principle of protein-dye binding. Anal. Biochem. 72, 248–254.

31. Clancy, B., and Cauller, L.J. (1998). Reduction of background autofluorescence in brain sections following immersion in sodium borohydride. J. Neurosci. Methods 83, 97–102.

32. Uhlen, M., Bandrowski, A., Carr, S., Edwards, A., Ellenberg, J., Lundberg, E., Rimm, D.L., Rodriguez, H., Hiltke, T., Snyder, M., and Yamamoto, T. (2016). A proposal for validation of antibodies. Nat. Methods 13, 823–827.

33. Foster, M.N., and Coetzee, W.A. (2016). KATP channels in the cardiovascular system. Physiol. Rev. 96, 177–252.

34. Thomzig, A., Wenzel, M., Karschin, C., Eaton, M.J., Skatchkov, S.N., Karschin, A., and Veh, R.W. (2001). Kir6.1 is the principal poreforming

subunit of astrocyte but not neuronal plasma membrane KATP channels. Mol. Cell. Neurosci. 18, 671–690.
35. RStudio Team. (2017). RStudio: Integrated Development for R. Boston, MA. Available at: http://www.rstudio.org (last accessed October 9, 2017).
36. Fox, J., and Weisberg, S. (2011). An R Companion to Applied Regression. Sage: Thousand Oaks, CA.
37. Vilalta, A., Sahuquillo, J., Rosell, A., Poca, M.A., Riveiro, M., and Montaner, J. (2008). Moderate and severe traumatic brain injury induce early overexpression of systemic and brain gelatinases. Intensive Care Med. 34, 1384–1392.
38. Simard, J.M., Sheth, K.N., Kimberly, W.T., Stern, B.J., del Zoppo, G.J., Jacobson, S., and Gerzanich, V. (2014). Glibenclamide in cerebral ischemia and stroke. Neurocrit. Care 20, 319–333.
39. Simard, J.M., Yurovsky, V., Tsymbalyuk, N., Melnichenko, L., Ivanova, S., and Gerzanich, V. (2009). Protective effect of delayed treatment with low-dose glibenclamide in three models of ischemic stroke. Stroke 40, 604–609.
40. Inoue, I., Nagase, H., Kishi, K., and Higuti, T. (1991). ATP sensitive K+ channel in the mitochondrial inner membrane. Nature 352, 244–247.
41. Ardehali, H., and O'Rourke, B. (2005). Mitochondrial K(ATP) channels in cell survival and death. J. Mol. Cell. Cardiol. 39, 7–16. 42.
42. Sun, X.L., Zeng, X.N., Zhou, F., Dai, C.P., Ding, J.H., and Hu, G. (2008). KATP channel openers facilitate glutamate uptake by GluTs in rat primary cultured astrocytes. Neuropsychopharmacology 33, 1336– 1342.
43. Rose, M.E., Huerbin, M.B., Melick, J., Marion, D.W., Palmer, A.M., Schiding, J.K., Kochanek, P.M., and Graham, S.H. (2002). Regulation of interstitial excitatory amino acid concentrations after cortical contusion injury. Brain Res. 935, 40–46.
44. Bullock, R., Zauner, A., Woodward, J.J., Myseros, J., Choi, S.C., Ward, J.D., Marmarou, A., and Young, H.F. (1998). Factors affecting excitatory amino acid release following severe human head injury. J. Neurosurgery 89, 507–518.
45. Jeong, H.K., Ji, K., Min, K., and Joe, E.H. (2013). Brain inflammation and microglia: facts and misconceptions. Exp. Neurobiol. 22, 59–67.

46. Ortega, F.J., Jolkkonen, J., and Rodriguez, M.J. (2013). Microglia is an active player in how glibenclamide improves stroke outcome. J. Cereb. Blood Flow Metab. 33, 1138–1139.
47. Ortega, F.J., Vukovic, J., Rodriguez, M.J., and Bartlett, P.F. (2014). Blockade of microglial KATP-channel abrogates suppression of inflammatory-mediated inhibition of neural precursor cells. Glia 62, 247–258.
48. Simard, J.M., Chen, M., Tarasov, K.V., Bhatta, S., Ivanova, S., Melnitchenko, L., Tsymbalyuk, N., West, G.A., and Gerzanich, V. (2006). Newly expressed SUR1-regulated NC(Ca-ATP) channel mediates cerebral edema after ischemic stroke. Nat. Med. 12, 433–440.
49. Simard, J.M., Woo, S.K., Tsymbalyuk, N., Voloshyn, O., Yurovsky, V., Ivanova, S., Lee, R., and Gerzanich, V. (2012). Glibenclamide-10-h treatment window in a clinically relevant model of stroke. Transl. Stroke Res. 3, 286–295.
50. Nistico, R., Piccirilli, S., Sebastianelli, L., Nistico, G., Bernardi, G., and Mercuri, N.B. (2007). The blockade of K(+)-ATP channels has neuroprotective effects in an in vitro model of brain ischemia. Int. Rev. Neurobiol. 82, 383–395.
51. Leon Guerrero, C.R., Pathak, S., Grange, D.K., Singh, G.K., Nichols, C.G., Lee, J.M., and Vo, K.D. (2016). Neurologic and neuroimaging manifestations of Cantu syndrome: a case series. Neurology 87, 270– 276.
52. Ortega, F.J., Gimeno-Bayon, J., Espinosa-Parrilla, J.F., Carrasco, J.L., Batlle, M., Pugliese, M., Mahy, N., and Rodriguez, M.J. (2012). ATPdependent potassium channel blockade strengthens microglial neuroprotection after hypoxia-ischemia in rats. Exp. Neurol. 235, 282–296.
53. Patel, A.D., Gerzanich, V., Geng, Z., and Simard, J.M. (2010). Glibenclamide reduces hippocampal injury and preserves rapid spatial learning in a model of traumatic brain injury. J. Neuropathol. Exp. Neurol. 69, 1177–1190.

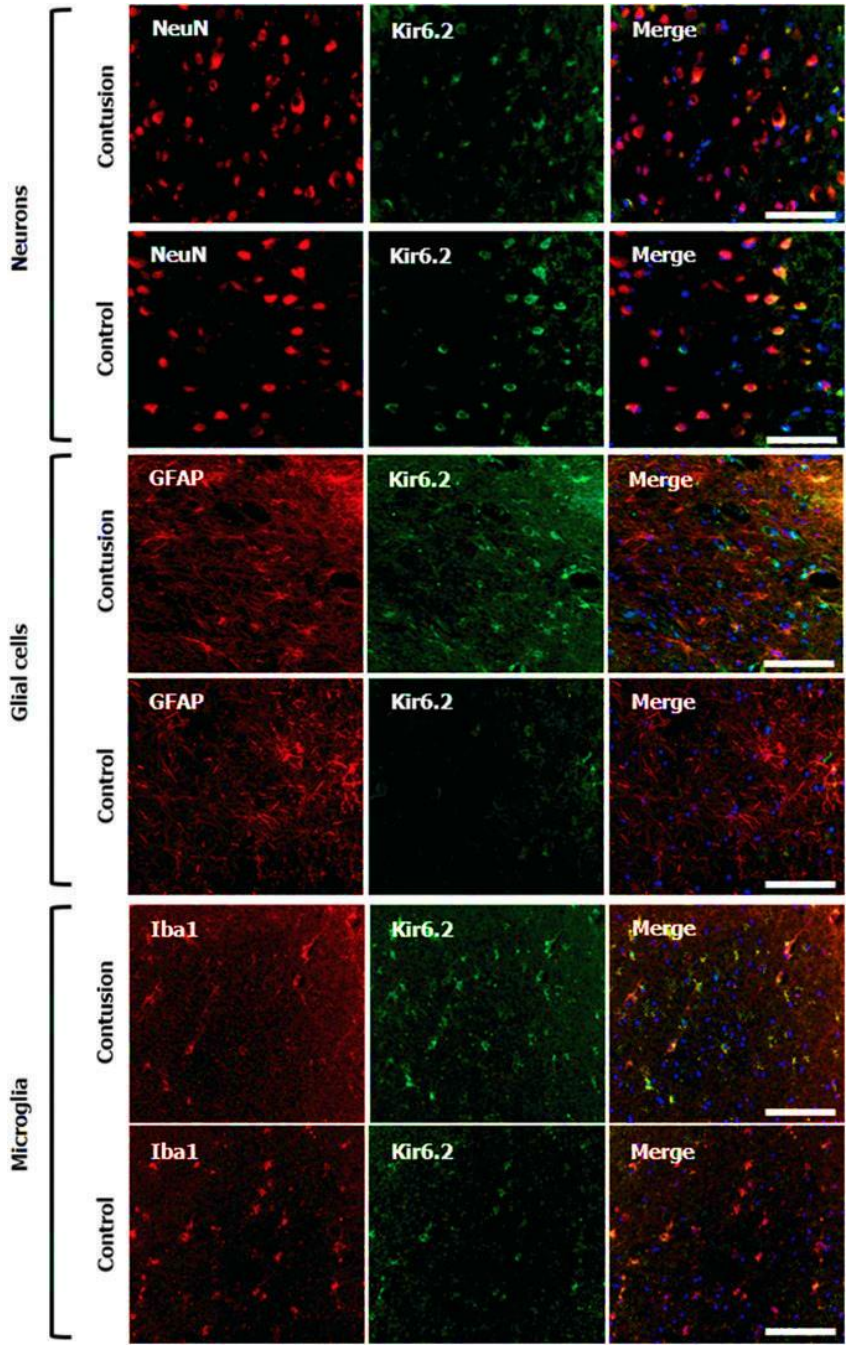


**SUPPLEMENTARY FIG. S1. Kir6.2 differential expression in neurons, glial cells, and microglia. Neurons:** fluorescent double labeling for NeuN (red) and Kir6.2 (green). Merged images are presented in the third column. We show

a similar expression of Kir6.2 in control and contusion samples. **Glial cells:** fluorescent double labeling for glial fibrillary acidic protein (GFAP) (red) and Kir6.2 (green). Merged images are presented in the last column. We observed a significant increase of Kir6.2 expression in contusion samples (this image corresponds to a score of 2 in our semiquantitative scale) in comparison with our controls (image corresponding to a median score of 0.5 in our semiquantitative scale). **Microglia:** fluorescent double labeling for Iba1 (red) and Kir6.2 (green). Merged images are presented in the third column. We observed a similar expression of Kir6.2 in both control and contusion samples (images corresponding to scores 2 and 3, respectively, in the semiquantitative scale). Original magnification = 20x. Scale: 100 μm. Nuclei were counterstained with 4,6-diamino-2-phenylindole (DAPI).

# RESULTADOS Y DISCUSIÓN

# RESULTADOS Y DISCUSIÓN

En esta sección, se resumirán los resultados, la discusión y las limitaciones, así como las futuras perspectivas, de los dos trabajos publicados que conforman esta tesis.

## 1. Modelo animal porcino de infarto maligno de la arteria cerebral media

En los últimos años, se han publicado muchos estudios en los que se demostraba la eficacia de diversos fármacos neuroprotectores en modelos animales de infarto cerebral[96–98]. A pesar de ello, la mayoría de las estrategias que se desarrollan, fallan a la hora de ser trasladadas al paciente. Existe un estudio que demuestra que de todos los fármacos desarrollados para el tratamiento del infarto cerebral entre 1995 y 2015, solo un 4% de ellos ha mostrado ser efectivo[99].

La mayoría de los modelos animales usados en la actualidad, se desarrollan en roedores, y aunque estos modelos son de gran importancia en los primeros pasos para la investigación de cualquier patología, es necesario el uso de modelos animales con un mayor parecido al humano, que permitan una mejor traslación de los resultados[93]. El objetivo de nuestro trabajo, fue el de conseguir desarrollar un modelo animal que nos permitiese el estudio del infarto cerebral maligno, así como de otras patologías relacionadas, como el TCE. Elegimos utilizar un modelo en cerdo común, por las ventajas que presentaba frente a los modelos habituales en roedores: el cerdo es un animal girencefálico, con una proporción sustancia

gris-sustancia blanca muy parecida a la del humano, y con un tamaño adecuado que nos permitía utilizar las mismas técnicas de MM cerebral usadas en el paciente neurocrítico.

## 1.1 Grupo de estudio

Este trabajo fue realizado con cerdos híbridos hembra (*Large White* x *Landrace*) de entre 2.5 y 3 meses de edad, con un peso de entre 30 y 40 kg. Todos los procedimientos fueron llevados a cabo con la aprobación del comité de ética del *Institut de Recerca de Vall d'Hebron* (número de protocolo 69/14) y de acuerdo con la legislación española y las directivas de la Unión Europea para la investigación animal (2010/63/EU).

Un total de 5 animales fueron incluidos en este trabajo. Todos ellos fueron inducidos a anestesia general y sometidos a una oclusión de las ACMs. Dos de los animales (#1 y #4) murieron en un período breve de isquemia y no pudieron completar el protocolo experimental. Ambos animales presentaron hipotensión severa 30 minutos después de la oclusión de las ACMs, que no pudo ser revertida con fluidoterapia y drogas vasoactivas, sufriendo los dos animales finalmente un paro cardíaco.

## 1.2 Período de isquemia y tamaño del infarto

La mediana del período de isquemia al que se sometieron los 5 animales de estudio fue de 6,5 horas (mín: 4 h; máx.: 7,5 h). En cuanto al tamaño del infarto provocado, la mediana fue de 12,3 $cm^3$ (mín: 6,6 $cm^3$; máx.: 15,8 $cm^3$), que en porcentaje representó el 18,4% del tamaño cerebral total (mín: 9,5 %; máx.: 25,1 %). En la **Tabla 4** se resumen los datos obtenidos con cada uno de los animales de experimentación.

**Tabla 4.** Tiempo de isquemia y volumen de infarto en los animales de experimentación

| Animal | Período isquémico (h) | Volumen de infarto ($cm^3$) | Volumen de infarto (%) |
|---|---|---|---|
| **1** | 4.5 | 12.3 | 18.4 |
| **2** | 6.5 | 9.1 | 13.8 |
| **3** | 7.5 | 14.2 | 23.6 |
| **4** | 4 | 6.6 | 9.5 |
| **5** | 7 | 15.8 | 25.1 |

## 1.3 Monitorización de la $PtiO_2$

En todos los animales, exceptuando el #5, la medida de la $PtiO_2$ permitió confirmar la inducción efectiva del infarto. Tras el clipaje de las ACMs de los animales, los niveles de $PtiO_2$ disminuyeron de forma inmediata alcanzando su mínimo valor después de alrededor de 60 min tras la colocación del clip. En el animal #5, los niveles de $PtiO_2$ se mantuvieron normales, pero se confirmó que las ACMs habían sido ocluidas mediante la realización de una angiografía cerebral. En este animal, estudios *post-mortem* mostraron que el sensor de $PtiO_2$ había sido colocado fuera del área infartada, por lo que sus medidas no se correspondían con la realidad. Los datos de la $PtiO_2$ de este animal fueron excluidos de nuestros análisis, al ser considerados erróneos.

En la **Tabla 5** se resumen los valores de la $PtiO_2$ de los animales de experimentación a nivel basal y durante la isquemia post-infarto, excluyendo al animal #5, por los problemas comentados anteriormente.

**Tabla 5.** Valores de $PtiO_2$ de los animales de experimentación en condiciones basales y de isquemia

| Condición | Tiempo (h) | $PtiO_2$ (mmHg) |
|---|---|---|
| Basal | 0 | **27.5** (24.4-39.2) |
| Isquemia | 1 | **0.45** (0-3.2) |
| Isquemia | 2 | **2.8** (1.0-4.6) |
| Isquemia | 3 | **2.2** (1.0-3.1) |
| Isquemia | 4 | **0.0** (0-4.7) |
| Isquemia | 5 | **2.0** (0-3.4) |

Los resultados están expresados como la mediana (mínimo-máximo)

## 1.4 Monitorización de la microdiálisis cerebral

El metabolismo cerebral fue estudiado mediante la monitorización de los niveles de glucosa, lactato, piruvato y glicerol. Para ello, se colocaron 2 catéteres de MD en el cerebro de los animales: uno en la zona del core del infarto y otro en la penumbra isquémica.

**Cambios en el core:** se detectó una reducción significativa de la concentración de glucosa cerebral en todos los animales, inmediatamente después de la oclusión de las ACMs, con excepción del animal #4. El análisis *post-mortem* de este animal reveló que el catéter de MD había sido colocado en el área infartada, pero había una importante circulación colateral alrededor del tejido necrótico, que podría explicar las lecturas de glucosa. En todos los animales, la bajada de la glucosa dio lugar a un descenso de los niveles de piruvato hasta niveles indetectables, acompañados de un

incremento en la concentración de lactato. Por todo lo anterior, hubo un aumento en el ratio lactato/piruvato. En los 5 animales se detectó también un aumento en la concentración de glicerol. Las variaciones en la concentración de metabolitos fueron descritas en comparación con los resultados obtenidos a nivel basal (**Tabla 6**).

**Tabla 6.** Valores de los metabolitos en condiciones basales y de isquemia en el core del infarto.

| Condición | Tiempo (h) | MD CORE (n= 5) | MD CORE (n= 3) | MD CORE (n= 3) | MD CORE (n= 3) | MD CORE (n= 3) |
|---|---|---|---|---|---|---|
| | | Glucosa (mM) | Lactato (mM) | Piruvato (mM) | LPR | Glicerol (µM) |
| BASAL | 0 | **1,59** (0,92–2,25) | **1,80** (1,2–2,5) | **0,101** (0,072–0,131) | **17,40** (16,1–18,8) | **44,20** (23,0–65,5) |
| ISQUEMIA | 1 | **0,70** (0,14–2,08) | **8,18** (1,56–13,4) | **0,074** (0,016–0,142) | **64,90** (19,5–853) | **77,60** (37,5–217) |
| ISQUEMIA | 2 | **0,09** (0–1,88) | **8,25** (7,25–9,85) | **0,015** (0–0,050) | **3241** (27,2-N/A) | **319** (116–544) |
| ISQUEMIA | 3 | **0,18** (0–2,59) | **7,29** (6,85–9,43) | **0,011** (0–0,047) | **3225** (187-N/A) | **462** (187–734) |
| ISQUEMIA | 4 | **0,15** (0–2,46) | **6,68** (5,84–10,7) | **0,008** (0–0,034) | **6282** (315-N/A) | **545** (306–794) |
| ISQUEMIA | 5 | **0,03** (0–2,02) | **8,87** (5,16–11,2) | **0,003** (0–0,032) | **4202** (346-N/A) | **588** (311–790) |

Resultados expresados como la mediana (mínimo-máximo)

**Cambios en la penumbra:** en esta zona, los cambios registrados en la concentración de los diferentes metabolitos, fueron más

heterogéneos. Se detectó una reducción de alrededor del 50% en los niveles de glucosa, que fue muy marcada en 2 de los animales (#3 y #4), indicando la posible transformación de penumbra en core. Los niveles de lactato aumentaron en la zona de penumbra, pero mucho menos que en el core. La misma tendencia se observó en el ratio lactato/piruvato. En cuanto al glicerol, se vio un aumento en su concentración, pero menos acusado que en el caso del core, exceptuando uno de los animales (#5) (**Tabla 7**).

**Tabla 7.** Valores de los metabolitos en condiciones basales y de isquemia en la penumbra del infarto.

| Condición | Tiempo (h) | MD PN (n= 3) | MD PN (n= 3) | MD PN (n= 3) | MD PN (n= 3) | MD PN (n= 3) |
|---|---|---|---|---|---|---|
| | | Glucosa (mM) | Lactato (mM) | Piruvato (mM) | LPR | Glicerol (µM) |
| **BASAL** | **0** | **2,72*** | **2,40*** | **0,24*** | **9,88*** | **15,1*** |
| **ISQUEMIA** | **1** | **1,22** (0,55–2,19) | **4,54** (4,40–7,32) | **0,25** (0,019–0,321) | **29,9** (13,72–244,5) | **148** (119–244) |
| **ISQUEMIA** | **2** | **1,40** (1,13–1,84) | **4,06** (2,62–4,97) | **0,18** (0,096–0,379) | **27,20** (10,7–27,7) | **103** (98,5–507) |
| **ISQUEMIA** | **3** | **1,21** (1,01–1,64) | **2,94** (2,58–3,40) | **0,26** (0,095–0,292) | **11,70** (9,89–31,2) | **111** (90,2–660) |
| **ISQUEMIA** | **4** | **1,13** (0,29–1,15) | **3,06** (1,91–4,85) | **0,21** (0,062–0,251) | **22,90** (7,6–49,5) | **115** (75,8–882) |
| **ISQUEMIA** | **5** | **1,13** (0,05–1,24) | **2,62** (1,98–8,13) | **0,25** (0,023–0,298) | **27,30** (7,87–116) | **141** (73,3–751) |

Resultados expresados como la mediana (mínimo-máximo).*Los valores basales de penumbra solo están disponibles de uno de los animales (#5). PN: PENUMBRA. LPR: ratio lactato-piruvato.

## 1.5 Análisis del perfil iónico en el espacio extracelular

A partir de las muestras de microdializado obtenidas del core y de la penumbra del infarto, se midieron las concentraciones de los iones $K^+$, $Na^+$ y $Cl^-$. Debido a la cantidad de microdializado que se necesitaba para medir estas concentraciones, no se pudieron obtener datos de las concentraciones en condiciones basales. Se demostró que el core isquémico presentaba un incremento de $K^+$ con respecto a la penumbra, mientras que la penumbra presentaba un ligero aumento de la concentración de $Na^+$ con respecto al core. No se detectaron diferencias en la concentración de $Cl^-$ entre core y penumbra. Los datos se resumieron en la **Tabla 8.**

**Tabla 8.** Concentración de los iones en zonas de penumbra y core

| Área monitorizada | $[Na^+]$ mmol/L | $[K^+]$ mmol/L | $[Cl^-]$ mmol/L |
|---|---|---|---|
| **Core isquémico** | 154.1 (135.3–199.8) | 27.9 (4.0–49.4) | 157.0 (132.3–187.0) |
| **Penumbra isquémica** | 164.0 (130.7–208.0) | 7.5 (3.7–44.0) | 157.7 (147.2–208.0) |

Resultados expresados como la mediana (mínimo-máximo)

## 1.6 Expresión de SUR1 y TRPM4

La expresión de SUR1 y TRPM4 fue analizada en diferentes tipos celulares: neuronas, células endoteliales y astrocitos. Para su estudio, se llevaron a cabo dos tipos de análisis (uno cuantitativo y otro semicuantitativo).

**Análisis cuantitativo:** este tipo de análisis se realizó en neuronas y vasos sanguíneos. Los resultados obtenidos para las dos subunidades, se muestran en la **Tabla 9.**

El análisis de expresión de SUR1 y TRPM4 en **neuronas**, mostró que existían diferencias significativas entre las 3 zonas de estudio (core, penumbra y tejido sano contralateral a la lesión). Se demostró que ambas subunidades se sobre-expresaban en neuronas tanto en muestras de penumbra (test de Tukey, SUR1/TRPM4: $p$ = 0,01) como de core (test de Tukey, SUR1/TRPM4: $p$ < 0,001), con respecto al lado sano contralateral a la lesión. Entre core y penumbra también había diferencias significativas, siendo mayor la expresión de ambas subunidades en el core (test de Tukey, SUR1: $p$ = 0,03; TRPM4: $p$ = 0,01). El análisis de la expresión de SUR1 y TRPM4 en **vasos sanguíneos** no mostró para SUR1 diferencias significativas entre las 3 zonas de estudio. TRPM4 mostró diferencias significativas entre el lado contralateral a la lesión y el core del infarto (test de Tukey, $p$ = 0,01).

**Tabla 9.** Expresión **de SUR1 y TRPM4 en neuronas y vasos sanguíneos**

| | **SUR1 (%) CL** | **SUR1 (%) PN** | **SUR1 (%) Core** | **TPRM4 (%) CL** | **TRPM4 (%) PN** | **TRPM4 (%) Core** |
|---|---|---|---|---|---|---|
| **Neuronas** | 3.63 (0-22.3) | 52.0 (18.6-62.6) | 79.3 (66.9-86.8 | 4.7 (0-19.9) | 32.9 (22.4-37.5) | 58.5 (40.1-64.5) |
| **Vasos sanguíneos** | 40 (4.6-55.7) | 65.3 (51.2-83.9) | 72.8 (32.2-88.7) | 61.3 (43.7-79.6 | 77.8 (75.6-79) | 87.2 (83.3-91.1) |

Resultados expresados como la mediana (mínimo-máximo). CL: contralateral; PN: penumbra.

**Análisis semicuantitativo:** este tipo de análisis nos permitió estudiar la expresión de SUR1 y TRPM4 en astrocitos. La cantidad de astrocitos presentes en las muestras de estudio era moderada. Tanto las muestras de penumbra como de core, presentaron una fuerte sobre-expresión de astrocitos SUR1-positivos en comparación con el tejido contralateral a la lesión. La expresión de astrocitos TRPM4-positivos fue moderada en core y penumbra, pero superior a la detectada en tejido contralateral a la lesión.

**Tabla 10.** Expresión de SUR1 y TRPM4 en astrocitos.

| Tipo de tejido | Cantidad de astrocitos | Astrocitos SUR1-positivos | Astrocitos TRPM4-positivos |
|---|---|---|---|
| Contralateral | 2 | 1 | 1 |
| Penumbra | 2 | 3 | 2 |
| Core | 2 | 3 | 2 |

Resultados expresados en una escala del 0 al 3, donde: 0: ninguna expresión, 1: en pocas células, 2: en muchas células, 3: en todas las células

## 1.7 DISCUSIÓN

El empleo de modelos animales que mimeticen las condiciones patológicas que tienen lugar en el humano, es esencial. Por esta razón, nuestro trabajo pretendía establecer un nuevo modelo animal de infarto maligno por oclusión de la ACM, que además fuese extrapolable a otras patologías como el TCE. El uso del cerdo común (*Sus scrofa domestica*) para el modelo, representaba varias ventajas con respecto al uso tradicional de modelos roedores, como se ha explicado con anterioridad: es un animal girencefálico y con

una proporción de sustancia gris-sustancia blanca, así como un tamaño cerebral más aproximado al humano[93].

Como ya se ha explicado previamente, el modelo se basó en la oclusión de las dos ACMs del animal, mediante el emplazamiento de dos clips quirúrgicos, tras haberle realizado una craniectomía frontotemporal. Este tipo de abordaje quirúrgico es más sencillo que el que proponen otros grupos, como el de la Universidad Aarhus de Dinamarca, en la que se ha establecido un modelo similar. Su modelo se basa en la oclusión transorbital de las ACMs[100], una aproximación mucho más compleja, que además solo permitía el acceso a una de las arterias, existiendo la duda de que el infarto no se produjese en su totalidad, y por lo tanto los volúmenes de infarto fuesen más variables.

Lo que conseguimos con nuestro modelo, fue generar un volumen de infarto consistente y reproducible entre los diferentes individuos de experimentación. Además, los volúmenes de infarto obtenidos eran comparables con aquellos obtenidos en previos modelos de infarto maligno en roedores[101,102]. Otra de las ventajas de nuestro modelo era la oclusión de las ACMs con clips quirúrgicos. Al no ser una oclusión permanente y que se puede retirar de forma sencilla, abre la posibilidad de generar otros modelos de infarto con reperfusión a diferentes tiempos post-isquemia.

### Neuromonitorización

El uso de un modelo animal de mayor tamaño que los roedores, permitió la neuromonitorización de parámetros como la $PtiO_2$ y la MD, que se monitorizan de forma rutinaria en los pacientes neurocríticos, y que son difíciles de monitorizar en animales de pequeño tamaño.

### *Medida de la $PtiO_2$*

La medida continua de la $PtiO_2$ en los animales de experimentación, nos permitió comprobar la correcta realización del infarto. En todos los animales de experimentación en los que el sensor fue colocado correctamente, hubo una bajada inmediata de la $PtiO_2$ a valores cercanos a 0mm Hg, que implicaba una correcta oclusión de las 2 ACMs del animal. Además, la medida de este parámetro actuaba como sustituta de la medida del flujo sanguíneo cerebral pudiendo detectar causas isquémicas y no isquémicas (hipoxia de baja extractividad, hipoxia por *shunt* o hipoxia por disperfusión)[103] de la hipoxia cerebral.

### *Estudio del perfil metabólico durante la isquemia cerebral*

El estudio del perfil metabólico cerebral mediante MD, nos permitió demostrar que los resultados obtenidos de la monitorización horaria de este parámetro, eran consistentes con los patrones detectados en pacientes neurocríticos.

En la zona de penumbra y en la de core, se produjo una reducción de los niveles de **glucosa**, en comparación con las medidas basales de este metabolito. Los bajos niveles de glucosa pueden deberse a la hiperglicólisis, la disfunción energética cerebral u otras causas como la hipoxia y/o la isquemia[104], que tienen lugar en la zona infartada y sus zonas circundantes. Estos niveles reducidos de glucosa ya se habían descrito previamente en pacientes con lesiones del SNC como el TCE, la HSA y el IMACM[88,105].

En cuanto al índice **lactato/piruvato**, en la zona de core se produjo un claro aumento de este índice, mientras que en la penumbra el incremento fue menos acusado. Un elevado índice

lactato/piruvato se relaciona con un aumento de la glicólisis o con la disfunción mitocondrial[106]. El hecho de que sea menor su aumento en la penumbra del infarto, puede deberse a que este tejido se encuentra en una situación menos comprometida que en el core de la lesión. Estos cambios también habían sido descritos previamente en humanos con IMACM[105].

También se detectó un incremento en la concentración de **glicerol**, menos acusado en la zona de penumbra. El glicerol es considerado un biomarcador de daño tisular. La concentración de este metabolito indica el nivel de daño en el parénquima cerebral, pero hay artículos que consideran que no permite la detección temprana de lesiones secundarias[107,108].

Desde un punto de vista metabólico, nuestro modelo permitió reproducir los cambios esperados en una situación de isquemia cerebral permanente, y además, detectar el deterioro metabólico de la zona de penumbra de la lesión.

### *Estudio del perfil iónico durante la isquemia cerebral*

La técnica de MD también nos permitió la medida del perfil iónico de las zonas de penumbra y core isquémico. Los resultados obtenidos de los iones analizados ($K^+$, $Na^+$ y $Cl^-$) también eran consistentes con los patrones encontrados en humanos[109]. El gran aumento de $K^+$ en la zona de core de la lesión con respecto a la zona de penumbra, demostró que el $K^+$ actuaba como un indicador claro del daño neuronal irreversible, que se había producido en esta zona. El cerebro sano dispone de mecanismos para controlar el aumento excesivo de $K^+$. Sin embargo, cuando se produce un evento isquémico, estos mecanismos se inactivan dando lugar a un

aumento de la concentración de este ion, que se puede acabar extendiendo a zonas de penumbra[110]. Con respecto al $Na^+$, se encontraron valores similares de este ion en core y en penumbra, siendo más altos en esta última zona. En algunos trabajos, se explica que durante la isquemia, el edema se desplaza hacia las zonas circundantes al core isquémico, lo que podría explicar la mayor presencia de $Na^+$ en la penumbra[111]. En el caso del $Cl^-$ no hubo diferencias de concentración entre penumbra y core isquémicos. El aumento del tamaño muestral, y el poder contar con la concentración de los metabolitos estudiados en condiciones basales, sería necesario para poder estudiar con más profundidad sus variaciones en las diferentes zonas de lesión.

## Expresión de SUR1 y TRPM4

Los desequilibrios iónicos que tienen lugar tras un evento isquémico, dan lugar a la formación de edema que puede derivar en la acumulación de agua en los espacios intra y extracelular. Estos mecanismos están directamente relacionados con la sobre-expresión de canales iónicos constitutivos o de nueva síntesis, como es el caso del canal SUR1-TRPM4[4]. Hay muchos estudios realizados en humanos y modelos animales en roedores[6,9,42,51,112], que demuestran la importancia de este canal en la formación del edema en diversas patologías del SNC (TCE, HSA, IMACM, etc). En este trabajo, hemos estudiado la expresión de las dos subunidades que componen el canal SUR1-TRPM4 en diferentes tipos celulares, obteniendo resultados similares y consistentes a aquellos estudios llevados a cabo en otros modelos animales y humanos.

La sobre-expresión de TRPM4 en vasos sanguíneos, neuronas y astrocitos de la zona de infarto, ya se había demostrado previamente

en muestras humanas de infarto cerebral[113], siendo los resultados similares a nuestros hallazgos. El estudio de la expresión de SUR1 en estos tipos celulares, también replicó diferentes estudios previos, llevados a cabo en humanos y modelos animales[6,7]. En este último caso, no se encontraron diferencias significativas entre la expresión de SUR1 en vasos sanguíneos del tejido contralateral y las zonas de penumbra o core, pero sí que observamos una tendencia que podría corroborarse aumentando el tamaño muestral de nuestro estudio.

De esta forma, podemos concluir que nuestro modelo ha permitido la reproducción de la expresión diferencial de canales iónicos con un papel esencial en la evolución de la patofisiología de las lesiones post-isquémicas.

### Limitaciones del estudio

Una de las principales limitaciones de este estudio, es que para poder llevar a cabo el diseño experimental propuesto, el investigador necesita de un profundo conocimiento de las características anatómicas, histopatológicas y clínicopatológicas del cerebro de los animales de estudio. Los cerdos, al igual que otros modelos experimentales considerados de "gran tamaño", tienen la desventaja de que tienen una circulación carótida externa prominente, que forma una *rete mirabilis* y a partir de la cual se origina la arteria carótida interna[114,115]. Esta circulación colateral, ha causado que algunos investigadores rechacen al cerdo como posible modelo animal de isquemia cerebral. La presencia de la *rete mirabilis* impide la oclusión de la arteria carótida y sus ramas, usando microcatéteres intravasculares[115]. Sin embargo, estos problemas anatómicos también los podemos encontrar en otros modelos animales de mayor tamaño como gatos, cabras, perros y ovejas[116,117]. La segunda diferencia

anatómica importante entre cerdos y humanos, es que las arterias posteriores comunicantes tienen un gran tamaño en cerdos. Esto provoca que la conexión entre los sistemas circulatorios anterior y posterior esté muy desarrollada en estos animales, en comparación con lo que ocurre en humanos. También es importante añadir que en cada hemisferio del cerebro del cerdo, hay 2 ACMs (una lateral y otra rostral), al contrario que en el humano, que solo hay una por hemisferio. Además de las características anatómicas, existen otro tipo de limitaciones en este estudio. Al tratarse de un estudio piloto, el tamaño muestral es muy reducido. En este trabajo, no intentamos obtener datos estadísticamente significativos, pero sí describir la viabilidad de realizar un modelo de infarto hemisférico en el cerdo común y demostrar sus ventajas con respecto a otros modelos alternativos como los realizados en roedores.

Otra de las limitaciones importantes, fue que el estudio no estaba diseñado para realizar un infarto con reperfusión, y por lo tanto no se han presentado datos de las lesiones post-reperfusión o del tiempo necesario para revertir el infarto. Relacionado con esto, también podemos decir que nuestro modelo se diseñó solamente con el propósito de estudiar las fases iniciales del infarto, y por lo tanto no tenemos datos de supervivencia de los animales o de las secuelas neurológicas a largo plazo de los mismos (las cuales se han estudiado en profundidad en modelos en roedores[118]).

Por último, añadir que la necesidad de usar agentes anestésicos con posibles efectos neuroprotectores (propofol, zolazepam y manitol), no es lo ideal para la realización de nuestro estudio. Sin embargo, prescindir de su uso es complicado, al ser necesarios para el acceso microquirúrgico que permite el clipaje de las 2 ACMs.

# 2. Expresión de Kir6.2 en las contusiones cerebrales post-traumáticas

La expresión de Kir6.2 a nivel cerebral, ha sido estudiada previamente en modelos animales en roedores[119,120], aunque también se ha demostrado su expresión en patologías humanas del SNC, como el Alzheimer[121]. Sin embargo, hasta la publicación de nuestro estudio, no se había estudiado su expresión en tejido cerebral procedente de pacientes que habían sufrido un TCE. En nuestro trabajo, se analizó la expresión de Kir6.2 en diferentes tipos celulares (neuronas, células endoteliales, astrocitos y microglía) tanto de tejido sano, como de tejido procedente de muestras pericontusionales.

## 2.1 Grupo de estudio

En este segundo trabajo, se incluyeron muestras de tejido pericontusional procedentes de pacientes que habían sufrido un TCE, entre enero de 2006 y julio de 2015. En todos los casos se obtuvo el consentimiento informado de los pacientes o de un representante legal de los mismos (protocolo PR-ATR-68/2007).

La cohorte de pacientes de este estudio estaba compuesta por 42 pacientes, de los cuales 29 (69%) eran hombres y 13 (31%) mujeres, con una mediana de edad de 48 años (mín: 14; máx: 74 años). De estos pacientes, se obtuvieron 43 muestras (2 de ellas de un mismo paciente) a diferentes horas post-TCE, con una mediana de tiempo post-traumatismo de 23 horas (mín: 5, máx: 246 horas). En todos los casos, se calculó el volumen de la contusión, obteniendo una mediana de 44 mL (mín: 13, máx: 170

mL). De los pacientes incluidos en este estudio, 21 (49%) presentaron a su llegada una GCS superior a 9, y por lo tanto fueron catalogados como TCEs moderados. La mortalidad de esta cohorte de pacientes fue de un 7%.

## 2.2 Grupo control

El grupo control estaba constituido por muestras procedentes de resecciones cerebrales de zonas macroscópicamente sanas, efectuadas para acceder a tumores de la base del cráneo extra-axiales o lesiones intraventriculares. Estas muestras fueron recogidas entre abril de 2011 y septiembre de 2015. Al igual que en el grupo de estudio, en todos los casos se obtuvo un consentimiento informado de los pacientes o de un representante legal (protocolo PR-ATR-286/2013).

La cohorte de pacientes que formaba el grupo control estaba compuesta por 6 pacientes, cuyos datos demográficos se indican en la **Tabla 11.**

**Tabla 11.** Datos demográficos de los pacientes control

| | | | | Calidad del tejido | |
|---|---|---|---|---|---|
| **Caso** | **Edad** | **Sexo** | **Patología primaria** | **Edema** | **Ischemia** |
| 1 | 57 | M | Meningioma meningotelial | 0 | 2 |
| 2 | 59 | M | Meningioma psamomatoso | 0 | 1 |
| 3 | 31 | M | Schwannoma facial | 0 | 1 |
| 4 | 2 | H | Tumor rabdoide | 1 | 2 |
| 5 | 66 | H | Quiste epidermoide | 1 | 2 |
| 6 | 25 | M | Lesión del lóbulo izquierdo temporal | 1 | 0 |

0: ausente; 1: leve; 2: moderado; y 3: severo. M: mujer; H: hombre

En todos los tejidos provenientes de pacientes control, se analizó el grado de isquemia y/o edema presentes. En la escala usada para evaluar estos dos parámetros (0: ausente; 1: leve; 2: moderado; y 3: severo), se descartaron todos aquellos tejidos con isquemia y/o isquemia superiores a 2.

## 2.3 Expresión global de Kir6.2

Los niveles de Kir6.2 se compararon mediante western blot (WB) entre muestras de contusión y de tejido sano (**Fig.7**). Se evaluaron 33 muestras provenientes de 32 pacientes con TCE (21 hombres y 11 mujeres). Los resultados fueron comparados con 5 muestras control. El análisis de los datos mostró un aumento significativo en la expresión de Kir6.2 en muestras de contusión (mediana: 1,03; mín.: 0,32, máx.: 1,84) en comparación con los controles (mediana: 0,64; mín.: 0,38, máx.: 0,93) (test Wilkoxon; $p$ = 0.014).

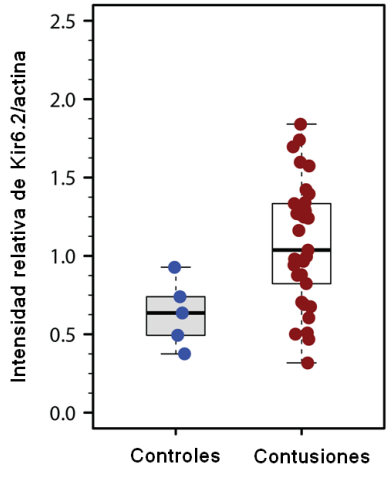


**Fig. 7. Niveles de Kir6.2 en muestras de control y contusión.** Box-plots de la intensidad relativa de Kir6.2 en muestras de control y contusión, mostrando un aumento significativo de esta proteína en las muestras de contusión (p = 0.014). Datos normalizados con β-actina.

## 2.4 Expresión de Kir6.2 en diferentes tipos celulares

La expresión de Kir6.2 en diferentes tipos celulares, fue estudiada por inmunofluorescencia en 29 muestras de contusión provenientes de 28 pacientes (23 hombres y 5 mujeres), que fueron comparadas con 4 muestras control. Se estudió la presencia o ausencia de esta subunidad mediante análisis cuantitativos y semicuantitativos.

**Análisis cuantitativo.** Este análisis fue llevado a cabo para cuantificar neuronas y vasos.

- **Neuronas.** La mediana del porcentaje de neuronas Kir6.2-positivas en controles fue de 16,5% (mín.: 6,1, máx.: 59,0 %), mientras que en el caso de las contusiones fue de un 1,8% (mín.: 0, máx.: 69,3 %). No se observaron diferencias significativas entre ambos grupos (**Figura 8**).
- **Vasos sanguíneos.** No se encontró expresión de Kir6.2 en ninguna de las muestras de contusión o de tejido sano. Por esta razón, no se realizó ningún tipo de cuantificación en este tipo celular.

**Análisis semicuantitativo.** Este tipo de análisis fue realizado en astrocitos y microglía.

- **Astrocitos (células GFAP-positivas).** En 1 control y 4 de las 29 muestras de contusión examinadas, no encontramos células GFAP-positivas, por lo que excluimos estas muestras de nuestro análisis. El estudio de las demás muestras, demostró que los tejidos control presentaban una muy baja expresión de Kir6.2 en células GFAP-positivas (mediana: 0,5; mín.: 0, máx.: 1), en comparación con los tejidos de contusión (mediana: 2; mín.: 0, máx.: 3). Estas diferencias eran estadísticamente significativas (test Wilkoxon, $p$ = 0,03), como se muestra en la **Figura 8**.

- **Microglía (células Iba1-positivas).** En 2 de los 4 controles y en 7 de las 29 muestras de contusión, no observamos células Iba1-positivas, por lo que como en el caso anterior, descartamos estas muestras para nuestro análisis. En las muestras incluidas en el análisis, encontramos que la expresión de Kir6.2 en células Iba1-positivas de muestras control era elevada (mediana: 2), al igual que en las muestras de contusión (mediana: 2,25; mín.: 1, máx.: 3), como se indica en la **Fig. 8.** Las diferencias entre las muestras de contusión y control no eran significativas (test Wilkoxon, $p$ = 0.29).

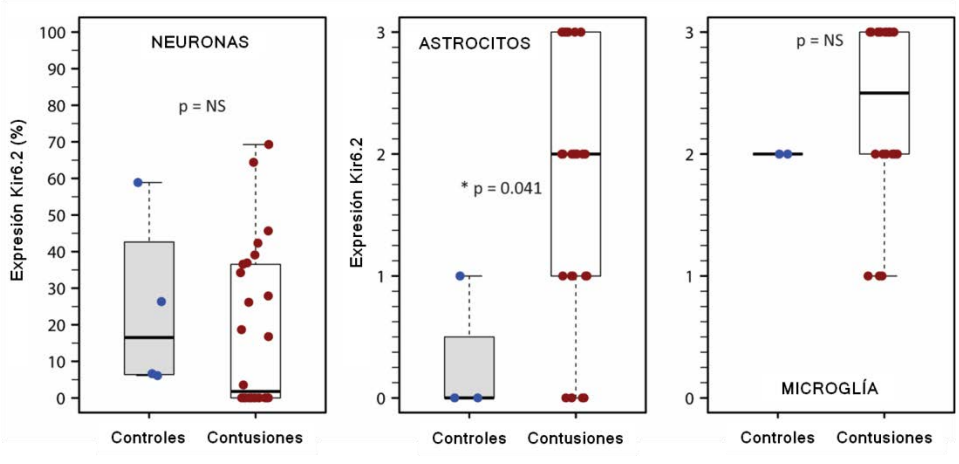


**Fig.8. Expresión de Kir6.2 en neuronas, astrocitos y microglía.** De izquierda a derecha, box-plots representativos de la expresión de Kir6.2 en neuronas (en porcentaje), en astrocitos y microglía (usando una escala semicuantitativa del 0 al 3). Los resultados mostraron un incremento significativo de Kir6.2 en astrocitos de las muestras de contusión (test Wilkoxon, $p$ = 0,03). No se encontraron diferencias significativas para neuronas y microglía. Los asteriscos indican diferencias estadísticamente significativas (*p < 0.05). NS: No significativo.

En todos los tipos celulares se estudió si existía una correlación temporal entre la expresión de Kir6.2 y el tiempo post-TCE de las muestras. No se encontraron diferencias significativas en ninguno de los casos.

## 2.5 DISCUSIÓN

Los mecanismos moleculares y las cascadas bioquímicas, implicadas en la evolución de las contusiones cerebrales postraumáticas, inducen un grado variable de alteración de la BHE. Esto da lugar al aumento de la permeabilidad a iones, que puede desembocar en la extravasación de proteínas y la transformación hemorrágica de la lesión, en última instancia. Entre los canales iónicos implicados en este proceso, cabe destacar el canal SUR1-TRPM4, que ha demostrado jugar un papel muy importante en la formación del edema cerebral[4,122]. En estudios clínicos y experimentales, la inhibición de este canal por sulfonilureas, ha inducido una reducción del edema[8,51,101]. Sin embargo, SUR1 también se asocia con otra subunidad formadora de poro, constituyendo el canal SUR1-Kir6.2. Modelos animales en roedores, han demostrado que la depleción de este canal genera una mayor vulnerabilidad a la hipoxia cerebral en los animales[14]. Nuestro trabajo constituye el primer estudio en el que analiza la expresión de Kir6.2 en muestras cerebrales de tejido pericontusional de pacientes que han sufrido un TCE.

### Expresión y distribución celular de Kir6.2

Los resultados que presentamos en nuestro trabajo, demuestran que Kir6.2 no se expresa en vasos sanguíneos, se expresa muy poco en neuronas y moderadamente en microglía. Sin embargo, encontramos que la expresión de esta subunidad era muy elevada

en astrocitos. Como el tejido necrótico de nuestras muestras fue excluido de los análisis en todos los casos, podemos decir que la sobreexpresión de Kir6.2 en astrocitos se da en tejido cerebral estructuralmente preservado. Este tejido fue denominado por Kurland *et al* "penumbra" peri-contusional[24], un tejido muy similar a la zona de penumbra isquémica descrita en los infartos cerebrales, un concepto que ya hemos descrito con anterioridad[95].

La expresión de Kir6.2 en astrocitos se localizaba no solo a nivel de membrana, sino que también la podíamos observar en el citoplasma celular. Estos resultados, sugerían que Kir6.2 probablemente se encontraba localizado en el retículo endoplásmico (donde se sintetiza), y también en las mitocondrias. Los canales mito$K_{ATP}$ ya habían sido descritos previamente en células del hígado de ratas[123]. Estos canales son los responsables de regular el volumen de las mitocondrias, así como su potencial de membrana, y podrían ser de gran importancia en los procesos moleculares implicados en el precondicionamiento isquémico[124].

### Importancia de la expresión de Kir6.2 en astrocitos

Los astrocitos, son células del SNC que, entre otras funciones, actúan como recaptadores del glutamato presente en el espacio extracelular. Su actividad permite que los niveles de glutamato se mantengan por debajo de niveles que podrían ser tóxicos para las neuronas[105]. En modelos experimentales y estudios llevados a cabo en clínica, se ha demostrado que después de un TCE, los niveles de glutamato extracelular aumentan de forma considerable[125,126]. Existen algunos estudios, que relacionan los canales mito$K_{ATP}$ con el transporte de glutamato al interior de los astrocitos[127], mecanismo que podría dar explicación a la sobre-expresión de Kir6.2 en tejido

pericontusional, y a la vez apoya la hipótesis del papel neuroprotector que tendría esta subunidad. Sin embargo, solamente podemos considerar esto como una hipótesis de trabajo que necesita de más experimentos y datos para poder ser demostrada o refutada.

### Expresión de Kir6.2 en microglía

La moderada expresión de Kir6.2 en microglía fue un resultado inesperado. Previos estudios demostraban que la microglía presentaba un aumento en la expresión de SUR1 y los canales $K_{ATP}$, después de recibir estímulos pro-inflamatorios[128,129]. También se había descrito en estos estudios, que los canales $K_{ATP}$ regulaban la liberación de mediadores inflamatorios y factores tróficos[128]. Creemos que el principal problema en nuestro estudio, que no nos permitió detectar un aumento de la expresión de Kir6.2 en la microglía, fue el hecho de que en nuestras muestras control había presencia de microglía activa, probablemente debida a la manipulación de las muestras durante su explantación quirúrgica. Para poder llegar a conclusiones más sólidas, deberíamos aumentar nuestro tamaño muestral tanto de tejido control como de tejido pericontusional.

### Co-existencia de Kir6.2 y TRPM4

SUR1 actúa como regulador de las dos subunidades formadoras de poro Kir6.2 y TRPM4. El canal SUR1-Kir6.2 se expresa de forma constitutiva en las neuronas del SNC[130], mientras que el canal SUR1-TRPM4 se expresa *de novo* tras algunas patologías del mismo[112]. El bloqueo de estos canales tiene efectos contrarios en las lesiones traumáticas e isquémicas del SNC. La apertura del canal SUR1-Kir6.2 induce la hiperpolarización de la célula y tiene un efecto neuroprotector durante episodios de hipoxia/isquemia o de estrés metabólico[131]. Por otro lado, el canal SUR1-TRPM4 promueve la despolarización de las células, y puede inducir (junto con otros

mecanismos) la formación de edema citotóxico y en último caso la muerte oncótica celular[42].

Como ya hemos explicado anteriormente, el bloqueo de SUR1 con sulfonilureas como la glibenclamida, ha demostrado ser beneficioso para el tratamiento de las lesiones secundarias isquémicas y traumáticas[8,10,51]. El bloqueo de SUR1, induciría el bloqueo de las 2 subunidades formadoras de poro (Kir6.2 y TRPM4), lo que podría parecer contradictorio al tener ambas funciones opuestas. Sin embargo, existen trabajos en los que se plantea que la excesiva activación de los canales $K_{ATP}$ durante situaciones patológicas, podría tener efectos deletéreos[132,133]. La hipótesis que plantean estos trabajos es que la activación excesiva de estos canales durante la isquemia, aumenta la salida de $K^+$ al espacio extracelular, reduciéndose su concentración en el interior de la célula. Este desequilibrio iónico, podría inducir la activación de la bomba $Na^+/K^+$, incrementándose el consumo de ATP residual que quedaría en la célula, e induciendo su muerte temprana por falta de energía. Es por este motivo, por el que el bloqueo de los canales $K_{ATP}$ durante situaciones de isquemia, permite una reducción del consumo de ATP y la preservación de la función celular[133]. Otros estudios apoyan la hipótesis de los efectos deletéreos de un aumento en la función de los canales $K_{ATP}$[134,135]. Uno de ellos se centra en el estudio del síndrome de Cantú, una patología que resulta de mutaciones presentes en los genes que codifican la subunidad SUR2, que se une a la subunidad formadora de poro Kir6.1. Esta mutación altera la función de los canales $K_{ATP}$, provocando que estos permanezcan abiertos cuando deberían encontrarse cerrados. La sobre-activación de estos canales induce problemas en la vasoconstricción[134]. Otro de los estudios, llevado a cabo en un modelo experimental, muestra que la microglía reactiva sobreexpresa SUR1 y Kir6.2 bajo condiciones de isquemia cerebral. Se considera que la sobre-expresión de estos canales $K_{ATP}$ regula la liberación de mediadores

pro-inflamatorios como el óxido nítrico, la interleucina 6 y el factor de necrosis tumoral alpha[135].

Todo esto sugiere que el bloqueo de SUR1 y por lo tanto de las subunidades formadoras de poro Kir6.2 y TRPM4, podría ser beneficioso para el tratamiento de patologías del SNC, como los TCEs, los infartos cerebrales, etc.

### Limitaciones del estudio

La principal limitación de este trabajo fue el reducido número de muestras control, así como el tipo de muestras control con las que contábamos. Como ya hemos explicado anteriormente, estas muestras proceden de pacientes a los que se les opera para acceder a lesiones extra-axiales de la base del cráneo o para acceder a lesiones intraventriculares. Estas muestras, por lo tanto, no son comparables a las muestras controles de animales o al tejido *post-mortem*. En una trabajo anterior de nuestro grupo[6], demostramos que en este tipo de controles había un incremento moderado de SUR1, más acusado en vasos sanguíneos. En el trabajo actual, lo que encontramos fue que había una expresión moderada de Kir6.2 en la microglía de los controles. Este tipo de controles también se habían reportado anteriormente en algunos modelos animales. En un modelo animal en rata de TCE leve/moderado, llevado a cabo por Patel y colaboradores[136], demostraron que aquellos animales denominados "sham" (a los que se les hacía una craneotomía sin lesión por impacto cortical), presentaban también expresión de SUR1 en las células endoteliales. Todo esto, confirma que cualquier intervención (incluyendo la cirugía en sí misma y la resección del tejido), puede inducir una activación de la síntesis de SUR1 y Kir6.2 en el cerebro. A pesar de estas limitaciones, creemos que nuestros

controles eran adecuados, siempre que fuesen interpretados como "controles sham".

Otra de las limitaciones de este estudio era que no estaba diseñado para manipular Kir6.2, ya que solo describimos su expresión en diferentes tipos celulares. Por lo tanto, solo podemos hacer hipótesis sobre los beneficios potenciales de la manipulación de este canal. Como tampoco hicimos un estudio en detalle de la localización de Kir6.2 en los diferentes compartimentos celulares, tampoco podemos concluir si el aumento de Kir6.2 se centra en la mitocondria o en la membrana celular.

# CONCLUSIONES

# CONCLUSIONES

## *CAPÍTULO 1*

1. El desarrollo de un modelo animal porcino de infarto maligno, mediante craneotomía frontotemporal y clipaje de las 2 ACMs es factible y reproducible.
2. Nuestro modelo animal porcino de IMACM permite, mediante la MM de los animales, la reproducción de los desajustes metabólicos e iónicos que tienen lugar tras la isquemia cerebral en humanos. Además, también permite el estudio de las diferentes zonas del área infartada como la penumbra y el core isquémicos, que nos ayudan a una mejor comprensión de la patofisiología y la evolución del edema cerebral isquémico. Este modelo podría ser extrapolable a otras patologías como la isquemia post-traumática.
3. El análisis de las muestras cerebrales de nuestro modelo animal, reproduce la expresión diferencial que tiene lugar en humanos, de canales iónicos (SUR1 y TRPM4) con un papel esencial en la evolución de la patofisiología de las lesiones post-isquémicas y post-traumáticas.
4. Este modelo animal permitirá probar nuevas estrategias terapéuticas que podrían ser útiles a la hora de reducir el edema cerebral, y así poder mejorar el pronóstico funcional de los pacientes con patologías similares.

*CAPÍTULO 2*

5. La subunidad formadora de poro Kir6.2, regulada por SUR1, se sobre-expresa en el citoplasma y en la membrana plasmática de astrocitos de tejido cerebral pericontusional humano. La expresión de esta proteína, no sigue un patrón temporal determinado.
6. Kir6.2 se expresa en microglía y neuronas, pero no en vasos sanguíneos de muestras de tejido cerebral control y pericontusional humanos.
7. Nuestros hallazgos sugieren que los canales regulados por SUR1, TRPM4 y Kir6.2, juegan un papel esencial en la patofisiología molecular de las contusiones cerebrales traumáticas. Su modulación farmacológica podría actuar como una potencial diana terapéutica.

# ANEXOS

## Anexos I

# Kir6.2 pore-forming unit is overexpressed under hypoxia but does not influence glutamate uptake in human cultured astrocytes

**Lidia Castro[1], Noelia Montoya[1], David Sánchez-Ortiz[1], Maria-Antonia Poca[1,2], Susana González-Granero[3], J.M. García-Verdugo[3], Joan Seoane[4], J. Marc Simard[5] and Juan Sahuquillo[1,2].**

**1** Neurotraumatology and Neurosurgery Research Unit (UNINN), Vall d'Hebron Research Institute (VHIR), Universitat Autònoma de Barcelona, Barcelona, Spain, **2** Department of Neurosurgery, Vall d'Hebron University Hospital, Universitat Autònoma de Barcelona, Barcelona, Spain, **3** Comparative Neurobiology Unit, University of Valencia, Valencia, Spain. **4** Cancer and Genetic Expression Unit, Vall d'Hebron University Hospital Oncology Institute (VHIO), Barcelona, Spain, **5** Departments of Neurosurgery, Physiology and Pathology, University of Maryland School of Medicine, Baltimore, MD, USA.

## Abstract

Adenosine triphosphate (ATP)-sensitive potassium ($K_{ATP}$) channels are a collection of structurally distinct channels that couple the cell's energetic status—by sensing intracellular concentrations of ATP ($[ATP]_i$)— with electrophysiological membrane potential. Experimental evidence has showed that in acute lesions of the central nervous system (CNS), the sulfonylurea receptors (SURs) and specifically SUR1—the regulatory subunit of pancreatic and neuronal $K_{ATP}$ channels— are involved in the generation and propagation of brain edema and hemorrhagic conversion. Most $K_{ATP}$ channels in human brain are constituted by the complex SUR1-Kir6.2, which function is still poorly understood. The subunit Kir6.2 of these channels has been demonstrated to be overexpressed in human brain contusions (BCs), and specifically in astrocytes, the most important scavengers of glutamate and $K^+$ of the brain's extracellular space. Our aim was to study the expression of the subunit Kir6.2 under hypoxic and normoxic conditions in human cultured

astrocytes, and also to find if there was a correlation between Kir6.2 expression and glutamate uptake by these cells. Our results showed that Kir6.2 subunit was overexpressed in astrocytes subjected to 24 h of severe hypoxia (0.5% $O_2$; 5% $CO_2$). However, we did not find any relationship between Kir6.2 upregulation under hypoxic conditions and the rate of glutamate uptake by the astrocytes. We also showed that there was no effect in glutamate uptake when plasmalemmal Kir6.2 or mito$K_{ATP}$ channels were inhibited by haloperidol and 5-hydroxidecanoate (5-HD), respectively. Our data suggest the need of further research on SUR1-regulated ionic channels, to develop a better understanding of the pathophysiological role of $K_{ATP}$ channels in BCs and their potential therapeutic applications in acute brain injuries and ischemia.

**Keywords:** hypoxia; human cultured astrocytes; Kir6.2; SUR1; brain contusions

## Introduction

Potassium ($K^+$) channels are expressed in all cell membranes and are involved in many physiological functions.[1] All $K^+$ channels are formed structurally by four subunits assembled around a central water-filled pore through which $K^+$ diffuses out of the cell due to its natural electrochemical gradient, excluding other cations such as $Na^+$, $Ca^{2+}$ and $Mg^{2+}$.[1] Adenosine triphosphate (ATP)-sensitive potassium ($K_{ATP}$) channels were first discovered by Noma in 1983 in the cardiomyocytes of guinea pigs and rabbits.[2] $K_{ATP}$ are a collection of structurally distinct channels that couple the cell's energetic status—by sensing intracellular concentrations of ATP ($[ATP]_i$)— with electrophysiological membrane potential.[3-5] In mammals, $K_{ATP}$ channels are expressed in excitable and endocrine tissues, including cardiomyocytes, pancreatic β-cells, skeletal and smooth muscles, kidney, pituitary, placenta, and brain.[3,5-8]

$K_{ATP}$ channels are hetero-octameric complexes with four pore-forming inwardly-rectifying potassium channel subunits (Kir6.1 or Kir6.2) and four regulatory sulfonylurea receptor subunits (SUR1, SUR2A, or SUR2B).[9] In

pancreatic β-cells, most $K_{ATP}$ channels (SUR1-Kir6.2) are embedded in the plasmalemma, they are opened by default, and they are regulated by blood glucose. When blood glucose concentration increases, $[ATP]_i$ also increases, the $K_{ATP}$ channels close and the plasma membrane depolarizes. Membrane depolarization activates voltage-dependent $Ca^{2+}$ channels, induces $Ca^{2+}$ entry into the cytosol and the release of insulin.[8,10,11] $K_{ATP}$ channels expressed in the mammalian brain have the same structure as the pancreatic β-cell channels —four SUR1 regulatory subunits and four Kir6.2 pore-forming subunits[12]— but their functions are still poorly understood. It has been shown that $K_{ATP}$ channels are activated in the setting of energy failure, both in the myocardium and the brain, and channel opening results in cell hyperpolarization, vasodilation and cardio- and neuro-protective effects.[11,13,14]

Experimental evidence has accumulated that in acute lesions of the central nervous system (CNS) such as aneurysmatic subarachnoid hemorrhage (aSAH), stroke, traumatic brain injury (TBI), and spinal cord injury, the SURs and specifically SUR1—the regulatory subunit of pancreatic and neuronal $K_{ATP}$ channels— are involved in the generation and propagation of ischemic and contusion-induced brain edema and in the hemorrhagic conversion of ischemic stroke and traumatic brain contusions (BCs).[15-17] SUR receptors are not directly involved in ionic transport but they associate with pore-forming subunits to form transmembrane cation channels. Consequently, the deleterious effects of SUR1-overexpression are associated with the pore-forming subunit they regulate, but not with the SUR1 subunit by itself.[4,15] Simard et al. have shown that SUR1 coassembles with the transient receptor potential melastatin 4 (TRPM4) cation channel to form the SUR1-TRPM4 complex.[18-21]. SUR1-TRPM4 is not present in the healthy brain but it is transcriptionally upregulated *de novo* in all the cells of the neurovascular unit in brain ischemia and acute brain injuries.[21,22] A growing body of evidence indicates that SUR1–TRPM4 is a key mediator of brain edema development in ischemic stroke, intracerebral hemorrhage, aSAH, TBI, and the hemorrhagic encephalopathy of prematurity.[23] It has been hypothesized that the main function of SUR1-TRPM4 is to protect the tissue from excessive calcium influx during pathological conditions.[21] However,

sustained channel opening in the setting of ischemia and brain injury is deleterious, and a decrease in ATP—a common situation after ischemic stroke and acute brain injury—, leads to a persistently opened channel that results in a strong inward flux of $Na^+$, cell depolarization and cytotoxic edema.[23] Cytotoxic edema does not cause brain swelling, but initiates a $Na^+$ transendothelial gradient that generates the osmotic force that drives ionic edema, vasogenic edema, loss of endothelial tight junction integrity, the final structural failure of the endothelial cells and the breakdown of the blood-brain barrier (BBB) by oncotic death of endothelial cells.[24] Glibenclamide, a second-generation sulfonylurea, blocks SUR1–TRPM4 with high affinity and specificity, and intravenous glibenclamide has shown effectiveness in reducing ischemic brain edema in rat models of permanent focal ischemia and the hemorrhagic transformation of the infarcts.[25]

Both Kir6.2 and TRPM4 are upregulated in astrocytes of rodents and humans with TBI.[26,27] Recently, we showed that Kir6.2, the canonical pore-forming subunit that coassembles with SUR1, is upregulated in human BCs.[26] The Kir6.2 pore-forming subunit was weakly expressed in neurons, but significantly overexpressed in astrocytes of BCs, and not-detectable in endothelial cells.[26] In astrocytes, Kir6.2 was apparently localized not only in the membrane but also in the cytoplasm[26], suggesting that Kir6.2 is present in the plasmalemma but also in the endoplasmic reticulum and in the mitochondria (mito$K_{ATP}$). Inoe et al. have suggested that mito$K_{ATP}$ could be a key player in the cardio- and neuroprotective molecular processes of ischemic pre-conditioning.[28]

This differential profile of expression, with TRPM4 being overexpressed in endothelial cells and Kir6.2 being overexpressed in astrocytes, suggests that Kir6.2, contrary to the TRPMP4, is not a relevant player in the generation of brain edema. Gerzanich et al. have shown that in a rat model, inhibiting the expression of SUR1 and TRPM4, but not Kir6.2, reduces the hemorrhagic progression of BCs.[19] In animal models, they showed that blocking SUR1-TRPM4 with antisense oligonucleotides reduced brain swelling in ischemia and TBI. However, the role for astrocytes' SUR1-Kir6.2 has not

been identified yet. We speculated that Kir6.2 upregulation observed around BCs might be induced by the hypoxic environment of BCs.[26]

Regarding the potential function of $K_{ATP}$ channels, experimental evidence has shown that mito$K_{ATP}$ and not plasma membrane $K_{ATP}$ are the major players in myocardial preconditioning-induced protection.[29] Astrocytes are the most important scavengers of glutamate and $K^+$ of the brain's extracellular space. They maintain extracellular glutamate concentrations below toxic levels via the astrocytic glutamate transporters (GluTs).[30] Glutamate is a key mediator of hypoxic and ischemic brain damage, and agents that block glutamate receptors significantly reduce neurotoxicity.[31] In cultured astrocytes, Sun et al. showed that mito-$K_{ATP}$ activation by $K_{ATP}$ channel openers increased glutamate transport into astrocytes.[30] We hypothesized that the overexpression of Kir6.2 pore-forming units is induced by different classes of brain hypoxia and that their overexpression could be pivotal for the uptake of glutamate by astrocytes. In an attempt to test these hypothesis, we aimed to study whether hypoxia induced Kir6.2 overexpression in cultured astrocytes and whether plasmalemmal Kir6.2 and mito-$K_{ATP}$ blockage modified glutamate uptake by them. We used an *in vitro* model of human astrocytes in which we reproduced a hypoxic environment to mimic what is found in stroke and in pericontusional brain tissue. Here we show that hypoxia induces HIF-1α and Kir6.2 overexpression but neither the inhibition of plasmalemmal Kir6.2 nor the mito$K_{ATP}$ did influence the astrocyte capacity for glutamate uptake.

## Materials and methods

### Cell culture

Human cryopreserved astrocytes isolated from human fetal brain cerebral cortex (1800; ScienCell Research Laboratories, CA, USA), were incubated in astrocyte medium (AM) (1801; ScienCell Research Laboratories) in poly-L-lysine pretreated plates. AM was supplemented with fetal bovine serum (FBS) (0010; ScienCell Research Laboratories), astrocyte growth supplement (1852; ScienCell Research Laboratories) and

penicillin/streptomycin (0503; ScienCell Research Laboratories). When cells reached 85-90% confluence, they were counted and seeded into pretreated poly-L-lysine wells-plates at different densities depending on the experiment. Immunocytochemistry showed positive staining of most of the cells (~99%) for the astrocytic biomarker S100B (ab4066; Abcam, Cambridge, UK) (**Figure 1**).

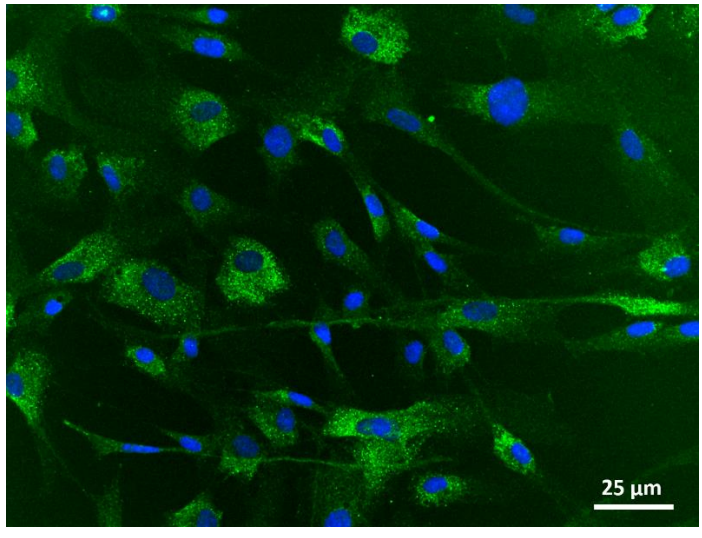


**FIG. 1.** Fluorescent labelling for S100β protein (green) showed that ~99% of the cells were positive for this astrocyte marker. Original magnification = 40X. Scale: 25 µm. Nuclei were counterstained with DAPI (4,6-diamino-2-phenylindole).

## Blockers of plasmalemmal and mitochondrial Kir6.2

Haloperidol and 5-hydroxidecanoate (5-HD) were used as blockers of the plasmalemmal Kir6.2 (haloperidol) and mitochondrial $K_{ATP}$ channels (5-HD) respectively.[30,32] Both blockers were tested *in vitro* to select the optimal dose that did not reduce cell's viability significantly. For this purpose, we performed 3-(4,5-dimethylthiazol-2-yl)-2,5-diphenyltetrazolium bromide (MTT) viability assays [33] in 96-wells plates where astrocytes were seeded at a density of $20x10^3$ cells/mL and treated with different concentrations of both drugs that were compared with their vehicle (VH), which was sterile *Milli-Q* water. These experiments were performed using 3 measurements per

condition (haloperidol, 5-HD and VH), and each of them was considered as an independent biological unit of interest (BU).[34] Cells were treated with haloperidol or 5-HD for 24 h with the concentrations indicated in the first column of **Tables 1** and **2**, respectively. After 24 h treatment, supernatants were discarded and MTT was added at a final concentration of 5 mg/mL. MTT relies on a mitochondrial reductase to convert the tetrazole to formazan. The assumption is that the conversion is dependent on the number of viable cells. After 4 h of incubation at 37°C, MTT was discarded and the formazan crystals formed by the cells were solubilized with dimethylsulfoxide (DMSO). The optic density (OD) of each well was measured at an absorbance of 570 nm using a spectrophotometer (SPECTROstar$^{Nano}$; Biogen, Massachusets, USA), and the following equation was used to calculate cell viability: %cell viability=(ODtreatment*100)/ODvehicle. Results of viability experiments are summarized in **Tables 1** and **2**. We decided to use a final haloperidol concentration of 10 μM in our experiments at which less than 10% of the cells died (**Table 1**). For 5-HD, we used the concentration of 500 nM, in which around of 10% of the cells died because of the treatment (**Table 2**).

**Table 1. Viability assays for haloperidol**

| Haloperidol (μM) | Cells viability (%) |
|---|---|
| 0 μM (VH) | 100 |
| 10 μM | 91.1 (min-max: 81.7-100) |
| 50 μM | 69.0 (min-max: 53.9-82.0) |
| 100 μM | 29.6 (min-max: 24.7-33.2) |
| 250 μM | 13.4 (min-max: 12.9-13.9) |
| 500 μM | 14.4 (min-max: 13.9-15.0) |

Cell's viability (%) at different concentrations of haloperidol (μM). Final selected concentration was 10 μM. At this concentration, less than 10% of the astrocytes died.

**Table 2. Viability assays for 5-hydroxidecanoate**

| 5-Hydroxidecanoate (nM) | Cells viability (%) |
|---|---|
| 0 nM (VH) | 100 |
| 250 nM | 104.2 (min-max: 79.9-121.0) |
| 500 nM | 87.0 (min-max: 68.2-114.6) |
| 1000 nM | 64.7 (min-max: 50.8-76.4) |
| 2500 nM | 66.2 (min-max: 47.2-79.3) |
| 5000 nM | 51.6 (min-max: 47.2-54.8) |

Cell's viability (%) at different concentrations of 5-hydroxidecanoate (nM). Fin selected concentration was 500 µM at wich around 10% of the cells died.

## Hypoxia experiments

For the hypoxic challenge, cells were counted and seeded at $6.7x10^4$ cells/mL into 6-well plates (CLS351, Corning® Costar®, Merck KGaA, Darmstadt, Germany) with the supplemented AM and acclimated in a regular normoxic incubator for 20 h (Galaxy 170R; Eppendorf, Enfield, CT, USA). After this period, the medium was changed to phenol red and FBS-free medium to avoid interferences in quantification assays and the plates were left in the incubator for 4 h for acclimation. After this period, astrocytes received the following treatments: 10 µM haloperidol (766949.4; KernPharma, Barcelona, Spain); 500 nM 5-HD (H-135; Sigma-Aldrich, St. Louis, MO) or VH (deionized water) and the treated plates subjected to either hypoxic (0.5% $O_2$; 5% CO2; 75% humidity; 37°C; 3.8 mmHg $PaO_2$) or normoxic conditions (21% $O_2$; 5% $CO_2$; 75% humidity; 37°C; 158 mmHg $PaO_2$) maintained for 24 h. Hypoxia was induced in an Invivo$_2$ 300 workstation (Baker Ruskinn, Sanford, USA). Normoxic conditions were used as controls.

## Assays of glutamate uptake

Glutamate uptake determination was performed as described by Pinnes and Kanner in 1990,[35] with minor modifications. After 24 h of treatment (with haloperidol, 5-HD or VH), medium was removed by aspiration and 200 nM [$^3$H] L-(3, 4)-glutamate (NET490001MC; PerkinElmer,

Massachusetts, USA) was added to each well in a solution of phenol-red and FBS-free AM with 1 mg/mL HEPES (51558; Sigma-Aldrich), for 15 min at 37°C. After 15 min, glutamate uptake was stopped with 3 washes with NaCl 0.9% at 4°C and cells were lysed using NaOH 0.3M. Cell lysates were centrifuged at 10,000 rpm during 15 min and supernatants were used to measure radioactivity in a liquid scintillation analyzer (4810TR; Perkin Elmer), using Ultima Gold LLT (6013681; PerkinElmer) as the liquid scintillation cocktail. Glutamate uptake by astrocytes was measured in disintegrations per minute (DPMs) of tritiated glutamate that were converted into pmol/mg, after normalizing by the amount of protein of each sample by the Bradford's method.[36] With this methodology, the higher the amount of glutamate the cells took in during the experiment, the greater the amount of radioactivity measured in the scintillation analyzer. We performed replicates for each treatment and control using two wells of the same plate, treated exactly alike, to avoid unexpected variations due to technical issues during experiments. Values were considered acceptable if replicates did not differ more than 25%. We did not discard any of our replicates, and we calculated the mean of the replicates for our posterior calculations. The mean of the two replicas were taken as our experimental unit (EU).

## Western blot

After 24 h of hypoxia/normoxia, cultured cells were washed 3 times with NaCl 0.9% and harvested with ice-cold RIPA buffer (R0278; Sigma-Aldrich). To avoid protein degradation, proteases were inhibited by a protease inhibitor cocktail (11697498001; Roche Diagnostics, Mannheim, Germany). After homogenization, samples remained on ice for 20 min and were centrifuged at 12,000 rpm for 15 min at 4°C. The pellet was discarded and the supernatant was used to quantify protein concentration by the Bradford method using bovine serum albumin (A2153; Sigma-Aldrich) as the standard. Ten µg of protein were loaded on a 10% SDS polyacrylamide gel, separated electrophoretically, and transferred into a tank filled with 1x running buffer (Tris/Glycine/SDS; 161073; Bio-Rad, Hercules, CA) to a polyvinylidene difluoride (PVDF) membrane. A standard molecular

weight marker (Precision Plus Protein Standards-Dual Color; Bio-Rad) was included in a separate lane. The membrane with the transferred proteins was incubated at 4°C overnight in blocking solution with a primary antibody (rabbit anti-hypoxia inducible factor 1α (HIF1α) at 1:1,000; NB100-449; Novus Biologicals, CO, USA or rabbit anti-Kir6.2 at 1:10,000; APC-020; Alomone Labs, Jerusalem, Israel). Blocking solution was composed of 5% skimmed milk powder and tris-buffered saline (TBS) containing 0.1% Tween®-20 (TBST; P9416; Sigma-Aldrich). After washing in TBST, the horseradish peroxidase tagged species-appropriate secondary antibody (A0545; Sigma-Aldrich) was applied at a dilution of 1:2,000 for 1 h. The blot was washed and positive signals were detected by enhanced chemiluminescence (RPN2232; Amersham Biosciences, Bucks, UK) and 2 min exposure to radiographic films. The relative optical density of the resulting bands was normalized to the β-actin loading control.

## Immunocytochemistry (ICC)

After 24 h of hypoxia/normoxia, cultured cells were fixed with 4% paraformaldehyde solution for 30 min. After washing with phosphate buffered saline (PBS) 1X, cells were incubated in a blocking solution containing 4% donkey serum (D9663; Sigma-Aldrich) and 0.2% Triton-X (T8787; Sigma- Aldrich) diluted in PBS1X for 1 h at room temperature. After blocking, cells were incubated overnight at 4°C with the following primary antibodies: anti-S100B (1:100; ab4066; Abcam, Cambridge, UK), anti-Kir6.2 (1:300; APC-020; Alomone Labs) and anti-Kir6.1 (1:100; APC-105; Alomone Labs). Fluorescent-labeled, species-appropriate secondary antibodies were used for signal visualization. The omission of primary antibodies was used as a negative control. Cells were counterstained with polar mounting medium containing anti-fade reagent and the nuclear dye 4,6-diamino-2-phenylindole (DAPI; P36935; Invitrogen). Fluorescent signals were visualized using an epifluorescence microscope (BX61Olympus; Olympus Corporation, Tokyo, Japan). Mean intensity of Kir6.2 labelling was measured using the plug-in *Measure* of ImageJ v1.47 (Wayne Rasband, National Institutes of Health, Bethesda, MD).

### Statistical analysis

Descriptive statistics was obtained for each variable. The Shapiro-Wilk test and inverse probability plot were used to test whether data followed a normal distribution. The mean and the standard deviation were used to describe continuous variables that followed a normal distribution and the median, maximum, and minimum values for continuous variables that were not normally distributed. In the case of medians, the 95% CI was calculated by a bootstrap method. Between-group differences were determined by a two-tailed independent 2-sample t-test or the Wilcoxon-rank sum test, depending on the statistical distribution. Data are presented graphically using box-and-whisker plots. The threshold for statistical significance was $P < 0.05$. Statistical analyses were carried out with Microsoft-enhanced R distribution (Microsoft R Open 3.5.1, Microsoft Corporation 2017, https://mran.microsoft.com) and the integrated development environment R Studio v1.1.463 (RStudio, Inc., Boston, MA, USA; http://www.rstudio.com). The *rcompanion* package was used to calculate the 95% CI for the medians with the bootstrap bias corrected, accelerated method (BCa).[37] For conducting *post hoc* power analyses of the negative results obtained in our experiments we used the standalone power analysis program G*Power v3.1.9 for Windows platforms.[38,39]

## Results

### Effects of hypoxia on astrocytes

In the astrocytes subjected to 24 h of hypoxia (N=4) or normoxia (N=4) we analyzed the presence or absence of the subunit HIF1α by WB. As shown in **Figure 2**, samples under hypoxia showed a statistically significant increase in HIF1α expression (median: 0.47; min-max: 0.24-1.17) compared with normoxic astrocytes (median of 0.27; min-max: 0.08-0.48); (Wilcoxon rank-sum test, $P = 0.0078$).

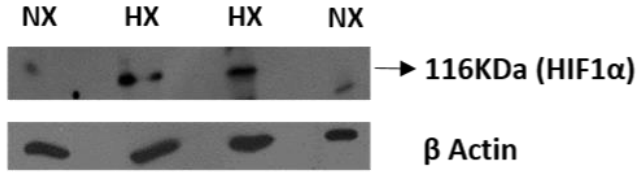


**FIG. 2.** Hypoxia in human astrocytes. Representative WB of human HIF1α in 4 specimens of astrocyte lysates is shown. Lanes 1 and 4 correspond to astrocytes under normoxia (NX) and lanes 2 and 3 correspond to lysates of astrocytes that underwent 24 h of hypoxia (HX). Hypoxic cells showed a band of 116 KDa corresponding to the hypoxia-inducible transcription factor 1α (HIF1α).

Kir6.2 expression was also analyzed by WB and ICC. Under normoxia (N=8), WB showed a median intensity of 0.80 (min-max: 0.23 - 1.16). Kir6.2 significantly increased to a median of 1.79 under hypoxic conditions (N=8; min-max: 0.53 - 3.02); (Wilcoxon rank-sum test, $P$ = 0.005) (**Figure 3A**). ICC also showed a significant increase in the expression of Kir6.2 after 24 h of the hypoxic challenge. The median intensity of Kir6.2 labelling (N =7) was 46.4 in normoxic cells (min-max: 25.9 – 68.8) and it increased significantly to 93.5 (min-max: 82.9 – 116.6) in hypoxic astrocytes (N=7; Wilcoxon rank-sum test, $P$ = 0.0006), as shown in **Figure 3B**. We also analyzed the expression of Kir6.1 subunit in cultured astrocytes by ICC but we did not find the expression of this subunit neither under normoxia nor under hypoxic conditions (data shown in **Figure S1**).

## Glutamate uptake under normoxic and hypoxic conditions

Glutamate uptake results are shown as the mean of two replicates performed for each experiment under hypoxic and normoxic conditions, and are summarized in **Table 3** for haloperidol (N=5) and **Table 4** for 5-HD (N=3). VH was used as a control of each treatment.

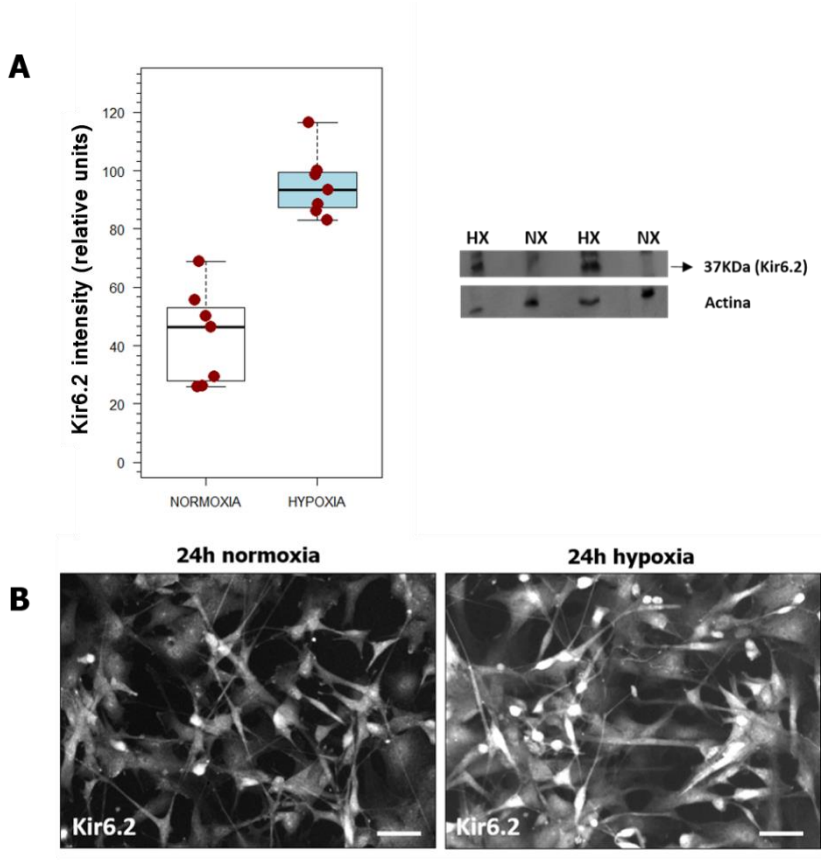


**FIG. 3. Kir6.2 expression in human astrocytes. A)** Left: Box-plots of Kir6.2 intensity (relative units), in normoxic and hypoxic astrocytes treated with vehicle (water). Kir6.2 expression was significantly increased under hypoxic conditions (Wilcoxon rank-sum test, $P$ = 0.005). Right: representative WB of Kir6.2 in 4 specimens of astrocytes lysates (lanes 2 and 4 correspond to astrocytes under normoxia (NX) and lanes 1 and 3, to lysates of astrocytes under hypoxia (HX)). Hypoxic cells showed an increase of Kir6.2 expression (band at 37 KDa). **B)** Fluorescence labelling of Kir6.2 in astrocytes after 24 h of normoxia (left) and hypoxia maintained for 24 h (right). A significant increase in Kir6.2 mean intensity labelling was observed during hypoxia (93.5) in comparison to normoxia (55.6). Original magnification = 40X. Scale: 50 µm. Nuclei were counterstained with DAPI. DAPI, 4,6-diamino-2-phenylindole.

To study glutamate uptake under hypoxia, we compared cells treated with VH under hypoxic and normoxic conditions. The median glutamate uptake in normoxic astrocytes was 75.9 pmol/mg (min-max: 37.2 - 144.9), and

the median for hypoxic astrocytes increased to 110.8 pmol/mg (min: 52.4, max: 152.8 pmol/mg). However, the observed moderate increase in glutamate uptake under hypoxia was not statistically significant compared with normoxic astrocytes ($P$ = 0.442, Wilkoxon rank-sum test for unpaired samples) (**Figure 4**). The required sample size to prove that the mean difference between hypoxic and normoxic conditions was statistically significant for an effect size of 0.42, $P$ < 0.05 and a power of 80% would be 188 (94 observation units per arm).

**Table 3. Glutamate uptake values under haloperidol treatment.**

| | Haloperidol (HX) (pmol/mg) | Haloperidol (NX) (pmol/mg) | Vehicle (HX) (pmol/mg) | Vehicle (NX) (pmol/mg) |
|---|---|---|---|---|
| **N1** | 87.23 | 74.19 | 93.98 | 69.94 |
| **N2** | 132.88 | 133.60 | 141.19 | 131.94 |
| **N3** | 147.94 | 126.68 | 152.81 | 139.1 |
| **N4** | 123.87 | 85.73 | 137.09 | 80.00 |
| **N5** | 88.86 | 86.70 | 97.85 | 71.88 |

Glutamate uptake (pmol/mg) under hypoxic (HX) and normoxic (NX) conditions. Haloperidol concentration: 10μM. Vehicle: water. N = 5.

**Table 4. Glutamate uptake values under 5-HD treatment.**

| | 5-HD (HX) (pmol/mg) | 5-HD (NX) (pmol/mg) | Vehicle (HX) (pmol/mg) | Vehicle (NX) (pmol/mg) |
|---|---|---|---|---|
| **N1** | 55.71 | 43.93 | 52.37 | 37.19 |
| **N2** | 136.98 | 136.49 | 123.82 | 144.87 |
| **N3** | 56.58 | 43.29 | 54.55 | 40.09 |

Glutamate uptake (pmol/mg) under hypoxic (HX) and normoxic (NX) conditions. 5-Hydroxidecanoate (5-HD) concentration: 500nM. Vehicle: water. N = 3.

## Changes in glutamate uptake under normoxia and hypoxia after selective blockage of membrane Kir6.2

Experiments were conducted as replicates of 2 wells under normoxia and hypoxia. Values were considered acceptable if replicates did not differ more

than 25%. Because in no case was variability within replicates above 25% and the experiments were consistent, the EU for this experiment was considered the seeded well under normoxia and hypoxia with the two treatments added (haloperidol and VH). Therefore, we had 4 experimental conditions: normoxia-VH, normoxia-haloperidol, hypoxia-VH and hypoxia-haloperidol. As in our previous experiments, normoxic astrocytes expressed Kir6.2 (**Figure 3B**). We decided to explore whether astrocytes with blockade of the plasmalemmal Kir6.2 incorporated less glutamate independently of the normoxic and hypoxic condition. When glutamate uptake was compared in all VH-treated cell independently of the conditions (hypoxia or normoxia), we did not find any statistically significant differences in glutamate uptake between wells treated with VH and those treated with haloperidol. Hypoxic and normoxic wells (N=20) treated with VH showed a median glutamate uptake of 113.8 pmol/mg (min: 62.3, max: 158.1; 95% CI: 81.4, 136.0) while the median glutamate uptake in the wells treated with haloperidol (N=20) was 108.9 (min: 72.3, max: 149.2; 95% CI: 83.8, 129.0). These differences were not statistically significant (Wilcoxon rank-sum test, W=218, $P$ = 0.636).

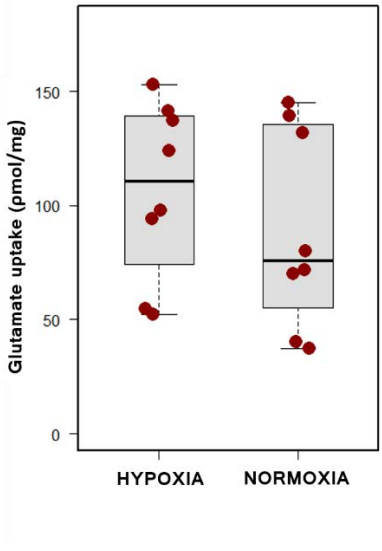


**FIG. 4. Glutamate uptake under hypoxic conditions.** Box plots show glutamate uptake (pmol/mg) in astrocytes treated with vehicle (water) under both hypoxic and normoxic conditions. The observed moderate increase in glutamate uptake under hypoxia was not statistically significant compared with normoxic astrocytes (P = 0.442, Wilcoxon rank-sum test for unpaired samples).

Normoxia. Regarding astrocytes incubated under normoxia, we did not observe any significant effect on glutamate uptake in those cells in which we blocked plasmalemmal Kir6.2 with haloperidol compared with VH-treated wells. The median glutamate uptake for the VH-treated cells in each well (N=10) was 81.4 pmol/mg (min: 62.3, max: 150.4; 95% CI: 69.9, 131.0). When the wells were pretreated with haloperidol the median glutamate uptake was 85.7 pmol/mg (min: 72.3, max: 134.1; 95% CI: 75.4, 128.0). These differences were not statistically significant (Wilcoxon rank-sum test, W=45, $P$ = 0.739).

Hypoxia. Hypoxic cells that overexpressed Kir6.2 and in which plasmalemmal Kir6.2 was blocked with haloperidol did not show any difference in glutamate uptake compared to cells pretreated with VH. When hypoxic cells received VH (N=10), the median glutamate uptake was 136.3 pmol/mg (min: 88.1, max: 158.6; 95% CI: 98.6, 145.0). When the wells were pretreated with haloperidol (N=10) the median glutamate uptake was 121.7 pmol/mg (min: 81.7, max: 149.2; 95% CI: 91.0, 136.0). These differences were not statistically significant (Wilcoxon rank-sum test, W=61, $P$ = 0.436).

## Inhibition of mito$K_{ATPs}$ did not change glutamate uptake by astrocytes

The blockage of mito$K_{ATP}$ channels with 5-HD showed no effects on glutamate uptake by astrocytes neither in hypoxic nor in normoxic conditions. In normoxia, the median glutamate uptake of the cells treated with VH (N=6) was 40.1 pmol/mg (min: 34.5, max: 163.5; 95% CI: 37.1, 126.0). When the wells were pretreated with 5-HD (N=6) the median glutamate uptake was 45.9 pmol/mg (min: 40.6, max: 138.1; 95% CI: 41.3, 135.0). This difference was not statistically significant (Wilcoxon rank-sum test, W=10, $P$ = 0.240). When the same treatments were applied to hypoxic astrocytes, 5-HD did not modify glutamate uptake. Hypoxic wells pretreated with VH (N=6) showed a median glutamate uptake of 55.4 pmol/mg (min: 49.6, max: 125.8; 95% CI: 51.5, 122.0). In the hypoxic astrocytes pretreated with 5-HD the median glutamate uptake was 56.9 (min: 54.1, max: 156.5; 95% CI: 54.1, 107.0). This difference

was not statistically significant (Wilcoxon rank-sum test, W=12, *P* = 0.377).

## Discussion

In 2015, Martinez-Valverde et al. reported that in human post-traumatic BCs, the non-constitutive regulatory unit SUR1 was overexpressed in all cell types of the neurovascular unit but this expression was especially prominent in neurons and endothelial cells around the contusion's core.[17] These authors' findings, endorsed the data from Simard's group pointing at SUR1-TRPM4 channel as a major molecular player in the pathophysiology of BCs and this finding opened the opportunity to modulate the mechanisms of their growth.[17] In a later study, Castro et al. found that the pore-forming subunit Kir6.2—but not Kir6.1—was significantly overexpressed in the astrocytes of human BC specimens.[26] Because SUR1 is the regulatory subunit for both TRMP4 and Kir6.2, and the SUR1-blocker glibenclamide protects the brain from ischemic swelling, our findings raised the question of what could be the pathophysiological role of the SUR1-Kir6.2 channel in traumatic BCs. Experimental and clinical evidence have shown that blocking the SUR1-TRMP4 channel is beneficial for the injured brain.[40,41] In experimental and clinical studies of ischemic stroke, blockade of the SUR1 regulatory subunit by sulfonylureas consistently reduces ischemia-induced brain edema and swelling.[25,40,42] Paradoxically, Kir6.2 and SUR1 null mice are extremely vulnerable to brain hypoxia and exhibit a reduced threshold for hypoxia-induced seizures.[11] In addition, experimental studies have shown that $K_{ATP}$ channels, and specifically mito$K_{ATP}$ —located in the inner mitochondrial membrane— play a key role in preconditioning cardio- and neuro-protection.[29,43] Tai et al. showed that diazoxide, a $K_{ATP}$ channel opener, conferred protection against cell death in PC12 cells exposed to the mitochondrial complex-I blocker rotenone.[43] They also showed that neuroprotection against rotenone toxicity was mediated by activation of the mito$K_{ATP}$ and not by the plasma membrane channels.[43]

Our results showed that the Kir6.2 subunit was overexpressed in astrocytes subjected to 24 h of severe hypoxia (0.5% $O_2$; 5% $CO_2$). This finding reproduces the results of Raeis et al. who showed *in vitro* that SUR regulatory units and Kir6 channels were overexpressed in cardiomyocytes subjected to 24 h of mild hypoxia (2% $O_2$; 5% $CO_2$).[44] These authors showed that in right atrial fragments from children operated for heart disease, low venous oxygen pressure and/or saturation predicted Kir6.1 upregulation while other clinical variables such as low pH, high potassium or low glucose did not correlate with Kir6.1 protein levels.[44] In the same study, the authors used atrial myocytes from neonate rats and exposed them to different conditions (low glucose, mild hypercapnia, high potassium and 2% $O_2$) and they showed that only hypoxia induced overexpression of the Kir6.1/Kir6.2 channel while there was not any significant contribution from low pH, low glucose, or high potassium.[44] These results, together with our previous findings of upregulation of Kir6.2 in astrocytes around BCs[26], suggest that brain hypoxia is a key etiological factor involved in the overexpression of SUR1-Kir6.2. Ischemia in the contusion core and dysperfusion hypoxia in the pericontusional brain —defined by Siggaard-Andersen, as a limitation of oxygen diffusion from the microcirculation to the cells due to edema—, might be critical drivers of Kir6.2 overexpression in BCs.[45,46]

In our experiments, as expected, we observed that severe hypoxia increased the expression of HIF1α, the oxygen-dependent subunit of HIF1 (**Figure 3**). The HIF1 pathway is involved in both the adaption to hypoxia and in governing immune responses. HIF1 is formed by a constitutively expressed β-subunit and a second oxygen-regulated α-subunit.[47] HIFα-subunit has an oxygen-dependent degradation domain that when hydroxylated makes it vulnerable to proteasomal degradation under normoxic conditions.[47] Under normoxia, HIF-1α is degraded by the proteasome and is inactivated. However, under hypoxic conditions, HIF-1 is stable, dimerizes with its constitutively expressed β-subunit and binds to the regulatory regions of its target genes.[47] HIF1 is a major regulator of oxygen within cells and regulates the expression of many genes involved in the adaptative mechanism of most cells to the lack of oxygen, including the shift to

anaerobic metabolism. Woo et al. showed that HIF1 also plays an important role in the transcriptional activation of *Abcc8*— the gene encoding SUR1— in brain ischemia and traumatic brain injury.[48] HIF1 activated *Abcc8* not directly but via upregulation of another transcription factor, the specificity protein 1 (Sp1).[48] Our experiments were not designed to study the regulation of the KCNJ11—the gene encoding Kir6.2— and therefore, whether or not HIF1 is the main activator of Kir6.2 or it is only one of the players in the whole process, as it occurs with SUR1 upregulation, requires further evaluation.

Brain $K_{ATP}$ channels are closed by default under physiological conditions, but they are activated under ischemia/hypoxia, ischemic preconditioning or metabolic inhibition.[30] When opened, they reduce membrane excitability by hyperpolarization of the resting membrane potential and protect the cells from death. We used haloperidol to block Kir6.2 because it dissolves in water and does not need the use of toxic solvents like DMSO. In addition, haloperidol selectively blocks only plasmalemmal Kir6.2 due to direct binding to this subunit and does not block mito$K_{ATP}$ subunits.[32] We did not use other $K_{ATP}$ inhibitors such as glibenclamide, because sulfonylureas inhibit both Kir6.2 and TRPM4 through SUR1 inhibition and both channels are overexpressed under hypoxia. Although we found a significant hypoxia-induced increase in Kir6.2, we did not find any relationship between Kir6.2 overexpression and the rate of glutamate uptake by astrocytes under hypoxia. We also showed that there was no effect in glutamate uptake when either the plasmalemmal Kir6.2 or mito$K_{ATP}$ channels were inhibited by haloperidol and 5-HD, respectively. Our results are in apparent contradiction with that of Sun et al. who showed that $K_{ATP}$ channel's openers facilitate glutamate uptake in rat cultured astrocytes.[30] In rodents, Kir6.1 is the predominant channel in astrocytes, while Kir6.2 expression is found only in neurons.[49,50] In astrocytes from human specimens, we reported that the predominant subunit observed was Kir6.2 and not Kir6.1 (**Figure S2**).[26] In specimens of human pericontusional tissue and controls and also in human astrocytes exposed to hypoxia *in vitro* we did not find Kir6.1 expression (**Figure S2**). These results are consistent with the findings reported by Erginel-Unaltuna et al. who found that in humans, KCNJ8/Kir6.1 is

expressed almost exclusively in the heart but not in other tissues.[51] It has been shown that the function of SUR1-Kir6.2 in humans is similar, if not identical, to the SURX-Kir6.1 in other mammals, and therefore the difference in the pore-forming unit in different species cannot explain the differences observed in the glutamate uptake. We need to emphasize that our study was designed to observe if the blockage of Kir6.2—either in the plasma membrane or in the mitochondria—, modified the uptake of glutamate by astrocytes. However, our negative findings do not allow us to disregard whether the activation of any of the plasmalemmal Kir6.2 and/or mitoKir6.2 by $K_{ATP}$ channel openers (KCOs) such as diazoxide, iptakalim or pinacidil can facilitate glutamate uptake by GluTs in astrocytes as suggested by others.[30]

There is a general agreement that the blockage of SUR1-TRMP4 is neuroprotective in many experimental models of CNS injuries.[21,24,25,40] However, experimental evidence shows that activation of the brain $K_{ATP}$ channels (SUR1-Kir6.2) is neuroprotective and their block can be deleterious and activate both apoptosis and necrotic cell death. Liu et al. showed that mice treated with low dose diazoxide— an activator of mito$K_{ATP}$ channels—, had a significant decrease (60% to 70%) in cortical infarct size after permanent occlusion of the middle cerebral artery.[52] In ischemic stroke, it has been proposed that activation of mito$K_{ATP}$ channels confers neuroprotection by attenuating mitochondrial $Ca^{2+}$ overload.[53] The molecular mechanisms responsible for Kir6.2-mediated neuroprotection are complex and not yet completely clarified. Among others, $K_{ATP}$ channels have been involved in glutamate homeostasis by astrocytes, in the regulation of astrocytic gap junctions, in preconditioning-triggered neuroprotection (mito$K_{ATP}$), in the modulation of glycolytic pathways under hypoxia and in the endoplasmic reticulum stress (ER stress) response to brain ischemia.[52-54] However, Nistico et al. have proposed that an excessive activation of the $K_{ATP}$ channels during oxygen and glucose deprivation on CA1 pyramidal neurons contribute to the ischemic damage and that $K_{ATP}$ channel blockers have neuroprotective actions in an *in vitro* model of brain ischemia.[55] In the same experiment, they showed that both tolbutamide and glibenclamide superfused for 30 min before and during the ischemic period, were able to

rescue the irreversible loss of field potentials typically obtained with 14-min oxygen and glucose deprivation.[55]

## Conclusions and recommendations for future research

Our findings suggest that hypoxia and the transcription factor HIF1 plays a pivotal role in activating Kir6.2 in cultured astrocytes exposed to severe hypoxia. However, blocking plasmalemmal or mito- Kir6.2 did not modify the glutamate uptake by astrocytes. The fact that SUR1 blockers reduce ischemic brain edema through the regulation of the non-constitutive SUR1-TRPM4 channels, and that the activation of the second unit regulated by SUR1 (Kir6.2) is neuroprotective under ischemia, is apparently contradictory. In addition, Nistico et al. have raised the hypothesis that the persistent and excessive activation of $K_{ATP}$ channels may contribute to the ischemic damage, and that blocking of these channels reduces ATP consumption and preserves cell's function.[55]

The failure of some bench-to-bed-side research in brain ischemia and CNS injuries is sometimes related to the incomplete or inaccurate understanding of the underlying molecular mechanisms and signaling pathways involved. To develop a better understanding of the pathophysiological role of $K_{ATP}$ channels in the neurovascular unit wwe need a deeper understanding of the role of SUR1-Kir6.2 in BCs and their potential therapeutic applications in TBI. This knowledge is needed to solve the paradox that blocking SUR1-TRPM4 is beneficial for the injured brain, while blocking SUR1-Kir6.2 might be potentially harmful, due to $K_{ATP}$ channel's protective role. [30,56] One of the mechanisms that needs to be explored is the additional complexity in the structure and regulation of $K_{ATP}$ channels that act as metabolic sensors in a large diversity of cell types. The canonical two-unit structure of $K_{ATP}$ channels, namely the pore-forming subunit (Kir6.x) and a sulfonylurea receptor regulatory subunit, seems to be an oversimplification. Emerging proteomic analysis have shown that $K_{ATP}$ channels are multisubunit macromolecular complexes and that key glycolytic enzymes are in fact relevant subunits involved in the $K_{ATP}$ structure.[57] Dhar-Chowdhury et al. demonstrated that some enzymes directly related to glycolysis—

glyceraldehyde-3-phosphate dehydrogenase, triose-phosphate isomerase and pyruvate kinase— are accessory subunits of the $K_{ATP}$ channels.[58]

The clarification of the underlying mechanisms involved in $K_{ATP}$ channels neuroprotection/damage is a unique opportunity to unravel the molecular pathophysiology of ischemic and brain injuries and also to design better targeted therapies. Further studies should be directed to study cells in which Kir6.2 and TRPM4 have been blocked independently. We are already working in gene silencing of Kir6.2 and TRPM4 in astrocytes and other cells of the perivascular unit by small interfering RNA (siRNA). By selective deleting these channels in astrocytes and exposing them to energy-limited conditions (ischemia and hypoxia) we can discriminate their differential role in changes in the energy metabolic profile and cell survival. A better understanding of the main roles involved in SUR1-regulated channels may help in designing targeted molecular therapies for CNS injuries that block the deleterious signaling pathways but that do not interfere with potential endogenous neuroprotective mechanisms.

### Author contributions to the study

Author contributions to the study and manuscript preparation include the following. Conception and design: Sahuquillo, Castro. Acquisition of data: Castro, Montoya, González-Granero, García-Verdugo. Analysis and interpretation of data: Sahuquillo, Castro, Simard. Statistical analysis: Sahuquillo and Castro. Drafting the article: Sahuquillo, Simard, Castro. Critically revising the article: all authors. Reviewed submitted version of manuscript: all authors. Approved the definitive version of the manuscript on behalf of all authors: Sahuquillo. Study supervision: Sahuquillo, Seoane, Simard.

## Acknowledgements

This work was supported in part by the Fondo de Investigación Sanitaria (Instituto de Salud Carlos III) with grant PI15/01228, which was co-financed by the European Regional Development and awarded to Dr. J.

Sahuquillo and by the grant AECC-GCT/2017 from the Asociación Española Contra el Cáncer to Drs J. Sahuquillo and J. Seoane.

## Author Disclosure Statement

JMS holds a U.S. patent (#7,285,574), ''A novel non-selective cation channel in neural cells and methods for treating brain swelling.'' JMS is a member of the scientific advisory board of and holds shares in Remedy Pharmaceuticals. No support, direct or indirect, was provided to JMS, or for this project, by Remedy Pharmaceuticals. All other authors report no conflict of interest concerning the materials or methods used in this study or the findings specified in this article.

## References

**1.** Miller, C. (2000). An overview of the potassium channel family. Genome biology 1, REVIEWS0004.

**2.** Noma, A. (1983). ATP-regulated $K^+$ channels in cardiac muscle. Nature 305, 147-148.

**3.** Ashcroft, F.M. (1988). Adenosine 5'-triphosphate-sensitive potassium channels. Annu Rev Neurosci 11, 97-118.

**4.** Nichols, C.G. (2006). KATP channels as molecular sensors of cellular metabolism. Nature 440, 470-476.

**5.** Liu, Z., Cai, H., Dang, Y., Qiu, C. and Wang, J. (2016). Adenosine triphosphate-sensitive potassium channels and cardiomyopathies (Review). Molecular medicine reports 13, 1447-1454.

**6.** Lybaert, P., Hoofd, C., Guldner, D., Vegh, G., Delporte, C., Meuris, S. and Lebrun, P. (2013). Detection of K(ATP) channels subunits in human term placental explants and evaluation of their implication in human placental lactogen (hPL) and human chorionic gonadotropin (hCG) release. Placenta 34, 467-473.

**7.** Insuk, S.O., Chae, M.R., Choi, J.W., Yang, D.K., Sim, J.H. and Lee, S.W. (2003). Molecular basis and characteristics of KATP channel in human corporal smooth muscle cells. International journal of impotence research 15, 258-266.

**8.** Szeto, V., Chen, N.H., Sun, H.S. and Feng, Z.P. (2018). The role of KATP channels in cerebral ischemic stroke and diabetes. Acta Pharmacol. Sin. 39, 683-694.

**9.** Flagg, T.P. and Nichols, C.G. (2011). "Cardiac KATP": a family of ion channels. Circ Arrhythm Electrophysiol 4, 796-798.

**10.** Yamada, K. and Inagaki, N. (2002). ATP-sensitive K(+) channels in the brain: sensors of hypoxic conditions. News Physiol Sci 17, 127-130.

**11.** Yamada, K. and Inagaki, N. (2005). Neuroprotection by KATP channels. Journal of molecular and cellular cardiology 38, 945-949.

**12.** Seino, S. (2003). Physiology and pathophysiology of KATP channels in the pancreas and cardiovascular system. Journal of Diabetes and its Complications 17, 2-5.

**13.** Stoller, D.A., Fahrenbach, J.P., Chalupsky, K., Tan, B.H., Aggarwal, N., Metcalfe, J., Hadhazy, M., Shi, N.Q., Makielski, J.C. and McNally, E.M. (2010). Cardiomyocyte sulfonylurea receptor 2-KATP channel mediates cardioprotection and ST segment elevation. Am J Physiol Heart Circ Physiol 299, H1100-1108.

**14.** Murry, C.E., Jennings, R.B. and Reimer, K.A. (1986). Preconditioning with ischemia: a delay of lethal cell injury in ischemic myocardium. Circulation 74, 1124-1136.

**15.** Benarroch, E.E. (2017). Sulfonylurea receptor-associated channels: Involvement in disease and therapeutic implications. Neurology 88, 314-321.

**16.** Kurland, D., Hong, C., Aarabi, B., Gerzanich, V. and Simard, J.M. (2012). Hemorrhagic progression of a contusion after traumatic brain injury: a review. J Neurotrauma 29, 19-31.

**17.** Martinez-Valverde, T., Vidal-Jorge, M., Martinez-Saez, E., Castro, L., Arikan, F., Cordero, E., Radoi, A., Poca, M.A., Simard, J.M. and Sahuquillo, J. (2015). Sulfonylurea Receptor 1 in Humans with Post-Traumatic Brain Contusions. J Neurotrauma 32, 1478-1487.

**18.** Jha, R.M., Kochanek, P.M. and Simard, J.M. (2018). Pathophysiology and treatment of cerebral edema in traumatic brain injury. Neuropharmacology.

**19.** Gerzanich, V., Stokum, J.A., Ivanova, S., Woo, S.K., Tsymbalyuk, O., Sharma, A., Akkentli, F., Imran, Z., Aarabi, B., Sahuquillo, J. and Simard, J.M. (2019). Sulfonylurea Receptor 1, Transient Receptor Potential Cation Channel Subfamily M Member 4, and KIR6.2:Role in Hemorrhagic Progression of Contusion. J Neurotrauma 36, 1060-1079.

**20.** Kurland, D.B., Gerzanich, V., Karimy, J.K., Woo, S.K., Vennekens, R., Freichel, M., Nilius, B., Bryan, J. and Simard, J.M. (2016). The Sur1-Trpm4 channel regulates NOS2 transcription in TLR4-activated microglia. J Neuroinflammation 13, 130.

**21.** Simard, J.M., Woo, S.K., Schwartzbauer, G.T. and Gerzanich, V. (2012). Sulfonylurea receptor 1 in central nervous system injury: a focused review. J Cereb Blood Flow Metab 32, 1699-1717.

**22.** Chen, M. and Simard, J.M. (2001). Cell swelling and a nonselective cation channel regulated by internal Ca2+ and ATP in native reactive astrocytes from adult rat brain. J Neurosci 21, 6512-6521.

**23.** Urday, S., Sheth, K.N. and Simard, J.M. (2017). Sur1–Trpm4-Promising Target for Brain Edema Treatment in Brain Edema. In: *Brain Edema*. Plesnila, N. (ed). Academic Press: San Diego, pps. 183-198.

**24.** Simard, J.M., Kent, T.A., Chen, M., Tarasov, K.V. and Gerzanich, V. (2007). Brain oedema in focal ischaemia: molecular pathophysiology and theoretical implications. The Lancet. Neurology 6, 258-268.

**25.** Simard, J.M., Tsymbalyuk, N., Tsymbalyuk, O., Ivanova, S., Yurovsky, V. and Gerzanich, V. (2010). Glibenclamide Is Superior to Decompressive Craniectomy in a Rat Model of Malignant Stroke. Stroke 41, 531-537.

**26.** Castro, L., Noelia, M., Vidal-Jorge, M., Sanchez-Ortiz, D., Gandara, D., Martinez-Saez, E., Cicuendez, M., Poca, M.A., Simard, J.M. and Sahuquillo, J. (2018). Kir6.2, the Pore-Forming Subunit of ATP-Sensitive K(+)

Channels, Is Overexpressed in Human Posttraumatic Brain Contusions. J Neurotrauma.

**27.** Gorse, K., Lantzy, M.K., Lee, E.D. and Lafrenaye, A.D. (2018). Trpm4 induces astrocyte swelling but not death after diffuse traumatic brain injury. J Neurotrauma.

**28.** Inoue, I., Nagase, H., Kishi, K. and Higuti, T. (1991). ATP-sensitive K+ channel in the mitochondrial inner membrane. Nature 352, 244-247.

**29.** Grover, G.J. (1997). Pharmacology of ATP-sensitive potassium channel (KATP) openers in models of myocardial ischemia and reperfusion. Can J Physiol Pharmacol 75, 309-315.

**30.** Sun, X.L., Zeng, X.N., Zhou, F., Dai, C.P., Ding, J.H. and Hu, G. (2008). KATP channel openers facilitate glutamate uptake by GluTs in rat primary cultured astrocytes. Neuropsychopharmacology 33, 1336-1342.

**31.** Choi, D.W. (1988). Glutamate neurotoxicity and diseases of the nervous system. Neuron 1, 623-634.

**32.** Yang, S.B., Proks, P., Ashcroft, F.M. and Rupnik, M. (2004). Inhibition of ATP-sensitive potassium channels by haloperidol. Br J Pharmacol 143, 960-967.

**33.** Berridge, M.V., Herst, P.M. and Tan, A.S. (2005). Tetrazolium dyes as tools in cell biology: new insights into their cellular reduction. Biotechnology annual review 11, 127-152.

**34.** Lazic, S.E., Clarke-Williams, C.J. and Munafo, M.R. (2018). What exactly is 'N' in cell culture and animal experiments? PLoS Biol 16, e2005282.

**35.** Pines, G. and Kanner, B.I. (1990). Counterflow of L-glutamate in plasma membrane vesicles and reconstituted preparations from rat brain. Biochemistry 29, 11209-11214.

**36.** Bradford, M.M. (1976). A rapid and sensitive method for the quantitation of microgram quantities of protein utilizing the principle of protein-dye binding. Anal Biochem 72, 248-254.

**37.** Mangiafico, S. (2018). rcompanion: Functions to Support Extension Education Program Evaluation. R package version 1.13.2.

**38.** Faul, F., Erdfelder, E., Lang, A.G. and Buchner, A. (2007). G*Power 3: a flexible statistical power analysis program for the social, behavioral, and biomedical sciences. Behavior research methods 39, 175-191.

**39.** Faul, F., Erdfelder, E., Buchner, A. and Lang, A.G. (2009). Statistical power analyses using G*Power 3.1: tests for correlation and regression analyses. Behav Res Methods 41, 1149-1160.

**40.** Simard, J.M., Sheth, K.N., Kimberly, W.T., Stern, B.J., del Zoppo, G.J., Jacobson, S. and Gerzanich, V. (2014). Glibenclamide in cerebral ischemia and stroke. Neurocrit Care 20, 319-333.

**41.** Kimberly, W.T., Elm, J., Hinson, H., Molyneaux, B., Beslow, L., Sze, G., Ostwaldt, A.C., Del Zoppo, G., Simard, M. and Sheth, K. (2016). Games (glyburide advantage in malignant edema and stroke) RP trial: Intermediate endpoint analysis as proof-of-concept. Neurology. Conference: 68th American Academy of Neurology Annual Meeting, AAN 86.

**42.** Simard, J.M., Yurovsky, V., Tsymbalyuk, N., Melnichenko, L., Ivanova, S. and Gerzanich, V. (2009). Protective effect of delayed treatment with low-dose glibenclamide in three models of ischemic stroke. Stroke 40, 604-609.

**43.** Tai, K.K., McCrossan, Z.A. and Abbott, G.W. (2003). Activation of mitochondrial ATP-sensitive potassium channels increases cell viability against rotenone-induced cell death. J Neurochem 84, 1193-1200.

**44.** Raeis, V., Philip-Couderc, P., Roatti, A., Habre, W., Sierra, J., Kalangos, A., Beghetti, M. and Baertschi, A.J. (2010). Central venous hypoxemia is a determinant of human atrial ATP-sensitive potassium channel expression: evidence for a novel hypoxia-inducible factor 1alpha-Forkhead box class O signaling pathway. Hypertension 55, 1186-1192.

**45.** Siggaard-Andersen, O., Ulrich, A. and Gothgen, I.H. (1995). Classes of tissue hypoxia. Acta Anaesthesiol Scand Suppl 107, 137-142.

**46.** Sahuquillo, J., Poca, M.A. and Amoros, S. (2001). Current aspects of pathophysiology and cell dysfunction after severe head injury. Curr Pharm Des 7, 1475-1503.

**47.** Ziello, J.E., Jovin, I.S. and Huang, Y. (2007). Hypoxia-Inducible Factor (HIF)-1 regulatory pathway and its potential for therapeutic intervention in malignancy and ischemia. Yale J Biol Med 80, 51-60.

**48.** Woo, S.K., Kwon, M.S., Geng, Z., Chen, Z., Ivanov, A., Bhatta, S., Gerzanich, V. and Simard, J.M. (2012). Sequential activation of hypoxia-inducible factor 1 and specificity protein 1 is required for hypoxia-induced transcriptional stimulation of Abcc8. J Cereb Blood Flow Metab 32, 525-536.

**49.** Thomzig, A., Wenzel, M., Karschin, C., Eaton, M.J., Skatchkov, S.N., Karschin, A. and Veh, R.W. (2001). Kir6.1 is the principal pore-forming subunit of astrocyte but not neuronal plasma membrane K-ATP channels. Mol Cell Neurosci 18, 671-690.

**50.** Zhou, M., Tanaka, O., Suzuki, M., Sekiguchi, M., Takata, K., Kawahara, K. and Abe, H. (2002). Localization of pore-forming subunit of the ATP-sensitive K(+)-channel, Kir6.2, in rat brain neurons and glial cells. Brain Res Mol Brain Res 101, 23-32.

**51.** Erginel-Unaltuna, N., Yang, W.P. and Blanar, M.A. (1998). Genomic organization and expression of KCNJ8/Kir6.1, a gene encoding a subunit of an ATP-sensitive potassium channel. Gene 211, 71-78.

**52.** Liu, D., Lu, C., Wan, R., Auyeung, W.W. and Mattson, M.P. (2002). Activation of mitochondrial ATP-dependent potassium channels protects neurons

against ischemia-induced death by a mechanism involving suppression of Bax translocation and cytochrome c release. J Cereb Blood Flow Metab 22, 431-443.

**53.** Sun, X.L. and Hu, G. (2010). ATP-sensitive potassium channels: a promising target for protecting neurovascular unit function in stroke. Clin Exp Pharmacol Physiol 37, 243-252.

**54.** Zhong, C.J., Chen, M.M., Lu, M., Ding, J.H., Du, R.H. and Hu, G. (2019). Astrocyte-specific deletion of Kir6.1/K-ATP channel aggravates cerebral ischemia/reperfusion injury through endoplasmic reticulum stress in mice. Exp Neurol 311, 225-233.

**55.** Nistico, R., Piccirilli, S., Sebastianelli, L., Nistico, G., Bernardi, G. and Mercuri, N.B. (2007). The blockade of K(+)-ATP channels has neuroprotective effects in an in vitro model of brain ischemia. Int Rev Neurobiol 82, 383-395.

**56.** Nagy, K., Kis, B., Rajapakse, N.C., Bari, F. and Busija, D.W. (2004). Diazoxide preconditioning protects against neuronal cell death by attenuation of oxidative stress upon glutamate stimulation. J Neurosci Res 76, 697-704.

**57.** Leonoudakis, D., Conti, L.R., Radeke, C.M., McGuire, L.M. and Vandenberg, C.A. (2004). A multiprotein trafficking complex composed of SAP97, CASK, Veli, and Mint1 is associated with inward rectifier Kir2 potassium channels. J Biol Chem 279, 19051-19063.

**58.** Dhar-Chowdhury, P., Harrell, M.D., Han, S.Y., Jankowska, D., Parachuru, L., Morrissey, A., Srivastava, S., Liu, W., Malester, B., Yoshida, H. and Coetzee, W.A. (2005). The glycolytic enzymes, glyceraldehyde-3-phosphate dehydrogenase, triose-phosphate isomerase, and pyruvate kinase are components of the K(ATP) channel macromolecular complex and regulate its function. J Biol Chem 280, 38464-38470.

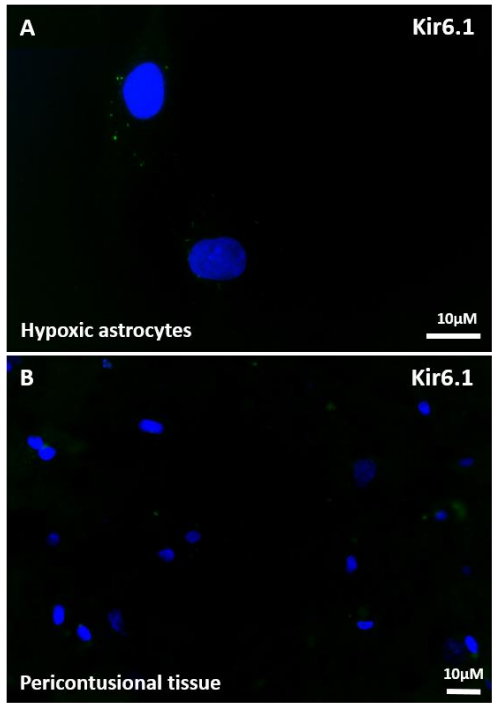


**SUPPLEMENTARY FIG. S1. Kir6.1 expression in human astrocytes and brain tissue. A)** Fluorescent labelling for Kir6.1 (green) of cultured hypoxic human astrocytes. Original magnification = 60X. Scale: 10 µm. **B)** Fluorescent labelling for Kir6.1 (green) from human pericontusional tissue. Original magnification = 40X. Scale: 10 µm. Nuclei were counterstained with DAPI (4,6-diamino-2-phenylindole).

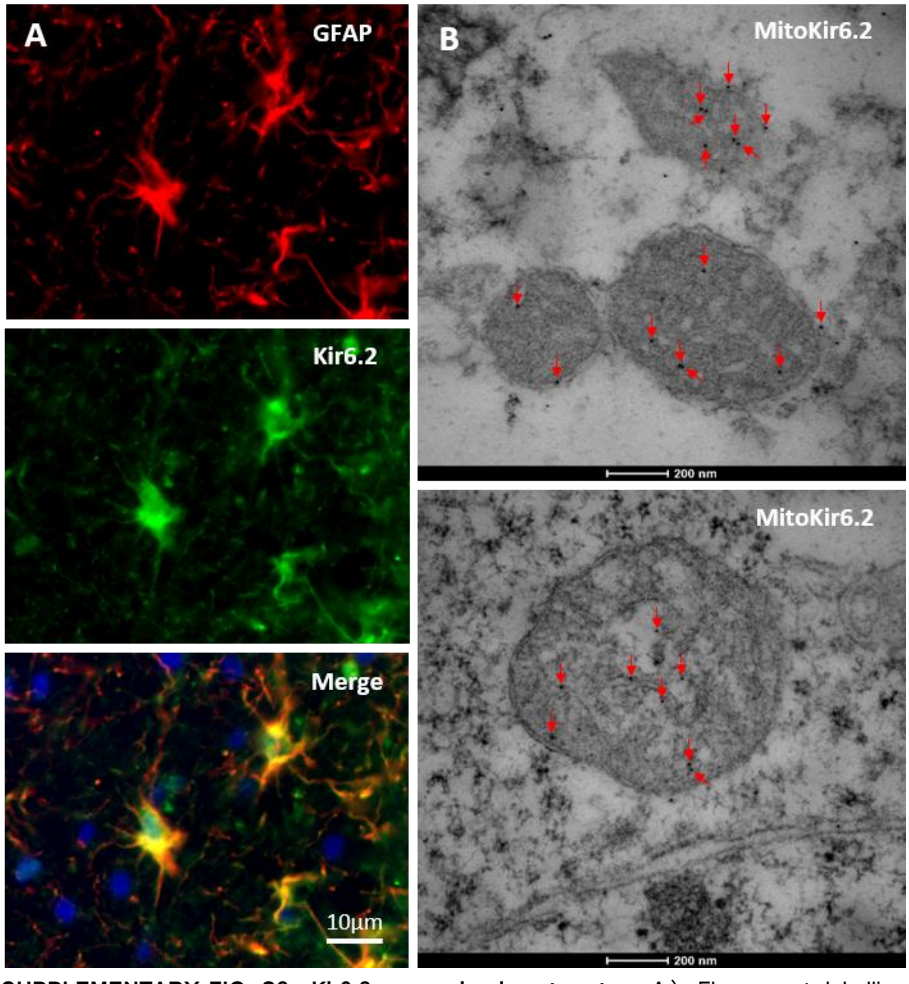


**SUPPLEMENTARY FIG. S2. Kir6.2 expression in astrocytes.** A) Fluorescent labelling for GFAP (red) and Kir6.2 (green) from human pericontusional tissue. Merged image is presented below. Original magnification = 60X. Scale: 10 µm. Nuclei were counterstained with DAPI (4,6-diamino-2-phenylindole). B) Transmission electron microscopy images (FEI Tecnai G2 Spirit BioTwin, using the digital camera Morada, Soft Imaging System, Olympus) from immunogold labelling of Kir6.2 (APC-020; Alomone Labs) in mitochondria from human pericontusional tissue. Black dots marked with red arrows show Kir6.2 subunits. Scale: 200nm.

# I. Estudio de la función de Kir6.2 en cultivos primarios de astrocitos humanos

Tras haber estudiado en el segundo capítulo que compone esta tesis doctoral la expresión de Kir6.2 en muestras cerebrales humanas de tejido pericontusional, decidimos estudiar las posibles funciones de esta subunidad *in vitro.* El tipo celular en el que observamos que Kir6.2 se expresaba de forma diferencial, eran los astrocitos (principales captadores del glutamato extracelular a nivel cerebral), por lo que para realizar nuestro modelo, usamos cultivos de astrocitos de origen humano. En nuestro estudio, intentamos reproducir un ambiente hipóxico para mimetizar las condiciones presentes en el infarto y las contusiones cerebrales. Para ello, sometimos a los astrocitos a condiciones de hipoxia severa, y analizamos los efectos de la hipoxia en la expresión de Kir6.2 en nuestras células. También estudiamos la posibilidad de que esta subunidad estuviese involucrada en la captación de glutamato por los astrocitos. Para realizar este estudio, se usaron inhibidores de Kir6.2 a nivel de membrana (haloperidol) e inhibidores de Kir6.2 a nivel mitocondrial (5-hidroxidecanoato (5-HD)).

## I.I Efectos de la hipoxia en los astrocitos

Mediante WB comprobamos que los astrocitos sometidos a hipoxia expresaban de forma significativa el factor inducible por hipoxia 1α (HIF1α) (mediana: 0,47; mín.: 0,24, máx.: 1,17) en comparación con los astrocitos sometidos a normoxia (mediana: 0,27; mín.: 0,08, máx.: 0,48) (test Wilkoxon; $p$ = 0.0078). De esta manera confirmábamos que nuestras condiciones hipóxicas eran las adecuadas.

La expresión de Kir6.2 se estudió en astrocitos sometidos a hipoxia (N=8) y a normoxia (N=8). El resultado mostró que durante condiciones hipóxicas, Kir6.2 se encontraba significativamente más expresado (mediana: 1,79; mín.: 0,53, máx.: 3.02) que en condiciones de normoxia (mediana: 0,80; mín.: 0,23, máx.: 1,16) (test Wilkoxon; $p$ = 0.005). Esto también fue comprobado mediante inmunocitoquímica, donde la mediana de la intensidad del marcaje de Kir6.2 (N=7) fue de 46,4 (mín.: 25,9; máx.: 68,8) en las células normóxicas, aumentando hasta 93,5 (mín.: 82,9; máx.: 116,6) en astrocitos hipóxicos (N=7) (test Wilkoxon; $p$ = 0.0006).

## I.II Captación de glutamato bajo condiciones de normoxia e hipoxia

Los resultados de captación de glutamato en las células tratadas con vehículo (VH) mostraron que en los astrocitos normóxicos la media de captación era de 75,9 ρmol/mg (mín.: 37,2; máx.: 144,9), mientras que en los hipóxicos era de 110,8 ρmol/mg (mín.: 52,4; máx.: 152,8). A pesar de que se observaba un incremento moderado en la captación de glutamato de los astrocitos hipóxicos, este no era estadísticamente significativo (test Wilcoxon para muestras no pareadas; $p$ = 0.442) (**Fig. 9**).

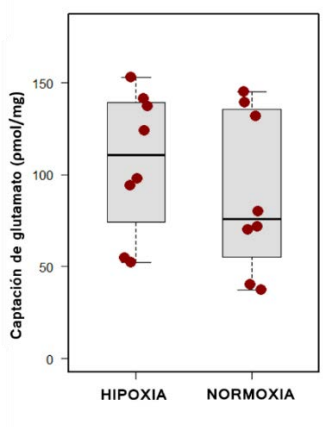


**Fig.9. Captación de glutamato bajo condiciones hipóxicas.** Box plots de la captación de glutamato (ρmol/mg) por los astrocitos tratados con vehículo, bajo condiciones de hipoxia y normoxia. No se observa un incremento significativo de la captación de glutamato por los astrocitos hipóxicos (p = 0.442).

## I.III Captación de glutamato tras el bloqueo selectivo de Kir6.2 a nivel de membrana

El bloqueo de la subunidad Kir6.2 de membrana, mediante el fármaco haloperidol, no mostró tener efectos sobre la captación de glutamato por los astrocitos (N=10).

**Normoxia:** al comparar los astrocitos tratados con haloperidol y los tratados con VH en normoxia, no vimos cambios estadísticamente significativos. La mediana de captación de glutamato de las células tratadas con VH era de 81,4 pmol/mg (mín.: 62,3; máx.: 150,4), mientras que la mediana de las células tratadas con haloperidol era de 85,7 pmol/mg (mín.: 72,3; máx.: 134,1) (test Wilcoxon; $p$ = 0.739).

**Hipoxia:** tampoco encontramos diferencias significativas entre las células tratadas con haloperidol y las tratadas con VH en condiciones hipóxicas. La mediana de captación de glutamato en las células tratadas con VH era de 136,3 pmol/mg (mín.: 88,1; máx.: 158,6), mientras que la de las células tratadas con haloperidol era de 121,7 pmol/mg (mín.: 81,7; máx.: 149,2) (test Wilcoxon; $p$ = 0.436).

## I.IV Captación de glutamato tras el bloqueo selectivo de los canales $K_{ATP}$ en mitocondria

El bloqueo de los canales $K_{ATP}$ con 5-HD no mostró tener ningún efecto sobre la captación de glutamato por los astrocitos, tanto en situaciones de normoxia como de hipoxia (N=6).

**Normoxia:** la mediana de captación de glutamato por los astrocitos tratados con VH fue de 40,1 pmol/mg (mín.: 34,5; máx.: 163,5). Cuando las células fueron tratadas con 5-HD, la mediana de captación de glutamato fue de 45,9 pmol/mg (mín.: 40,6; máx.: 138,1)(test Wilcoxon; $p$ = 0.240).

**Hipoxia:** en condiciones hipóxicas, las células tratadas con VH mostraron una mediana de captación de glutamato de 55,4 pmol/mg (mín.: 49,6; máx.: 125,8), mientras que la mediana de las células tratadas con 5-HD fue de 56,9 pmol/mg (mín.: 54,1; máx.: 156,5)(test Wilcoxon; $p$ = 0.377).

## I.V DISCUSIÓN

Un estudio de nuestro grupo llevado a cabo en el año 2015, demostró la sobreexpresión de la subunidad SUR1 en muestras humanas de contusiones cerebrales post-traumáticas[7]. Esta sobreexpresión se centraba especialmente en neuronas y células endoteliales de tejido pericontusional, aunque también se demostró en células gliales. Estos hallazgos corroboraban los datos obtenidos por otros autores, que apuntaban al canal SUR1-TRPM4, como uno de los principales mecanismos implicados en la patofisiología de la evolución de las contusiones cerebrales[4,122]. Posteriormente, también en nuestro grupo, se encontró que la subunidad formadora de poro Kir6.2 estaba expresada de forma significativa en astrocitos de tejido pericontusional[137].

SUR1 es la unidad reguladora tanto para TRPM4, como para Kir6.2. Hay evidencias clínicas y experimentales que muestran que el bloqueo del canal SUR1-TRPM4 en diferentes patologías del SNC, es beneficioso[8,10,51,101], ya que entre otras cosas permite reducir el tamaño del edema cerebral. Paradójicamente, hay trabajos en los

que ratones que no expresan SUR1 y Kir6.2 son extremadamente vulnerables a la hipoxia cerebral y en ellos se ve reducido el umbral de las lesiones inducidas por hipoxia[14]. Además, hay estudios experimentales donde los canales $K_{ATP}$, y específicamente los canales $K_{ATP}$ mitocondriales (mito$K_{ATP}$), tienen un papel esencial en la cardio y neuroprotección[138,139].

Nistico *et al* propusieron la hipótesis de que la activación persistente y excesiva de los canales $K_{ATP}$, podría contribuir al daño isquémico, y que el bloqueo de estos canales podría reducir el consumo de ATP preservando la función celular en condiciones patológicas[133].

### Expresión de Kir6.2 en condiciones hipóxicas

Nuestros resultados mostraban que la subunidad Kir6.2 estaba sobreexpresada en astrocitos sometidos a 24 h de hipoxia severa (0,5% $O_2$; 5% $CO_2$). Estos hallazgos, son similares a aquellos obtenidos por Raeis *et al* donde se muestra que tanto las subunidades SUR como las subunidades Kir6, se encuentran sobreexpresadas en cardiomiocitos sometidos a 24 h de hipoxia moderada (2% $O_2$; 5% $CO_2$)[140]. En este estudio, los autores usan miocitos cardíacos de ratas neonatas y los exponen a diferentes condiciones (baja glucosa, hipercapnia moderada, altas concentraciones de potasio, y 2% de $O_2$), y muestran que solamente la hipoxia y ninguno de los demás parámetros, es capaz de inducir la sobreexpresión de los canales Kir6.1 y Kir6.2. Estos resultados, junto con los obtenidos anteriormente en nuestro grupo donde se demostraba la sobreexpresión de Kir6.2 en astrocitos de tejido pericontusional humano[137], sugieren que la hipoxia cerebral es un factor involucrado en la sobreexpresión de los canales SUR1-Kir6.2. La isquemia en el core de las contusiones, y la hipoxia por

disperfusión en el tejido pericontusional[141,142], podrían ser los inductores de la sobreexpresión de Kir6.2 en las contusiones cerebrales.

En nuestros experimentos, como era de esperar, se observó un aumento en la expresión de HIF1α, la subunidad oxígeno dependiente de HIF. La vía de HIF1 está implicada en la adaptación celular a la hipoxia y en la regulación de las respuestas inmunes. HIF1 se forma a través de la subunidad constitutiva β y una segunda subunidad α oxígeno-dependiente. En condiciones de normoxia, HIF1α se degrada en el proteasoma y se inactiva. Sin embargo, en condiciones hipóxicas HIF1α permanece estable, dimeriza con HIF1β y se une a las regiones reguladoras de sus genes diana[143]. HIF1 regula la expresión de muchos genes involucrados en la respuesta adaptativa a la falta de oxígeno, incluyendo el cambio al metabolismo anaerobio. Hay trabajos que demuestran que HIF1 tiene una función importante en la activación transcripcional del gen ABCC8 (el que codifica para SUR1), durante la isquemia cerebral o las lesiones cerebrales traumáticas. La activación de ABCC8 por HIF1 no ocurre de forma directa, sino que tiene lugar a través de la activación de otro factor de transcripción, la proteína de especificidad 1 (Sp1)[144].

Nuestros experimentos no fueron diseñados para estudiar la regulación del gen que codifica para Kir6.2 (KCNJ11), y por lo tanto no podemos saber si HIF1 es uno de los principales activadores de Kir6.2 o si solamente es uno de los participantes en la vía de activación.

**Efectos de la modulación farmacológica de Kir6.2 en la captación de glutamato por los astrocitos**

Los canales $K_{ATP}$ cerebrales están cerrados en condiciones fisiológicas, pero se abren cuando hay situaciones de isquemia/hipoxia, precondicionamiento isquémico o inhibición metabólica[127]. Para llevar a cabo nuestros experimentos, bloqueamos Kir6.2 de membrana con haloperidol, un fármaco que se disuelve en agua y no necesita el uso de disolventes tóxicos como el dimetilsulfóxido (DMSO). Además, el haloperidol bloquea selectivamente Kir6.2 a nivel de membrana uniéndose directamente a esta subunidad[145]. No usamos otros inhibidores de canales $K_{ATP}$, como la glibenclamida, porque inhiben la subunidad SUR1 y por lo tanto afectarían tanto a Kir6.2 como a TRPM4.

Aunque encontramos un aumento significativo de Kir6.2 inducido por hipoxia, no encontramos una relación entre el aumento de su expresión y la captación de glutamato por los astrocitos. También mostramos que no había efecto en la captación de glutamato ni cuando estaba bloqueado Kir6.2 a nivel de membrana (con haloperidol), ni a nivel de mitocondria (con 5-HD). Estos resultados aparentemente contradecían aquellos obtenidos por Sun *et al*, donde se mostraba que fármacos que inducían la apertura de los canales $K_{ATP}$, facilitaban la captación de glutamato en astrocitos de rata[127]. En roedores, Kir6.1 es el canal predominante en los astrocitos, mientras que la expresión de Kir6.2 se restringe a las neuronas[120,146]. En los astrocitos humanos, nuestro grupo ha demostrado que la subunidad predominante es Kir6.2 y no Kir6.1. En astrocitos de tejido pericontusional y control, y también en astrocitos humanos sometidos a condiciones de hipoxia y normoxia, no encontramos expresión de Kir6.1. Estos resultados son consistentes con aquellos encontrados por Erginel-Unaltuna *et al*, que encontraron que KCNJ8/Kir6.1, se expresaba casi exclusivamente en corazón, pero no en otros tejidos de origen humano[147]. A pesar de

esto, se sabe que la función de SUR1-Kir6.2 en humano es similar, si no idéntica, a la función de SURX-Kir6.1 en otros mamíferos, y por lo tanto estas diferencias entre especies no pueden explicar las diferencias observadas en la captación de glutamato.

Debemos destacar que nuestro estudio fue diseñado para estudiar si el bloqueo de Kir6.2 (tanto de membrana como de mitocondria), modificaba la captación de glutamato por los astrocitos. Sin embargo, nuestros resultados negativos no nos permiten discernir si la activación de Kir6.2 por los fármacos que inducen la apertura de los canales $K_{ATP}$ (diazóxido, iptakalim, pinacidil...), facilitan la captación de glutamato por los transportadores de glutamato de los astrocitos, como se sugiere en otros trabajos[127].

### Futuros estudios

Los problemas a la hora de trasladar los resultados del laboratorio a la clínica, suelen estar relacionados con la falta comprensión de los mecanismos moleculares y las vías de señalización involucrados en la isquemia cerebral y las lesiones del SNC. Conocer la función de los canales $K_{ATP}$ podría ser un primer paso para mejorar el conocimiento de la función del canal SUR1-Kir6.2 en las contusiones cerebrales, y así encontrar posibles aplicaciones terapéuticas para los TCEs. Estos estudios son necesarios para resolver la paradoja que se plantea a la hora de bloquear SUR1, siendo este bloqueo beneficioso de cara al bloqueo de TRPM4, pero potencialmente peligroso de cara al bloqueo de Kir6.2 (con un papel protector).

Uno de los mecanismos que necesitan ser mejor estudiados, son la complejidad estructural y la regulación de estos canales, ya que la estructura canónica de los canales $K_{ATP}$, formados por dos tipos de subunidades (SURX y Kir6.X), parece ser una simplificación de la

realidad. Existen estudios en los que se ha mostrado que los canales $K_{ATP}$ podrían estar constituidos por complejos macromoleculares con diversas subunidades, entre las que se incluyen enzimas glicolíticas[148]. Dhar-Chowdhury *et al* demostraron que algunas enzimas relacionadas directamente con la glicólisis (gliceraldehído-3-fosfato deshidrogenasa, triosa-fosfato isomerasa y piruvato quinasa), son subunidades accesorias de los canales $K_{ATP}$[149].

El estudio de los mecanismos implicados en la neuroprotección/daño causados por los canales $K_{ATP}$ es una oportunidad única para comprender la patofisiología molecular de las lesiones isquémicas y traumáticas, y también para diseñar nuevas dianas terapéuticas. Las aproximaciones futuras deben dirigirse al estudio del bloqueo de Kir6.2 y TRPM4, de forma independiente. La depleción selectiva de estas subunidades en astrocitos y otras células de la unidad perivascular mediante RNA de interferencia, y la exposición de estas células a condiciones como la isquemia y la hipoxia, podría ayudar a estudiar su función diferencial. El mejor conocimiento de los canales regulados por SUR1 podría ayudar a diseñar nuevas terapias protectoras contra las diferentes lesiones del SNC.

## I.VI CONCLUSIONES (ANEXOS)

1. La subunidad Kir6.2 se sobreexpresa en cultivos primarios de astrocitos humanos sometidos a 24 horas de hipoxia severa (0,5% $O_2$; 5% $CO_2$).
2. La sobreexpresión de Kir6.2 en astrocitos humanos sometidos a hipoxia, no afecta a la captación de glutamato por los mismos.
3. La inhibición de Kir6.2 mediante inhibidores selectivos de Kir6.2 de membrana (haloperidol) y de mitocondria (5-HD), no afecta a la captación de glutamato por los astrocitos.

# BIBLIOGRAFÍA

# BIBLIOGRAFÍA


1. Maas, A. I. R., Stocchetti, N. & Bullock, R. Moderate and severe traumatic brain injury in adults. *Lancet Neurol.* **7,** 728–741 (2008).
2. Roozenbeek, B., Maas, A. I. R. & Menon, D. K. Changing patterns in the epidemiology of traumatic brain injury. *Nat. Rev. Neurol.* **9,** 231–236 (2013).
3. Godoy, D., Piñero, G., Cruz-Flores, S., Alcalá Cerra, G. & Rabinstein, A. Malignant hemispheric infarction of the middle cerebral artery. Diagnostic considerations and treatment options. *Neurologia* **31,** 332–343 (2013).
4. Simard, J. M., Kent, T. A., Chen, M., Tarasov, K. V & Gerzanich, V. Brain oedema in focal ischaemia: molecular pathophysiology and theoretical implications. *Lancet Neurol.* **6,** 258–268 (2007).
5. Maciel, C. B. & Sheth, K. N. Malignant MCA Stroke: an Update on Surgical Decompression and Future Directions. *Curr. Atheroscler. Rep.* **17,** (2015).
6. Mehta, R. I. *et al.* Sulfonylurea receptor 1 expression in human cerebral infarcts. *J. Neuropathol. Exp. Neurol.* **72,** 871–83 (2013).
7. Martínez-Valverde, T. *et al.* Sulfonylurea Receptor 1 in Humans with Post-Traumatic Brain Contusions. *J. Neurotrauma* **32,** 1478–1487 (2015).
8. Simard, J. M. & Kimberly, W. T. Glibenclamide in Cerebral Ischemia and Stroke. **20,** 319–333 (2014).
9. Mehta, R. I. *et al.* Sur1-Trpm4 Cation Channel Expression in Human Cerebral Infarcts. **74,** 835–849 (2016).
10. Zafardoost, P., Ghasemi, A. A., Salehpour, F., Piroti, C. & Ziaeii, E. Evaluation of the Effect of Glibenclamide in Patients With Diffuse Axonal Injury Due to Moderate to Severe Head Trauma. **21,** 0–3 (2016).
11. Sheth, K. N. *et al.* Human Data Supporting Glyburide in Ischemic Stroke. *Acta Neurochir. (Wien).* **121,** 13–18

(2016).

12. Miki, T., Nagashima, K. & Seino, S. The structure and function of the ATP-sensitive K+ channel in insulin-secreting pancreatic beta-cells. *J.Mol.Endocrinol.* **22,** 113–123 (1999).
13. Noma, A. ATP-regulated K+ channels in cardiac muscle. *Nature* **305,** 147–8 (1983).
14. Yamada, K. & Inagaki, N. Neuroprotection by KATP channels. *J. Mol. Cell. Cardiol.* **38,** 945–949 (2005).
15. Sheth, K. N. *et al.* Human Data Supporting Glyburide in Ischemic Stroke. *Acta Neurochir. (Wien).* **121,** 13–18 (2016).
16. Majdan, M. *et al.* Epidemiology of traumatic brain injuries in Europe: a cross-sectional analysis. *Lancet Public Heal.* **1,** e76–e83 (2016).
17. Pérez, K. *et al.* Incidence trends of traumatic spinal cord injury and traumatic brain injury in Spain, 2000-2009. *Accid. Anal. Prev.* **46,** 37–44 (2012).
18. Menon, D. K., Schwab, K., Wright, D. W. & Maas, A. I. Position statement: Definition of traumatic brain injury. *Arch. Phys. Med. Rehabil.* **91,** 1637–1640 (2010).
19. Hawryluk, G. W. J. & Manley, G. T. *Classification of traumatic brain injury. past, present, and future. Handbook of Clinical Neurology* **127,** (Elsevier B.V., 2015).
20. Marshall, L. *et al.* The diagnosis of head injury requires a classification based on computed axial tomography. *J. Neurotrauma* **9,** S287-92 (1992).
21. Steyerberg, E. W. *et al.* Predicting outcome after traumatic brain injury: Development and international validation of prognostic scores based on admission characteristics. *PLoS Med.* **5,** 1251–1261 (2008).
22. Teasdale, G. & Jennett, B. Assessment of coma and impaired consciousness. A practical scale. *Lancet* **2,** 81–84 (1974).
23. McKee Ann C., D. D. H. *The neuropathology of Traumatic brain injury. Handbook of Clinical Neurology* **127,** (2015).
24. Kurland, D., Hong, C., Aarabi, B., Gerzanich, V. & Simard,

J. M. Hemorrhagic Progression of a Contusion after Traumatic Brain Injury: A Review. *J. Neurotrauma* **29,** 19–31 (2012).

25. Newcombe, V. F. J. *et al.* Microstructural basis of contusion expansion in traumatic brain injury: Insights from diffusion tensor imaging. *J. Cereb. Blood Flow Metab.* **33,** 855–862 (2013).
26. Grysiewicz, R. A., Thomas, K. & Pandey, D. K. Epidemiology of Ischemic and Hemorrhagic Stroke: Incidence, Prevalence, Mortality, and Risk Factors. *Neurol. Clin.* **26,** 871–895 (2008).
27. Stroke GBD. UPDATE ON THE GLOBAL BURDEN OF ISCHAEMIC AND HAEMORRHAGIC STROKE IN 1990–2013: THE GBD 2013 STUDY. *Neuroepidemiology* **45,** 161–176 (2015).
28. Ovbiagele, B. & Nguyen-Huynh, M. N. Stroke Epidemiology: Advancing Our Understanding of Disease Mechanism and Therapy. *Neurotherapeutics* **8,** 319–329 (2011).
29. Werner, H. *et al.* 'Malignant' Middle Cerebral Artery Territory Infarction. *Arch. Neurol.* **53,** 309–3015 (1996).
30. Simard, J. M., Sahuquillo, J., Sheth, K. N., Kristopher, T. K. & Walcott, B. P. Managing Malignant Cerebral Infarction. **13,** 217–229 (2011).
31. Abbott, N. J., Patabendige, A. A. K., Dolman, D. E. M., Yusof, S. R. & Begley, D. J. Structure and function of the blood-brain barrier. *Neurobiol. Dis.* **37,** 13–25 (2010).
32. Reese, T. S. & Karnovsky, M. J. Fine Structural Localization of a Blood-Brain Barrier To Exogenous Peroxidase. *J. Cell Biol.* **34,** 207–217 (1967).
33. Chow, B. W. & Gu, C. The Molecular Constituents of the Blood-Brain Barrier. *Trends Neurosci.* **38,** 598–608 (2015).
34. Abbott, N. J., Rönnbäck, L. & Hansson, E. Astrocyte-endothelial interactions at the blood-brain barrier. *Nat. Rev. Neurosci.* **7,** 41–53 (2006).
35. Sandoval, K. E. & Witt, K. A. Blood-brain barrier tight junction permeability and ischemic stroke. *Neurobiol. Dis.* **32,**

200–219 (2008).

36. Cabezas, R. *et al.* Astrocytic modulation of blood brain barrier: perspectives on Parkinsonâ€™s disease. *Front. Cell. Neurosci.* **8,** 1–11 (2014).
37. Wong, A. D. *et al.* The blood-brain barrier: an engineering perspective. *Front. Neuroeng.* **6,** 1–22 (2013).
38. Hawkins, B. T. & Davis, T. P. The blood-brain barrier in health and disease. *Pharmacol. Rev.* **57,** 173–185 (2005).
39. Klatzo, I. Neuropathological aspects of brain edema. *J. Neuropathol. Exp. Neurol.* **26,** (1967).
40. Chinard, F. P. Starling's hypothesis in the formation of edema. **38,** (1962).
41. Stokum, J. A., Gerzanich, V. & Simard, J. M. Molecular pathophysiology of cerebral edema. *J. Cereb. Blood Flow Metab.* **36,** 513–538 (2016).
42. Simard, J. M. *et al.* Newly expressed SUR1-regulated NC(Ca-ATP) channel mediates cerebral edema after ischemic stroke. *Nat. Med.* **12,** 433–40 (2006).
43. Castejón, O. J. Formation of transendothelial channels in traumatic human brain edema. *Pathol. Res. Pract.* **179,** 7–12 (1984).
44. Weber, J. T. Altered calcium signaling following traumatic brain injury. *Front. Pharmacol.* **3 APR,** 1–16 (2012).
45. Valable, S. *et al.* VEGF-induced BBB permeability is associated with an MMP-9 activity increase in cerebral ischemia: both effects decreased by Ang-1. 1491–1504 (2005). doi:10.1038/sj.jcbfm.9600148
46. Leinonen, V., Vanninen, R. & Rauramaa, T. *Raised intracranial pressure and brain edema*. *Handbook of Clinical Neurology* **145,** (Elsevier B.V., 2017).
47. Hollenstein, K., JP, D. R. & P, L. K. Structure and mechanism of ABC transporters. *Curr. Opin. Struct. Biol.* **17,** 412–418 (2007).
48. Aittoniemi, J. *et al.* SUR1: A unique ATP-binding cassette protein that functions as an ion channel regulator. *Philos.*

*Trans. R. Soc. B Biol. Sci.* **364,** 257–267 (2009).

49. Liss, B. & Roeper, J. Molecular physiology of neuronal K-ATP channels (review). *Mol. Membr. Biol.* **18,** 117–127 (2001).
50. Tosun, C. *et al.* Inhibition of the Sur1-Trpm4 Channel Reduces Neuroinflammation and Cognitive Impairment in Subarachnoid Hemorrhage. **44,** 3522–3528 (2013).
51. Simard, M., Tsymbalyuk, N., Tsymbalyuj, O., Ivanova, S. & Gerzanich, V. Glibenclamide is superior to decompressive craniectomy in a model of malignant stroke. **41,** 531–537 (2010).
52. Guo, J. *et al.* Structures of the Calcium-activated Non-Selective Cation Channel TRPM4. **552,** 205–209 (2017).
53. Duan, J. *et al.* Structure of full-length human TRPM4. *Proc. Natl. Acad. Sci.* **115,** 2377–2382 (2018).
54. Cheng, H. *et al.* TRPM4 controls insulin secretion in pancreatic β-cells. *Cell Calcium* **41,** 51–61 (2007).
55. Schattling, B. *et al.* TRPM4 cation channel mediates axonal and neuronal degeneration in experimental autoimmune encephalomyelitis and multiple sclerosis. *Nat. Med.* **18,** 1805–1811 (2012).
56. Earley, S. TRPM4 channels in smooth muscle function. *Pflugers Arch. Eur. J. Physiol.* **465,** 1223–1231 (2013).
57. Chen, M., Dong, Y. & Simard, J. M. Functional Coupling between Sulfonylurea Receptor Type 1 and a Nonselective Cation Channel in Reactive Astrocytes from Adult Rat Brain. *J. Neurosci.* **23,** 8568–8577 (2003).
58. Kurland, D. B. *et al.* Glibenclamide for the treatment of acute CNS injury. *Pharmaceuticals* **6,** 1287–1303 (2013).
59. Haider, S., Antcliff, J. F., Proks, P., Sansom, M. S. P. & Ashcroft, F. M. Focus on Kir6.2: A key component of the ATP-sensitive potassium channel. *J. Mol. Cell. Cardiol.* **38,** 927–936 (2005).
60. Suzuki, M., Fujikura, K., Inagaki, N., Seino, S. & Takata, K. Localization of the ATP-sensitive K+ channel subunit Kir6.2 in

Mouse pancreas. *Diabetes* **46,** 1440–1444 (1997).

61. Teramoto, N. Physiological roles of ATP-sensitive K+channels in smooth muscle. *J. Physiol.* **572,** 617–624 (2006).
62. Davies, N. W. Modulation of ATP-sensitive K+ channels in skeletal muscle by intracelullar protons. *Lett. To Nat.* **346,** 818–822 (1990).
63. Quast, U. ATP-sensitive K+ channels in the kidney. *Naunyn Schmiedebergs Arch Pharmacol* **354,** 213–225 (1996).
64. Wu, S., Li, H. & Chiang, H. Characterization of ATP-sensitive potassium channels functionally expressed in pituitary GH3 cells. *J. Membr. Biol.* **178,** 205–2014 (2000).
65. Lybaert, P. *et al.* Detection of KATP channels subunits in human term placental explants and evaluation of their implication in human placental lactogen (hPL) and human chorionic gonadotropin (hCG) release. *Placenta* **34,** 467–473 (2013).
66. Levin, B. E., Dunn-meynell, A. A. & Routh, V. H. Brain glucosensing and the K. *Pharmacology* 459–460 (2001).
67. Li, N. *et al.* Structure of a Pancreatic ATP-Sensitive Potassium Channel. *Cell* **168,** 101–110.e10 (2017).
68. Héron-Milhavet, L. *et al.* Protection against hypoxic-ischemic injury in transgenic mice overexpressing Kir6.2 channel pore in forebrain. *Mol. Cell. Neurosci.* **25,** 585–593 (2004).
69. Sun, H. & Feng, Z. Neuroprotective role of ATP-sensitive potassium channels in cerebral ischemia. *Acta Pharmacol. Sin.* **34,** 24–32 (2013).
70. Hemphill, J. C., Andrews, P. & De Georgia, M. Multimodal monitoring and neurocritical care bioinformatics. *Nat. Rev. Neurol.* **7,** 451–460 (2011).
71. Haddad, S. H. & Arabi, Y. M. Critical care management of severe traumatic brain injury in adults. *Scand. J. Trauma. Resusc. Emerg. Med.* **20,** 12 (2012).
72. Roh, D. & Park, S. Brain Multimodality Monitoring: Updated Perspectives. *Curr Neurol Neurosci Rep* **16,** 1–17 (2016).
73. Carney, N. *et al.* Guidelines for the Management of Severe

Traumatic Brain Injury, Fourth Edition. *Neurosurgery* **24(Suppl 1,** 1 (2016).

74. Tasneem, N. *et al.* Brain Multimodality Monitoring: A New Tool in Neurocritical Care of Comatose Patients. *Crit. Care Res. Pract.* **2017,** (2017).
75. Nortje, J. & Gupta, A. K. The role of tissue oxygen monitoring in patients with acute brain injury. *Br. J. Anaesth.* **97,** 95–106 (2006).
76. Orakcioglu, B. *et al.* Evaluation of a novel brain tissue oxygenation probe in an experimental swine model. *Neurosurgery* **67,** 1716–1722 (2010).
77. De Georgia, M. A. Brain Tissue Oxygen Monitoring in Neurocritical Care. *J. Intensive Care Med.* **30,** 473–483 (2015).
78. Martini, R. P., Deem, S. & Treggiari, M. M. Targeting brain tissue oxygenation in traumatic brain injury. *Respir Care* **58,** 162–172 (2013).
79. Nortje, J. & Gupta, A. K. The role of tissue oxygen monitoring in patients with acute brain injury. *Br. J. Anaesth.* **97,** 95–106 (2006).
80. Bellander, B. M. *et al.* Consensus meeting on microdialysis in neurointensive care. *Intensive Care Med.* **30,** 2166–2169 (2004).
81. Olausson, P. *et al.* Relative recovery over time-an in vivo microdialysis study of human skeletal muscle. *Scand. J. Clin. Lab. Invest.* **73,** 10–16 (2013).
82. Borg, A. & Smith, M. Cerebral microdialysis: Research technique or clinical tool? *Neuromethods* **75,** 1–21 (2013).
83. Reinstrup, P. *et al.* Intracerebral microdialysis in clinical practice: baseline values for chemical markers during wakefulness, anesthesia, and neurosurgery. *Neurosurgery* **47,** 701–9 (2000).
84. Abi-Saab, W. M. *et al.* Striking differences in glucose and lactate levels between brain extracellular fluid and plasma in conscious human subjects: Effects of hyperglycemia and

hypoglycemia. *J. Cereb. Blood Flow Metab.* **22,** 271–279 (2002).

85. Schulz, M., Wang, L., Tange, M. & Bjerre, P. Cerebral microdialysis monitoring: determination of normal and ischemic cerebral metabolism in patients with aneurysmal subarachnoid hemorrhage. *J. Neurosurg.* **93,** 233–38 (2000).
86. Sánchez-Guerrero, A. *et al.* Reappraisal of the reference levels for energy metabolites in the extracellular fluid of the human brain. *J. Cereb. Blood Flow Metab.* **37,** 2742–2755 (2017).
87. Helbok, R. *et al.* Early brain injury after aneurysmal subarachnoid hemorrhage: A multimodal neuromonitoring study. *Crit. Care* **19,** 1–9 (2015).
88. De Lima Oliveira, M. *et al.* Cerebral microdialysis in traumatic brain injury and subarachnoid hemorrhage: State of the art. *Neurocrit. Care* **21,** 152–162 (2014).
89. Dohmen, C. *et al.* Prediction of malignant course in MCA infarction by PET and microdialysis. *Stroke* **34,** 2152–2158 (2003).
90. Arikan, F. *et al.* Malignant infarction of the middle cerebral artery in a porcine model. A pilot study. *PLoS One* **12,** 1–21 (2017).
91. Xiong, Y., Mahmood, A. & Chopp, M. Animal models of traumatic brain injury. *Nat Rev Neurosci.* **14,** 128–142 (2013).
92. Sommer, C. J. Ischemic stroke: experimental models and reality. *Acta Neuropathol.* **133,** 245–261 (2017).
93. Burkhardt, A. M. & Zlotnik, A. Translating translational research: Mouse models of human disease. *Cell. Mol. Immunol.* **10,** 373–374 (2013).
94. Sorby-Adams, A. J., Vink, R. & Turner, R. J. Large animal models of strocke and traumatic brain injury as translational tools. *Am. J. Physiol.* 17–24 (2018).
95. Bramlett, H. M. & Dietrich, W. D. Pathophysiology of cerebral ischemia and brain trauma: similarities and differences. *J.*

*Cereb. Blood Flow Metab.* **24,** 133–150 (2004).

96. Turski, L. *et al.* ZK200775: A phosphonate quinoxalinedione AMPA antagonist for neuroprotection. *Pharmacology* **95,** 10960–10965 (1998).
97. Zhang, C. *et al.* Cerebrolysin enhances neurogenesis in the ischemic brain and improves functional outcome after stroke. **88,** 3275–3281 (2010).
98. Schäbitz, W., Li, F. & Fisher, M. The N-Methyl-D-Aspartate Antagonist CNS 1102 Protects Cerebral Gray and White Matter From Ischemic Injury Following Temporary Focal Ischemia in Rats. *Stroke* **31,** 1709–1714 (2000).
99. Chen, X. & Wang, K. The fate of medications evaluated for ischemic stroke pharmacotherapy over the period 1995–2015. *Acta Pharm. Sin. B* **6,** 522–530 (2016).
100. Gjedde, A. *et al.* Relationship between residual cerebral blood flow and oxygen metabolism as predictive of ischemic tissue viability: sequential multitracer positron emission tomography scanning of middle cerebral artery occlusion during the critical first 6 hours after st. *J. Neurosurg.* **93,** 647–657 (2009).
101. Simard, J. M. *et al.* Protective Effect of Delayed Treatment With Low-Dose Glibenclamide in Three Models of Ischemic Stroke. *Stroke* **40,** 304–609 (2009).
102. Morancho, A. *et al.* A new method for focal transient cerebral ischaemia by distal compression of the middle cerebral artery. *Neuropathol. Appl. Neurobiol.* **38,** 617–627 (2012).
103. Sahuquillo, J. *et al.* Coexistence of Regional Cerebral Hypoxia with Normal or Hyperemic Brain Detected by Global Monitoring Methods. Analysis of Apparently Contradictory Findings Based on the Siggaard-Andersen Model of Tissue Hypoxia. *Acta Neurochir. (Wien).* **81,** 303–305 (2002).
104. Carteron, L., Bouzat, P. & Oddo, M. Cerebral microdialysis monitoring to improve individualized neurointensive care therapy: An update of recent clinical data. *Front. Neurol.* **8,** 1–10 (2017).
105. Nielsen, T. H. *et al.* Bedside Diagnosis of Mitochondrial

Dysfunction After Malignant Middle Cerebral Artery Infarction. *Neurocrit. Care* **21,** 35–42 (2013).

106. Carpenter, K. L. H., Jalloh, I. & Hutchinson, P. J. Glycolysis and the significance of lactate in traumatic brain injury. *Front. Neurosci.* **9,** 1–15 (2015).
107. Peerdeman, S. M., Girbes, A. R. J., Polderman, K. H. & Vandertop, W. P. Changes in cerebral interstitial glycerol concentration in head-injured patients; correlation with secondary events. *Intensive Care Med.* **29,** 1825–1828 (2003).
108. Clausen, T. *et al.* Association between elevated brain tissue glycerol levels and poor outcome following severe traumatic brain injury. *J. Neurosurg.* **103,** 233–8 (2005).
109. Martinez-Valverde, T. *et al.* Characterization of the Ionic Profile of the Extracellular Space of the Injured and Ischemic Brain: A Microdialysis Study. *J. Neurotrauma* **34,** 74–85 (2016).
110. Leis, J. A., Bekar, L. K. & Walz, W. Potassium homeostasis in the ischemic brain. *Glia* **50,** 407–416 (2005).
111. Betz, L., Keep, R. F., Beer, M. E. & Ren, X.-D. Blood-Brain Barrier Permeability and Brain Concentration of Sodium, Potassium, and Chloride During Focal Ischemia. *J. Cereb. Blood Flow Metab.* **14,** 29–37 (1994).
112. Woo, S. K., Kwon, M. S., Ivanov, A., Gerzanich, V. & Simard, J. M. The sulfonylurea receptor 1 (Sur1)-transient receptor potential melastatin 4 (Trpm4) channel. *J. Biol. Chem.* **288,** 3655–3667 (2013).
113. Mehta, R. I. *et al.* Sur1-Trpm4 Cation Channel Expression in Human Cerebral Infarcts. **74,** 835–849 (2015).
114. Imai, H. *et al.* A new model of focal cerebral ischemia in the miniature pig. *J. Neurosurg. Pediatr.* **104,** 123–132 (2006).
115. Burbridge, B., Matte, G. & Remedios, A. Complex intracranial arterial anatomy in swine is unsuitable for cerebral infarction projects. *Can. Assoc. Radiol. J.* **55,** 326–9 (2004).
116. Gillilan, L. A. Blood supply to brains of ungulates with and

without a rete mirabile caroticum. *J. Comp. Neurol.* **153,** 275–290 (1974).

117. Gillilan, L. A. Extra- and intra-cranial blood supply to brains of dog and cat. *Am. J. Anat.* **146,** 237–253 (1976).
118. Hernández-Jiménez, M. *et al.* Test repositioning for functional assessment of neurological outcome after experimental stroke in mice. *PLoS One* **12,** 1–13 (2017).
119. Thomzig, A., Laube, G., Prüss, H. & Veh, R. W. Pore-forming subunits of K-ATP channels, Kir6.1 and Kir6.2, display prominent differences in regional and cellular distribution in the rat brain. *J. Comp. Neurol.* **484,** 313–330 (2005).
120. Zhou, M. *et al.* Localization of pore-forming subunit of the ATP-sensitive K+-channel, Kir6.2, in rat brain neurons and glial cells. *Mol. Brain Res.* **101,** 23–32 (2002).
121. Patrylo, P. R. *et al.* Aberrant expression of the pore-forming KATP channel subunit Kir6.2 in hippocampal reactive astrocytes in the 3xTg-AD mouse model and human Alzheimer's disease. *Neuroscience* **336,** 81–101 (2016).
122. Jha, R. M. *et al.* Sulfonylurea Receptor-1: A Novel Biomarker for Cerebral Edema in Severe Traumatic Brain Injury. *Crit. Care Med.* **45,** e255–e264 (2017).
123. Inoue, I., Nagase, H., Kischi, K. & Higuti, T. ATP-sensitive K+ channel in the mitochondrial inner membrane. *Nature* **352,** 244–247 (1991).
124. Ardehali, H. & O'Rourke, B. Mitochondrial KATP channels in cell survival and death. *J. Mol. Cell. Cardiol.* **39,** (2005).
125. Rose, M. E. *et al.* Regulation of interstitial excitatory amino acid concentrations after cortical contusion injury. *Brain Res.* **943,** 15–22 (2002).
126. Bullock, R. *et al.* Factors affecting excitatory amino acid release following severe human head injury. *J. Neurosurg.* **89,** 507–518 (1998).
127. Sun, X.-L. *et al.* KATP channel openers facilitate glutamate uptake by GluTs in rat primary cultured astrocytes. *Neuropsychopharmacology* **33,** 1336–1342 (2008).

128. Ortega, F. J., Vukovic, J., Rodríguez, M. J. & Bartlett, P. F. Blockade of microglial KATP-channel abrogates suppression of inflammatory-mediated inhibition of neural precursor cells. *Glia* **62,** 247–258 (2014).
129. Ortega, F. J., Jolkkonen, J. & Rodríguez, M. J. Microglia is an active player in how glibenclamide improves stroke outcome. *J. Cereb. Blood Flow Metab.* **33,** 1138–1139 (2013).
130. Liss, B. & Roeper, J. Molecular physiology of neuronal K-ATP channels (review). *Mol. Membr. Biol.* **18,** 117–127 (2001).
131. Sun, H. & Feng, Z. Neuroprotective role of ATP-sensitive potassium channels in cerebral ischemia. *Acta Pharmacol. Sin.* **34,** 24–32 (2013).
132. Benarroch, E. E. Sulfonylurea receptor-associated channels: Involvement in disease and therapeutic implications. *Neurology* (2016). doi:10.1212/WNL.0000000000003523
133. Nisticò, R. *et al.* The Blockade of K+-ATP Channels has Neuroprotective Effects in an In Vitro Model of Brain Ischemia. *Int. Rev. Neurobiol.* **82,** 383–395 (2007).
134. Vo, K. D. *et al.* Neurologic and neuroimaging manifestations of Cantú syndrome. *Neurology* **87,** 270–276 (2016).
135. Ortega, F. J. *et al.* ATP-dependent potassium channel blockade strengthens microglial neuroprotection after hypoxia-ischemia in rats. *Exp. Neurol.* **235,** 282–296 (2012).
136. Patel, A. D., Gerzanich, V., Geng, Z. & Simard, J. M. Glibenclamide reduces hippocampal injury and preserves rapid spatial learning in a model of traumatic brain injury. *J. Neuropathol. Exp. Neurol.* **69,** 1177–90 (2010).
137. Castro, L. *et al.* Kir6.2, the Pore-Forming Subunit of ATP-Sensitive $K^+$ Channels, Is Overexpressed in Human Posttraumatic Brain Contusions. *J. Neurotrauma* **36,** 165–175 (2019).
138. Tai, K., McCrossan, Z. & Abbott, G. Activation of mitochondrial ATP-sensitive potassium channels increases cell

viability against rotenone-induced cell death. *J. Neurochem.* **84,** 1193–200 (2003).

139. Gover, G. Pharmacology of ATP-sensitive potassium channel (KATP) openers in models of myocardial ischemia and reperfusion. *Can J Physiol Pharmacol* **75,** 309–15 (1997).
140. Raeis, V. *et al.* Central venous hypoxemia is a determinant of human atrial ATP-sensitive potassium channel expression: Evidence for a novel hypoxia-inducible factor 1α-forkhead box class O signaling pathway. *Hypertension* **55,** 1186–1192 (2010).
141. Sahuquillo, J., Poca, M. & Amoros, S. Current Aspects of Pathophysiology and Cell Dysfunction after Severe Head Injury. *Curr. Pharm. Des.* **7,** 1475–1503 (2001).
142. Siggaard-Andersen, O., Ulrich, A. & Gothgen, I. Classes of tissue hypoxia. *Acta Anaesthesiol Scand Suppl* **107,** 137–42 (1995).
143. Ziello, J. E., Jovin, I. S. & Huang, Y. Hypoxia-Inducible Factor (HIF)-1 regulatory pathway and its potential for therapeutic intervention in malignancy and ischemia. *Yale J. Biol. Med.* **80,** 51–60 (2007).
144. Woo, S. K. *et al.* Sequential activation of hypoxia-inducible factor 1 and specificity protein 1 is required for hypoxia-induced transcriptional stimulation of Abcc8. *J. Cereb. Blood Flow Metab.* **32,** 525–36 (2012).
145. Yang, S. B., Proks, P., Ashcroft, F. M. & Rupnik, M. Inhibition of ATP-sensitive potassium channels by haloperidol. *Br. J. Pharmacol.* **143,** 960–967 (2004).
146. Thomzig, A. *et al.* Kir6.1 is the principal pore-forming subunit of astrocyte but not neuronal plasma membrane K-ATP channels. *Mol. Cell. Neurosci.* **18,** 671–690 (2001).
147. Erginel-Unaltuna, N., Yang, W. P. & Blanar, M. A. Genomic organization and expression of KCNJ8/Kir6.1, a gene encoding a subunit of an ATP-sensitive potassium channel. *Gene* **211,** 71–78 (1998).
148. Leonoudakis, D., Conti, L. R., Radeke, C. M., McGuire, L.

M. M. & Vandenberg, C. A. A Multiprotein Trafficking Complex Composed of SAP97, CASK, Veli, and Mint1 Is Associated with Inward Rectifier Kir2 Potassium Channels. *J. Biol. Chem.* **279,** 19051–19063 (2004).

149. Dhar-Chowdhury, P. *et al.* The glycolytic enzymes, glyceraldehyde-3-phosphate dehydrogenase, triose-phosphate isomerase, and pyruvate kinase are components of the K ATP channel macromolecular complex and regulate its function. *J. Biol. Chem.* **280,** 38464–38470 (2005).